International Journal of Extreme Manufacturing

Femtosecond laser direct writing of functional stimulus-responsive structures and applications

To cite this article before publication: Yuxuan Zhang *et al* 2023 *Int. J. Extrem. Manuf.* in press https://doi.org/10.1088/2631-7990/acf798

Femtosecond laser direct writing of functional stimulus-responsive structures and applications

Journal:	*International Journal of Extreme Manufacturing*
Manuscript ID	IJEM-110854.R1
Manuscript Type:	Topical Review
Keywords:	stimulus-responsive structures, femtosecond laser direct writing, laser-matter interaction, multifunctionality

IOP Publishing Journal Title
Journal **XX** (XXXX) XXXXXX https://doi.org/XXXX/XXXX

Femtosecond laser direct writing of functional stimulus-responsive structures and applications

Yuxuan Zhang, Dong Wu, Yachao Zhang, Yucheng Bian, Chaowei Wang*, Jiawen Li, Jiaru Chu and Yanlei Hu*

CAS Key Laboratory of Mechanical Behavior and Design of Materials, Key Laboratory of Precision Scientific Instrumentation of Anhui Higher Education Institutes, Department of Precision Machinery and Precision Instrumentation, University of Science and Technology of China, Hefei 230027, China

***Corresponding authors (**email: **chaoweiw@ustc.edu.cn**; **huyl@ustc.edu.cn)**

Received xxxxxx
Accepted xxxxxx
Published xxxxxx

Abstract

Diverse natural organisms possess stimulus-responsive structures to adapt to the surrounding environment. Inspired by nature, researchers have developed various smart stimulus-responsive structures with adjustable properties and functions to address the demands of ever-changing application environments that are becoming more intricate. Among many fabrication methods for stimulus-responsive structures, femtosecond laser direct writing (FsLDW) has received increasing attention because of its high precision, simplicity, true three-dimensional machining ability, and wide applicability to almost all materials. This paper systematically outlines state-of-the-art research on stimulus-responsive structures prepared by FsLDW. Based on the introduction of femtosecond laser-matter interaction and mainstream FsLDW-based manufacturing strategies, different stimulating factors that can trigger structural responses of prepared intelligent structures, such as magnetic field, light, temperature, pH, and humidity, are emphatically summarized. Various applications of functional structures with stimuli-responsive dynamic behaviors fabricated by FsLDW, as well as the present obstacles and forthcoming development opportunities, are discussed.

Keywords: stimulus-responsive structures, femtosecond laser direct writing, laser-matter interaction, multifunctionality

1. Introduction

In the natural world, numerous creatures have developed and formed diverse stimulus-responsive structures to adapt to different environments for better survival conditions. Honeybees can dynamically control their glossal surface and wettability regulated by erectable glossal hairs during foraging activities, which can reduce the energy consumption for impelling nectar and improve the nectar-trapping volume [1]. Chameleons can rapidly change their body colors with changes in the environment, which is beneficial for camouflage and predation [2]. For plants, pine cones, chiral pods, and wheat awns can be actuated by swelling or shrinking for the dispersal of seeds in response to variations in surrounding humidity [3-5]. Mimosa can generate closing motion immediately when its leaves are subjected to external touch [6]. Sunflowers are sensitive to light stimuli and always change their positions to face normal to the sun throughout the day [7]. Drawing inspiration from nature, researchers have made continuous efforts to prepare stimulus-responsive structures with tunable characteristics and advanced functionalities to fulfill the requirements of complicated and variable application scenarios and multifunction integration. These smart structures enabling controllable shape or phase changes upon various chemical and physical stimuli can be widely applied in diverse fields, e.g., stimulus-responsive swelling and shrinking for cell culture/manipulation and precise disease treatment [8-10], stimulus-responsive reversible wettability switching for liquid transport, oil/water separation and bioinspired adhesives [11-13], and stimulus-responsive bending/crawling/locomotion for various robotics [14, 15]. In one very interesting example, cone-shaped hollow microhelices with excellent locomotion abilities were flexibly

fabricated and utilized for accomplishing nanocargo loading/release and targeted neural stem cell delivery under external magnetic field excitation [16]. Apart from humidity, stress, light, and magnetic field, other external stimulants, such as electric field, pH, and temperature, have also been exploited to trigger modifications in the form and/or characteristics and other dynamic behaviors of stimuli-responsive structures [17-19].

Under the background of continuous deepening of fundamental research and growing need for intelligent applications, versatile artificial structures with intelligent response capabilities have aroused extensive attention. In the last few years, the most promising stimuli-responsive structures with multiple customized functions have been made from shape memory polymers (SMPs) [20, 21], liquid crystal (LC) polymeric materials [22, 23], hydrogels [24, 25], and tailored composite materials [26], among others. Furthermore, various manufacturing methods have been devised to prepare these intelligent structures with favorable characteristics of fast responses to external stimuli, such as fused deposition modeling, stereolithography, direct ink writing, digital light processing, electrospinning, and selective laser sintering [22, 27-35]. However, these fabrication techniques are subject to inherent limitations, including poor material applicability, low resolution, poor biocompatibility, complicated multiple processing steps, restrictions in surface design, and difficulty in fabricating three-dimensional (3D) structures with sophisticated morphologies. For example, the dependence on melting and cooling processes makes the use of the fused deposition modeling method suitable only for thermoplastic polymers. The direct ink writing strategy is restricted in geometric complexity and relies on fast solidifying viscoelastic inks that do not easily deform or collapse [28]. Nowadays, there is a growing interest in the development of stimuli-responsive micro/nano functional devices that exhibit highly integrated structures and customized multiple functionalities. In comparison to traditional macroscale stimuli-responsive structures, the micro/nano counterparts offer several advantages, including superior precision, sensitivity, rapid response, high integration, versatile functionality, and compact size. Additionally, they often feature complex and multi-material spatial microstructures. These micro/nano functional devices play a crucial role in cutting-edge research areas such as materials science, nanotechnology, biotechnology, as well as in various industrial and commercial applications including microelectronics, microelectromechanical systems, micro/nano optics, lab-on-a-chip devices, and biomedical diagnostics [27, 36-41]. However, conventional manufacturing technologies are no longer adequate to meet the demands of highly integrated and precise manufacturing required for reliable and high-performance micro/nanoscale devices with desired stimuli-responsiveness and quality. The fabrication of these structures presents significant challenges in terms of exceptional precision, quality assurance, integration of multiple materials, compatibility, and scalability. With the rapid development of ultrafast laser systems, femtosecond (10^{-15} s) laser direct writing (FsLDW) technique has arisen as an attractive and promising manufacturing tool for the fabrication of smart and multifunctional stimulus-responsive structures owing to its distinct benefits of high spatial precision and accuracy, simplicity, surface and volume machining capability, mask-free processing, true 3D manufacturing capability, and wide applicability to almost all materials. The ultrashort pulse duration and immensely high peak intensity of femtosecond laser bring unprecedented physical conditions for modern extreme manufacturing and scientific experimental research [42-48]. FsLDW technology can promote the flexible and efficient manufacturing of well-designed structures with on-demand stimulus-responsive behaviors, thus further facilitating current tendencies of miniaturization, functionalization, integration, and ultimate practical application of these intelligent structures in diverse fields such as microfluidics [49-51], optics [52-54], robotics [55], and biomedical engineering [10, 56, 57].

In this review, we outline the recent progress of FsLDW technology in the manufacturing of smart stimulus-responsive structures (**Figure 1**). Firstly, the basic principles of femtosecond laser interaction with different types of materials as well as the commonly used FsLDW-based fabrication strategies are introduced. Then, we present various functional stimulus-responsive structures fabricated by using FsLDW technology, such as magnetic-responsive structures, light-responsive structures, temperature-responsive structures, pH-responsive structures, and humidity-responsive structures. Subsequently, versatile applications of these intelligent structures with different stimulus-sensitive behaviors are highlighted and discussed. In the end, current limitations and challenges along with future perspectives of FsLDW-based stimulus-responsive structures are shared.

2. Principles and strategies of FsLDW

To effectively fabricate desired stimulus-responsive structures with the required resolution and functionalities based on FsLDW technology, it is necessary to figure out the basic physical mechanisms and processing strategies.

2.1. Interaction principles between the femtosecond laser and matter

Because the pulse width of femtosecond laser is exceedingly brief, it can reach incredibly high peak power and energy density ($> 10^{14}$ W cm^{-2}) at lower pulse energy after focusing. The processing mechanism of FsLDW differs from that of conventional long pulse lasers and continuous lasers. It

possesses the benefits of a small heat-affected region, high processing accuracy beyond the optical diffraction limit, true 3D processing ability and the ability to process almost any material. When a femtosecond laser interacts with various materials, there will be complicated nonlinear physical effects such as multiphoton absorption, nonequilibrium thermal relaxation, Coulomb explosion, avalanche ionization, and multiphoton ionization [58-60]. The interaction process of femtosecond laser with metallic and nonmetallic materials will be classified and described below.

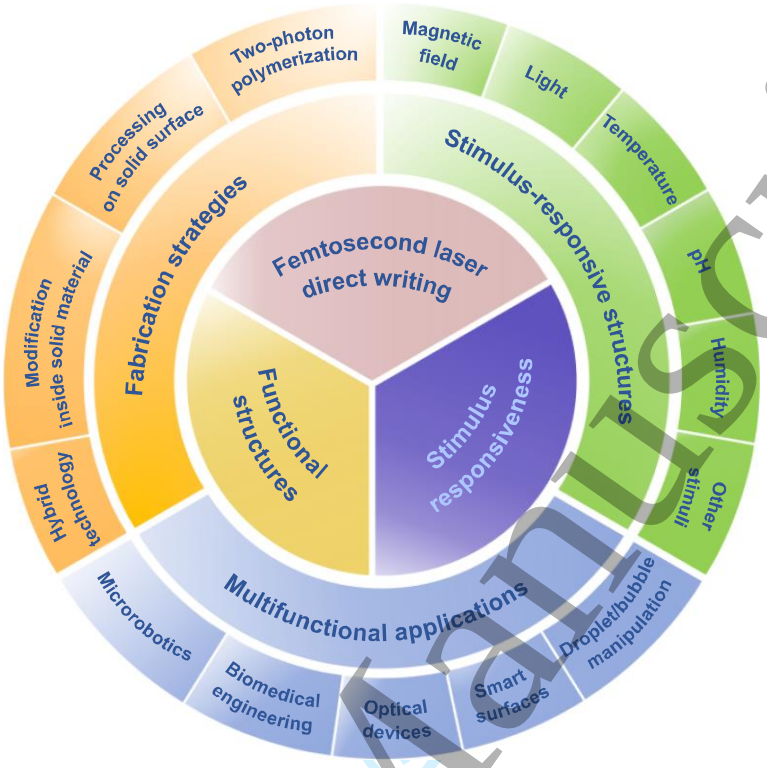

Figure 1. Schematic illustration of functional stimulus-responsive structures fabricated by femtosecond laser direct writing.

2.1.1. Interaction between the femtosecond laser and metallic materials. Metals possess plentiful free electrons, which can absorb energy from photons and be heated when interacting with a femtosecond laser. Then, the heated free electrons impact with other electrons, transmitting energy between them. The increasing electrons that are heated can amplify interplay between the electrons and the lattice, culminating in the heating of the lattice. Upon heating the lattice to a sufficiently high temperature, melting and ablation can occur in the metallic material at the time scale of picosecond (10^{-12} s) to nanosecond (10^{-9} s). A variety of mechanisms [61], including evaporation [62, 63], phase explosion [64, 65], and fragmentation[66, 67], can lead to the laser ablation. According to the time evolution, the process of interaction between metal and femtosecond laser involves excitation of light and electron heating, coupling and relaxation of electron-phonon energy, and removal of material [68, 69]. Electrons typically require several hundred femtoseconds to achieve thermal equilibrium after absorbing laser energy. However, the transfer of energy from the electronic system to the lattice generally takes around 1 to 100 picoseconds, which is significantly greater compared to the time required for electrons to reach a thermo-equilibrium state [69]. Therefore, the energy change of the electron and lattice during femtosecond laser irradiation can be regarded as a nonequilibrium process capable of greatly diminishing the area of the heat-affected region formed [42, 70]. Researchers have put forward various hypotheses and frameworks to elucidate the ways in which ultrafast lasers interact with metallic materials. For example, Liu and coworkers introduced the ablation threshold theory [71], which holds that the minimum required laser energy must be guaranteed to achieve material removal and processing [72]. During the process of femtosecond laser-metal interaction, electrons and lattice can be analyzed as two independent systems. Anisimov et al. proposed a classic two-temperature model of femtosecond laser-metal interaction based on a one-dimensional unsteady heat conduction equation in 1974, which considers the complex interactions between photons and electrons and between electrons and the lattice [73]. With the development of related research fields, the classical two-temperature model has been optimized. In 2005, Jiang et al.

introduced an enhanced two-temperature model, which solved the problem that the classical model cannot accurately depict the interaction between ultrafast lasers and metals at high laser fluences. They used full-scale quantum calculations to determine the paramount parameters, such as electron relaxation time, conductivity, and heat capacity, which expands the application range of the two-temperature model and improves the accuracy to theoretically predict the ablation threshold for the interaction between femtosecond laser and gold film [74]. Researchers have also begun to investigate the process of interaction between materials and femtosecond lasers by combining the molecular dynamics model with the two-temperature model. The molecular dynamics model can directly describe the particles movement on the nanoscale and can be utilized for elucidating the mechanism of lattice phase transition during the femtosecond laser-matter interaction [75-77].

2.1.2. Interaction between the femtosecond laser and nonmetallic materials. Nonmetallic materials have significantly fewer free electrons compared to metal materials. The electron density and conductivity of nonmetallic materials in the conduction band are usually low, and the majority of electrons are confined to the valence band. When matter is exposed to a femtosecond laser, the initial event involves the electrons absorbing photon energy. For metals, the primary absorption mechanism is linear absorption, while for nonmetallic materials such as dielectrics and semiconductors, non-linear absorption plays a more predominant role [78]. The first stage of the interaction between nonmetallic materials and femtosecond lasers can be broadly conceptualized as initiating with the generation of a sufficient number of free electrons through photoexcitation. For a semiconductor with a narrow bandgap smaller than the photon energy, a single photon absorption is sufficient to directly excite valence band electrons to the conduction band [79]. However, for the wide-bandgap semiconductors and dielectrics, the energy of the bandgap exceeds the photon energy (**Figure 2**). In this case, the generation of free electrons is mainly attributed to the combined mechanisms of multiphoton ionization, tunnel ionization, and avalanche ionization. Multiphoton ionization is the phenomenon wherein valence band electrons absorb the collective energy of multiple photons, facilitating the valence band electrons to be excited into the conduction band and become free electrons [71, 80, 81]. Tunnel ionization is a quantum mechanical process and plays a key role in femtosecond laser-matter interaction. The strong electric field generated by the ultrashort femtosecond laser pulses allows electrons to tunnel through the energy barrier around the nucleus, leading to their escape from the atom or molecule and resulting in ionization and turning into free electrons [59, 82]. Tunnel ionization and multiphoton ionization engage in a competitive relationship, and which one is dominant can be determined by Keldysh parameter [59]. Upon absorption of photon energy, low-energy free electrons undergo a transformation into high-energy counterparts within the conduction band, assuming the role of seed electrons. Seed electrons possess considerable kinetic energy and can interact with electrons in the valence band. Hence, two low-energy free electrons will be produced after the collision between a seed electron and a valence electron, which can also absorb the energy of photons, and then impact and ionize again. This process can undergo repeated iterations, giving rise to a cascade effect akin to an avalanche, known as avalanche ionization [58, 80]. Multiphoton ionization and tunnel ionization can provide the initial seed electrons for avalanche ionization (**Figure 3**). As for the most solid nonmetallic materials, the following stage after the femtosecond laser photoexcitation is phase transition. After the first stage, there is a gradual accumulation of free electrons within the material, leading to energy transfer to the lattice. The interaction between these free electrons and the lattice can potentially induce a phase transition and material removal through melting, gasification, Coulomb explosion, and electrostatic ablation [60, 83].

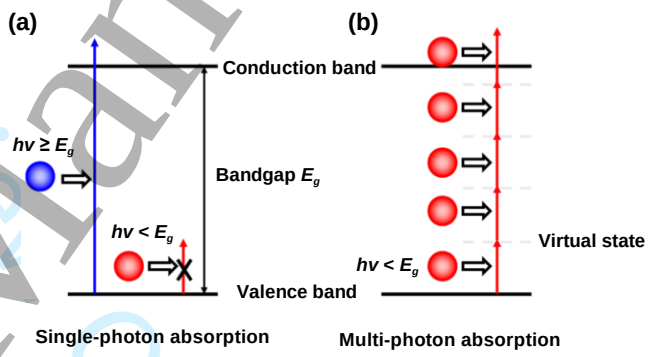

Figure 2. Schematics showing the process of electron excitation. (a) Single-photon absorption. (b) Multi-photon absorption. Reproduced from [43]. CC BY 3.0. Copyright © 2019 The Author.

The mechanism of the femtosecond laser-nonmetallic material interaction can undergo variations when utilizing photopolymer materials for micro/nanostructure fabrication. This process primarily relies on the photopolymerization, involving the bonding reaction of monomers and oligomers. The comprehensive process primarily encompasses the generation of free radicals and subsequent cross-linking of monomers/oligomers initiated by the free radicals [38, 84-86]. Photoinitiators are commonly employed to initiate the photopolymerization reactions, which exhibit sensitivity to UV/visible light and can experience a transformation that generates reactive species such as free radicals and photoacids upon light absorption [87-89]. The excitation of an electron in a valence band from the ground state to higher energy levels can occur through multiple photon absorption. When photoinitiator molecules simultaneously absorb the energy of

two or more photons, they experience electronic transitions, leading to their excitation from the ground state to the excited singlet state. Subsequently, via intersystem crossing, they transition to the triplet state, resulting in the formation of free radicals. Apart from the multiple photon absorption, the electron can acquire sufficient energy through multiphoton ionization to surpass the ionization threshold, leading to its separation from the valence shell of photoinitiator or monomer molecules, following the phenomenon of avalanche ionization and free-radicals generation [38, 85]. It is worth noting that

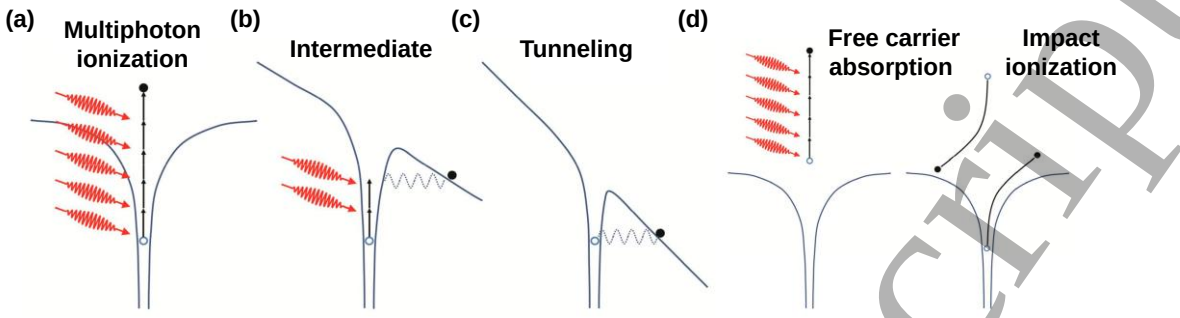

Figure 3. Schematic illustrations showing photoionization processes. (a) Multiphoton ionization. (b) Combination of multiphoton ionization and tunnel ionization. (c) Tunnel ionization. (d) Avalanche ionization. Reproduced from [81]. CC BY 4.0. Copyright © 2017 The Authors.

multiphoton ionization and multiple photon absorption can occur concurrently, representing parallel processes that compete with each other. The manner in which photoexcitation occurs is contingent upon the band gap of the photopolymer, which can be modulated through the utilization of photoinitiators. Additionally, the selection of laser parameters, encompassing pulse duration, laser central wavelength, pulse repetition rate, and photon beam density, further governs the process of photoexcitation [85, 90, 91]. Following the generation of free radicals, the polymerization reaction is initiated, leading to the formation of a cross-linked network of monomers or oligomers, ultimately yielding the creation of polymerized voxels, which serve as the primary microstructure building units [92, 93]. Interestingly, the polymerization reaction process is usually accompanied by a quenching effect, which hinders the progress of polymerization. It is crucial to employ an appropriate laser exposure dose, determined by laser power and exposure time, to ensure that the production of free radicals surpasses the quenching effect, providing an adequate supply for polymerization reactions to take place. Furthermore, it is noteworthy that photopolymer materials possess not only a polymerization threshold but also a distinct damage threshold. Excessive exposure dose during processing can result in local overheating, leading to micro-explosions and material damage. Therefore, it is essential to select laser parameters within the range of the polymerization threshold and the damage threshold [94-98]. Commonly employed photopolymers can be formulated by utilizing readily available materials such as epoxies, acrylates, and hydrogels. To impart additional stimuli-responsiveness and multifunctionalities, these photopolymer materials are often supplemented with appropriate dopants, including magnetic nanoparticles, organic dyes, and carbon nanomaterials, thereby facilitating the production of tailored composite materials [99-102].

2.2. Manufacturing strategies of FsLDW

In addition to the development of femtosecond laser-matter interaction mechanisms, many feasible manufacturing strategies at diverse scales based on FsLDW have been proposed.

2.2.1. Femtosecond laser two-photon polymerization.

Since Kawata and coauthors made a significant breakthrough by reporting the fabrication of microbull sculptures with an impressive spatial resolution of 120 nm in 2001, two-photon polymerization possessing good material penetration and spatial selectivity has become one of the most widely used technologies to fabricate 3D micro/nanoscale devices in polymers (**Figure 4(a) and (b)**) [103]. Generally, the typical

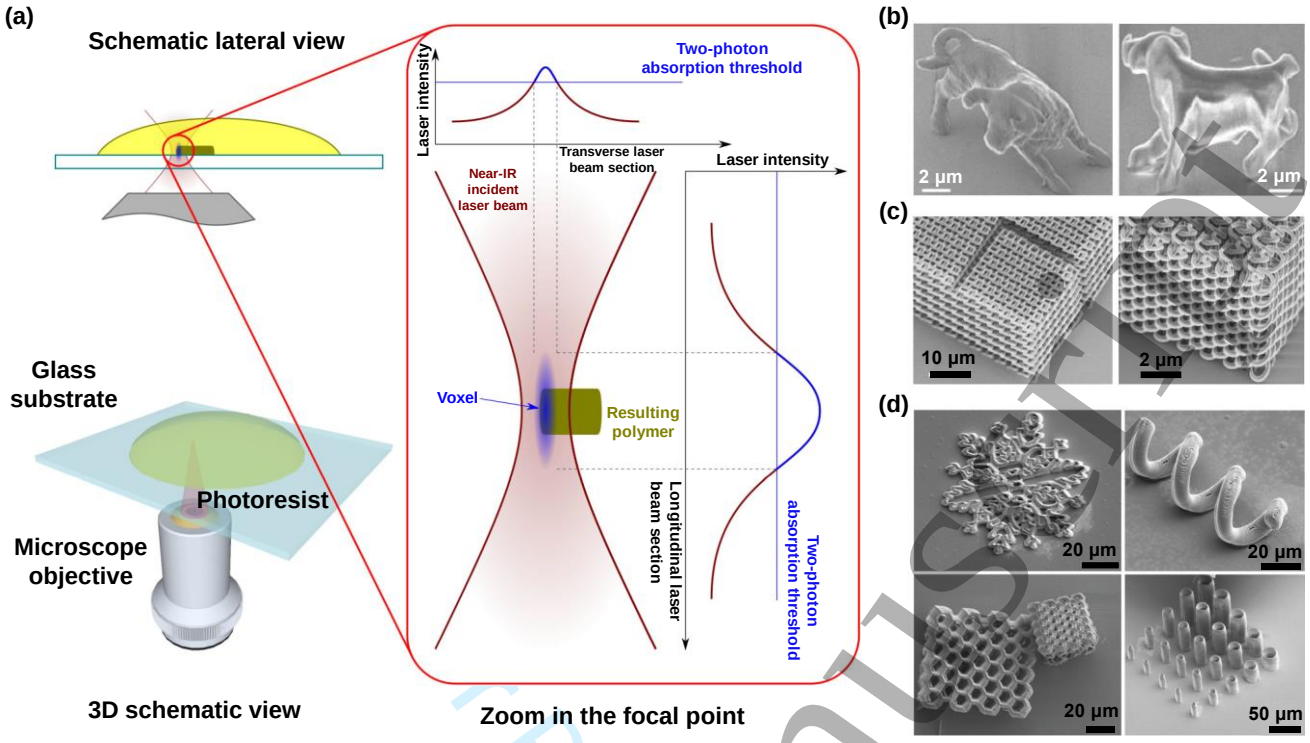

Figure 4. Femtosecond laser two-photon polymerization and the fabricated typical structures. (a) Schematics and working principle. Reproduced from [104]. CC BY 4.0. Copyright © 2022 The Authors. (b) Microbull sculptures. Reprinted by permission from Springer Nature Customer Service Centre GmbH: Springer Nature, Nature [103], Copyright (2001). (c) Spiral architectures. [105] John Wiley & Sons. © 2005 WILEY-VCH Verlag GmbH & Co. KGaA, Weinheim. (d) Various conductive and bioactive microstructures. [106] John Wiley & Sons. © 2022 Wiley-VCH GmbH.

two-photon polymerization process involves the requirement for the target transparent photosensitive materials to synchronously absorb two or more photons to obtain enough photon energy, which is regulated by a transient virtual transition state characterized by an exceedingly brief duration within the femtosecond range. Following the occurrence of two-photon absorption, which is a third-order nonlinear optical process arising from the interaction between the material and the femtosecond laser's light, the molecules of the target material can present high energy states. Two-photon polymerization only occurs near the focus of the laser with high laser intensity, which can localize a large number of photons in a tiny focusing area. Furthermore, lasers with longer wavelengths and lower energy are generally selected for two-photon polymerization processing. In this case, single-photon polymerization cannot occur at the unfocused position of the femtosecond laser. Thus, the photopolymerization reactions of monomers and photoinitiator molecules can only be induced at the laser focus without impact on other positions. Through precise control of either the laser focus or the sample's relative movement, the target materials can gradually polymerize along the focus scanning path, which can realize the fabrication of intricate micro/nanoscale structures with arbitrary morphology and resolution less than the applied diffraction limit in a maskless and facile process [86, 104, 107-111]. Micro/nanostructure fabrication through the principle of two-photon or multiphoton polymerization using a femtosecond laser represents an advanced processing technology for photosensitive polymers, which synergistically integrates the versatility of 3D printing with exceptional resolution of photolithography technology and holds great potential for the precision manufacturing of micro/nano-architectures with customized and complicated constructs [103, 112, 113]. The desired micro/nano-structures are typically fabricated using photoresists whose ingredients include photoinitiators for generating free radicals after excitation, monomers or oligomers acting as the fundamental structural framework, and cross-linkers responsible for guaranteeing insolubility in developing solvents. For instance, Seet and colleagues demonstrated the preparation of photonic crystals with square and circular 3D spiral architectures using SU-8 photoresist and femtosecond laser two-photon polymerization strategy (**Figure 4(c)**), showing characteristics of photonic stop-gaps at infrared wavelengths [105]. Tian and collaborators fabricated the microlens array with different curvature unit lenses using the commercial negative photoresist SU-8 , which possessed unique imaging and focus capabilities and can be applied to improve the optical system performance of field curvature correction and real-time 3D imaging [114]. In addition to photopolymers, microstructured

metals, metal oxides, carbon materials, proteins, and composite materials have been easily prepared through two-photon or multiphoton polymerization processes [106, 115-117]. For instance, Dadras et al. manufactured various 3D organic semiconductor composite microstructures and microelectronic devices by using newly developed photosensitive resin doped with organic semiconductor materials (**Figure 4(d)**) [106]. Moreover, many smart and responsive materials have been developed for the fabrication of stimulus-responsive structures based on femtosecond laser two-photon polymerization. Functional groups in monomers, nanoparticle dopants, or appropriate surface modifications can make the prepared structures respond to various external stimuli [118-121].

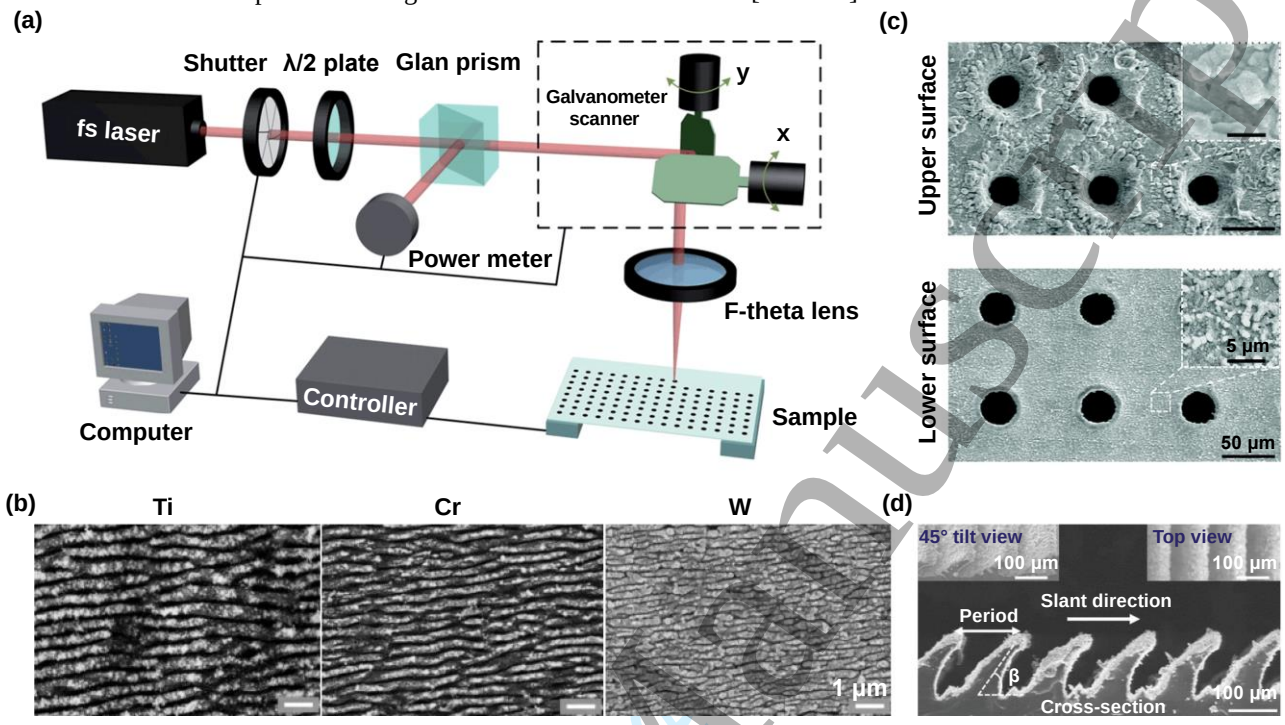

Figure 5. Femtosecond laser processing on the surface of solid material. (a) Schematic diagram. Reproduced from [122] with permission from the Royal Society of Chemistry. (b) LIPSS structures produced on different substrates. Reprinted from [123], Copyright (2013), with permission from Elsevier. (c) Microhole arrays. Reproduced with permission from [124]. Copyright 2017, Royal Society of Chemistry. (d) Slant microwall arrays. [125] John Wiley & Sons. © 2020 Wiley-VCH GmbH.

2.2.2. Femtosecond laser processing on the surface of solid material. When the used laser energy density is slightly higher than the solid material energy threshold, the laser-induced periodic structures (LIPSS) can be generated on the material surface (**Figure 5**). Since the pioneering work of Birnbaum et al. in 1965, the formation of LIPSS has been observed on various materials, such as semiconductors, metals, and dielectric materials, when exposed to laser irradiation [126-130]. It is believed that the generation mechanisms of the LIPSS of different materials using ultrashort pulse lasers are different, which mainly include scattered light interference theory, surface plasmon polariton theory, self-organization theory, and evanescent wave theory [131-134]. Diverse laser parameters, including laser power, pulse number, pulse width, repetition frequency, laser polarization direction, incident laser wavelength, incident angle, and focusing position, can affect the generation of periodic structures on the surface of solid materials [135-137]. Moreover, the morphologies of LIPSS can also be influenced by the material properties and environments. Albu et al. used femtosecond lasers with different wavelengths to process titanium/chromium/tungsten (Ti/Cr/W) in air and liquid environments (**Figure 5(b)**), and found that structures periods formed in liquids were much smaller than those formed in air [123]. The generation of micro/nano periodic surface structures through femtosecond laser irradiation has a profound impact on the surface properties of materials. These structures can significantly alter characteristics such as friction, wettability, and optical behavior, which hold immense promise for a wide range of applications across various fields such as national defense, biochemistry, and high-end manufacturing [138-140]. For example, Jiang et al. used a copper foil template with LIPSS and a template-directed chemical vapor deposition method to fabricate hierarchically structured few-layer graphene films with superhydrophobicity and beautiful structural color [141]. When the laser energy surpasses the damage threshold of the solid material, direct ablation of the material surface occurs. In this circumstance, the target material can be converted into

vapor and plasma near the focal point and be removed. Moreover, some nanoparticles and micro/nano debris can be generated, which can increase the surface roughness. Various microscale structures, such as microholes, micropillars, and microgrooves, can be manufactured by using this technology [51, 122, 125, 142-144]. For example, Zhang and coworkers designed a Janus oil barrel with controllable microhole arrays fabricated by femtosecond laser drilling (**Figure 5(c)**), which exhibited the capability for spontaneous absorption and storage of spilled oil with high flux [124]. Sohn et al. fabricated periodic micrograting and micropillars on the surface of fused silica glass through irradiating with a femtosecond laser beam, and then obtained different microlens arrays by several laser polishing cycles [145]. Wu et al. prepared the slant microwall arrays using one-step femtosecond laser oblique ablation (**Figure 5(d)**), which can be used for high-performance droplet manipulation [125].

2.2.3. Femtosecond laser modification processing inside solid material. One significant benefit of employing ultrashort pulses is the ability to regulate the thermal impact of light-matter interactions. Furthermore, the interaction between the femtosecond laser and materials can exhibit nonlinearity, which indicates that materials transparent to the incident wavelength, such as glass and related transparent dielectrics, can be processed for creating intricate and arbitrary free-form 3D micro/nanoscale structures [146]. Usually, the femtosecond laser beam is precisely focused into the bulk of solid material samples using a microscopic objective to realize on-demand localized modifications and precise fabrications (**Figure 6(a)**). The processing results are greatly affected by the energy density at the laser focus and

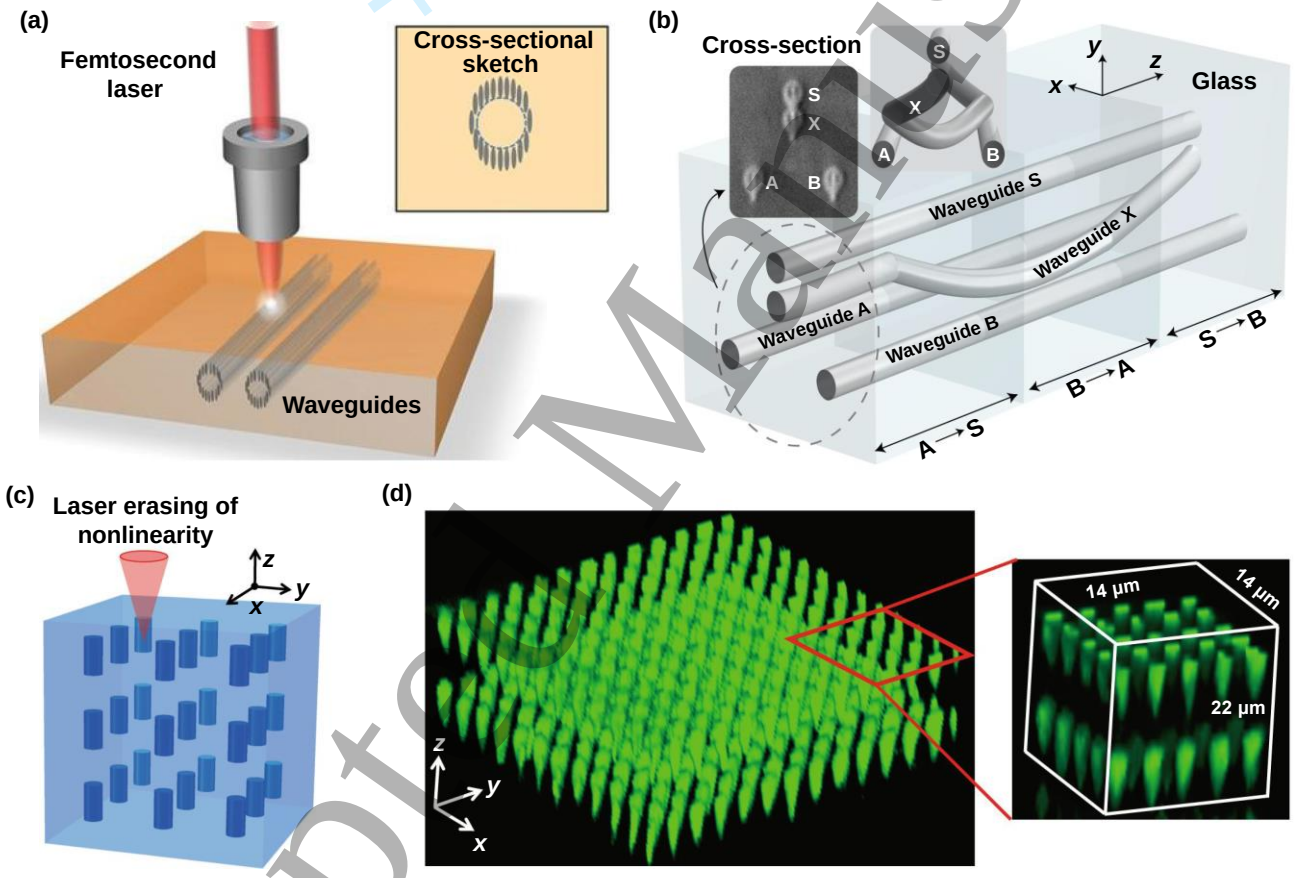

Figure 6. Femtosecond laser modification processing inside solid material. (a) Fabrication schematic. [147] John & Sons. © 2013 WILEY-VCH Verlag GmbH & Co. KGaA, Weinheim. (b) Schematic of the braiding structure and cross section photos of produced waveguides. Reprinted by permission from Springer Nature Customer Service Centre GmbH: Springer Nature, Nature Photonics [148], Copyright (2022). (c) Schematic of the fabrication of the 3D nonlinear photonic crystal. (d) Image of the nonlinear photonic crystal structure showing the first two layers. Reproduced with permission from Springer Nature Customer Service Centre GmbH: Springer Nature, Nature Photonics [149], Copyright (2018).

the damage threshold of the material. Under conditions where the laser energy density at the focal point remains below the material's damage threshold, a color center can be generated [150]. When the pulse energy at the laser focus approaches or

slightly exceeds the material damage threshold, modifications of the refractive index can be induced in the material, which can be categorized into refractive index increase modification and refractive index decrease modification depending on used laser irradiation parameters and material characteristics. The femtosecond laser-induced internal refractive index change can be used to construct 3D optical microcomponents including optical waveguides and optical couplers [147, 151-156]. In cases where the energy at the laser focus significantly exceeds the material's damage threshold, microcavities or microcracks can be generated at the focus, which is generally accompanied by relatively violent phase and structural changes [42, 157, 158]. Since the energy density at the focus point of the tightly focused ultrashort pulse laser is extremely high and the nonlinear interaction with the material only occurs on a very small scale, the processing resolution is great, which is suitable for manufacturing 3D complex micro/nanostructures in transparent solid materials including glass and crystals [42, 159, 160]. For example, Wolf and colleagues introduced a novel fabrication approach for the point-by-point femtosecond inscription of fiber Bragg grating arrays with diverse configurations within seven-core spun optical fibers [161]. Zhang and colleagues manufactured a photonic chip composed of three straight waveguides and a curved waveguide in boroaluminosilicate glass through FsLDW (**Figure 6(b)**), which could be used for two-mode photonic braiding [148]. Wei et al. fabricated a 3D nonlinear photonic crystal in lithium niobate using a selective femtosecond laser erasing technique (**Figure 6(c) and (d)**), which shows great potential in nonlinear imaging, nonlinear beam shaping, and 3D nonlinear holography [149].

2.2.4. Hybrid FsLDW fabrication technology. Apart from the FsLDW technologies mentioned above, hybrid processing techniques integrating FsLDW with other manufacturing strategies have also attracted wide attention, such as etching-assisted femtosecond laser micromachining, femtosecond laser-induced plasma-assisted ablation (LIPAA), and FsLDW-based soft transfer [43, 44, 162, 163]. By combining FsLDW technology and wet/dry etching technology, well-designed structures with high accuracy and great surface roughness can be obtained. The femtosecond-laser-induced phase and structural modifications can enhance the etch rate inside the transparent hard materials, which can facilitate the matter removal from the modified region during subsequent etching processes [164-166]. The etching-assisted femtosecond laser processing strategy integrates the advantages of subwavelength resolution beyond the diffraction limit based on FsLDW and surface quality improvement based on polishing effect of the etching process, which can realize preparation of high-quality complex micro/nano-structures with superior resolution on the surface or inside transparent hard materials through a relatively facile and cost-effective process. For instance, Liu and coworkers manufactured artificial compound eyes using curved sapphire substrates based on a dry-etching-assisted FsLDW strategy, with a root-mean-square value of the surface roughness of only 1.1 nm (**Figure 7(a) and (b)**), which presented brilliant wide field-of-view imaging and focusing characteristics [167]. Ródenas et al. found that the chemical etching rate of nanopores in yttrium aluminum garnet and sapphire crystals could experience a remarkable amplification of over five orders of magnitude through combining direct laser writing with wet etching. And they fabricated sub-wavelength diffraction gratings and nanostructured optical waveguides in yttrium aluminum garnet, as well as millimeter-long nanopores in sapphire (**Figure 7(c)-(e)**), proving the value of this hybrid technology in the realms of crystalline nonlinear optics and 3D nanophotonics [168]. The femtosecond LIPAA utilizes the strong high-energy plasma produced by the interaction between a femtosecond laser and the target material to strengthen the laser ablation at the rear surface of the transparent substrate material, thereby enabling the fabrication of microstructures characterized by superior quality and reduced surface roughness [44]. For instance, Liu et al. manufactured microstructures with high aspect ratio on the sapphire substrates through using femtosecond LIPAA and subsequent optimized laser ablation (**Figure 7(f) and (g)**), which could avoid laser heating and internal crack formation [169]. In addition, FsLDW-based soft transfer hybrid technology has also aroused great interest from researchers due to its flexibility and high efficiency for fabricating soft functional structures [51, 170]. Li and coworkers facilely prepared slanted shape memory microcones through oblique FsLDW and a subsequent replica-molding method (**Figure 7(h) and (i)**), which enabled the reversible morphology switching-based regulation of wettability and droplet adhesion [171].

3. Stimulus-responsive structures through FsLDW

By integrating different processing strategies based on FsLDW technology with intelligent materials such as SMPs, LC polymeric materials, and smart hydrogels, various stimulus-responsive structures capable of responding to different external stimuli can be fabricated flexibly and efficiently. This section summarizes the recent research progress of different stimulus-responsive structures prepared by FsLDW according to their types of environmental stimuli.

3.1. Magneto-responsive structures

Magnetic fields have attracted great attention and become the preferred stimulation strategy to actuate stimulus-responsive structures because of their attractive advantages of being remotely controllable, safe, instantly responsive, and biocompatible [17, 50, 121, 172]. At present, to render the fabricated structures based on FsLDW technology with the

required magnetic responsiveness, magnetic elements such as Fe_3O_4 nanoparticles, NdFeB particles, and iron powder can be incorporated with the raw materials to obtain magnetic composites for fabrication, or magnetic materials can be coated on the surface of prefabricated unresponsive structures [173-177]. When subjected to external magnetic fields and spatial gradients, these structures can undergo complex predesigned behaviors including deformation and locomotion under actuating magnetic torques and forces, showing expansive application prospects in microfluidics [50, 51], robotics [178], cell/drug delivery [179, 180], etc.

For example, Yasa et al. developed a magnetically steerable cell microtransporter for active and precisely localized stem

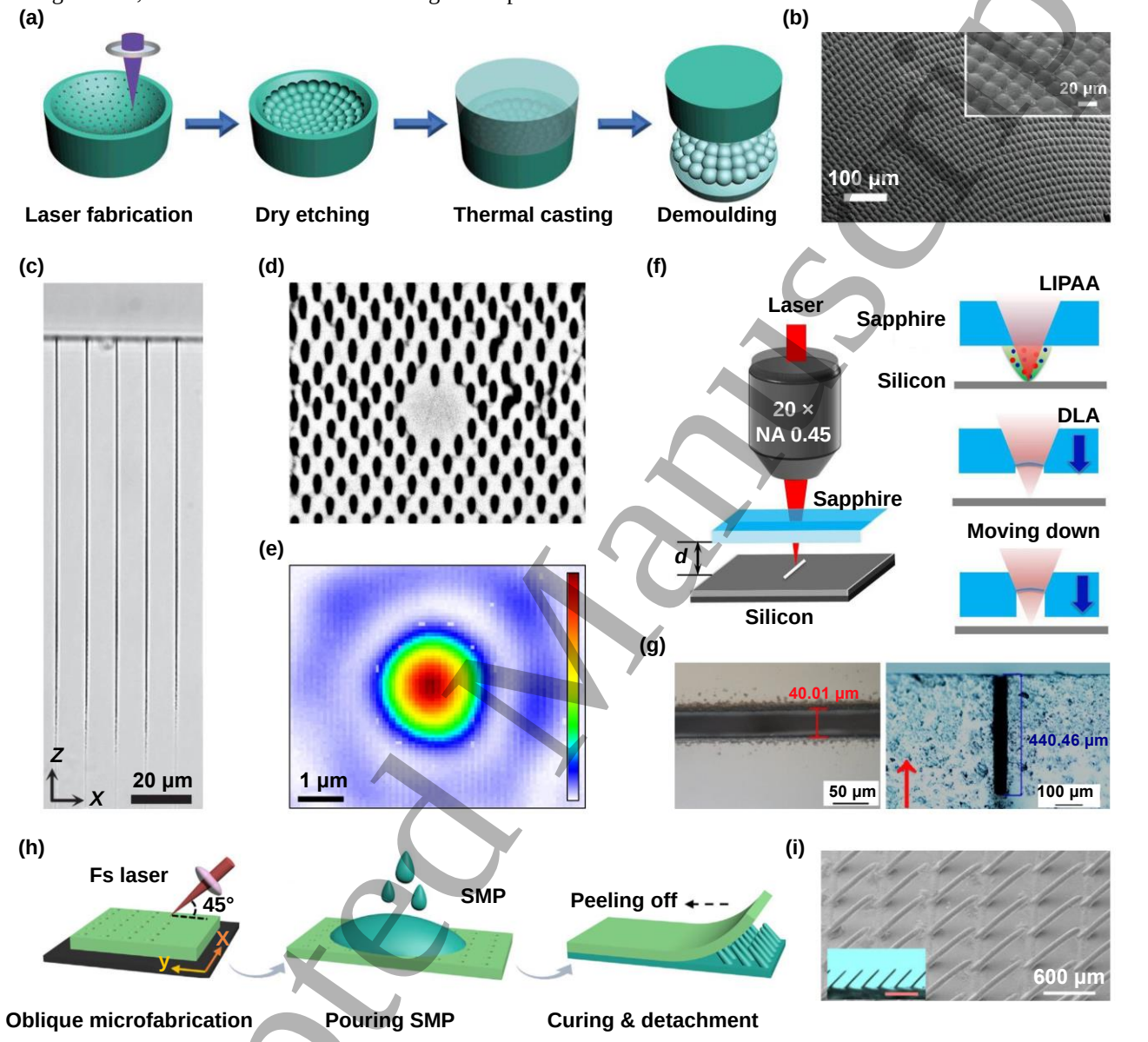

Figure 7. Hybrid FsLDW fabrication technology. (a) Schematic of dry-etching-assisted FsLDW fabrication of a compound eye. (b) SEM images showing the compound eye. [167] John Wiley & Sons. © 2019 WILEY-VCH Verlag GmbH & Co. KGaA, Weinheim. (c) Top-view optical microscope image of nanopores fabricated by combining direct laser writing with wet etching. (d) Nanostructured waveguide with hexagonal structure. (e) Diffraction-limited near-field image of the waveguide output mode. Reproduced with permission from Springer Nature Customer Service Centre GmbH: Springer Nature, Nature Photonics [168], Copyright (2018). (f) Schematics showing the experimental setup for fabrication of high-aspect-ratio microstructure based on femtosecond LIPAA. (g) Fabricated high-aspect-ratio microgroove on sapphire. Reprinted from [169], Copyright (2020), with permission from Elsevier. (h) Schematics showing the fabrication procedure of slanted shape memory microcones. (i) SEM image of the microcones. Reprinted from [171], with the permission of AIP Publishing.

cell delivery by using a trimethylolpropane ethoxylate triacrylate (TMPETA)-based hydrogel containing superparamagnetic iron oxide nanoparticles through FsLDW technology (**Figure 8(a) and (b)**) [179]. Similarly, a magnetically powered biodegradable microswimmer based on the magnetic hydrogel composite, which was synthesized by using poly(ethyleneglycol) diacrylate (PEG-DA), pentaerythritol triacrylate (PE-TA), and superparamagnetic Fe_3O_4 nanoparticles, was manufactured utilizing the femtosecond laser two-photon polymerization strategy. The prepared magnetically responsive microswimmer with multi-segment architecture and good degradability could realize undulatory locomotion and move forward under the driving of an external oscillating magnetic field, which presented great prospect in real-time and *in vivo* medical applications [181]. In addition to directly preparing magneto-responsive structures using magnetic composites, magnetically responsive structures can also be fabricated by modifying the surfaces of prefabricated nonresponsive structures with magnetic materials [120, 121, 182]. For example, Xu et al. first fabricated microcarriers using the negative-tone photoresist and two-photon polymerization-based FsLDW strategy and then coated the nonmagnetic structures with 50 nm Fe by electron beam evaporation to prepare magnetic micromotors (**Figure 8(c) and (d)**) [183]. Besides the fabrication of a single simple structure, complicated magnetic structures can also be manufactured by integrating multimaterial components through assembly strategies [184]. In a very fascinating example, Hu et al. fabricated Janus microparticle-based magnetic micromachines with diverse programmed shape transformations and functions using two-photon polymerization-based FsLDW technology and a hierarchical assembly strategy (**Figure 8(e) and (f)**). The inherent magnetic shape anisotropy of Janus microparticles brought excellent magnetic programmability to these deformable magneto-responsive soft structures [185].

By combining FsLDW technology with other advanced manufacturing technologies, a variety of flexible magnetic-responsive structures can be fabricated. For example, a multifunctional lubricated slippery magnetic-responsive microplate array was developed through a hybrid process of FsLDW and soft-transfer-based fabrication technology. A polytetrafluoroethylene (PTFE) mold with high-aspect-ratio microgroove array was first obtained through femtosecond laser ablation. Then, the composite material consisting of carbonyl iron powder and liquid polydimethylsiloxane (PDMS) and the PTFE mold were utilized to prepare the magnetic-responsive microplate array. Furthermore, the surfaces of the microplates were ablated again using a femtosecond laser to form microstructured surfaces, which could ensure the better storage of lubricating oil for the multifunctional lubricated slippery magnetic-responsive microplate array to realize high-performance multi-substance transport (**Figure 8(g) and (h)**) [163]. Likewise, Li et al. developed shape memory magnetic microcones using iron-particle-doped epoxy resin through a FsLDW-based microdrilling and replica-molding strategy, which can be applied for versatile droplet manipulation and information encryption [142].

3.2. Light-responsive structures

Intelligent light-responsive structures hold significant appeal due to their ability to be remotely and precisely controlled and multidimensionally (e.g. wavelength, intensity, and irradiation time) modulated rapidly in a noninvasive manner [186], which are generally actuated based on photochemical mechanisms (e.g., photoisomerization) or photothermal effects [187-195]. These smart structures possess the capability to undergo reversible changes in their physical and chemical characteristics, including alterations in morphology and surface wettability, under light of an appropriate wavelength [188-190, 194, 196]. For example, Pennacchio et al. designed a photoactuable cell confining system using an advanced azobenzene-containing gelatin-based hydrogel with great biocompatibility and biodegradability by means of two-photon-polymerization-based FsLDW technology. The molecules of used azobenzene-based cross-linkers could realize isomerization between more stable *trans* isomers and less stable *cis* isomers under sufficient light irradiation, which endowed the fabricated microstructures with on-demand deformation for confinement and mechanical stimulation of living cells (**Figure 9(a) and (b)**) [57]. Similarly, light-responsive microactuators were fabricated using liquid crystalline networks based on the azobenzene-doped mesogen mixtures. Trans-cis photoisomerization in azobenzene induced the shape morphing and nonreciprocal movement of the light-activated actuators manufactured by femtosecond laser two-photon polymerization [197]. Zeng et al. proposed microscale light-fueled walkers based on azobenzene-containing liquid crystalline elastomers, which possessed dynamic behaviors, demonstrating capabilities such as directional or random walking, rotating, and jumping (**Figure 9(c)-(e)**) [196]. Furthermore, Ulrich and colleagues fabricated visible light-responsive photochromic 3D microobjects by using the formulated modular thiol-ene resin and femtosecond laser two-photon polymerization strategy, which could dynamically realize photoisomerization-based reversible color tuning [198].

In addition to photoisomerizable functional groups, photothermal-conversion-based elements, such as gold nanorods (AuNRs), reduced graphene oxide (RGO), carbon nanotubes, and Fe_3O_4 nanoparticles, can also be utilized in light-responsive structures [193, 199-201]. For example, Bai et al. designed a sunlight-driven recoverable superhydrophobic surface using FsLDW technology and a photo-responsive SMP composite, which was developed

through mixing a thermal-responsive SMP matrix and RGO. Since RGO presented excellent photothermal conversion properties, it could heat the prepared RGO-SMP composite above the glass transition temperature under enough light irradiation. The micropillar structures on the RGO-SMP composite surface were constructed by orthogonally crossed line-by-line femtosecond laser ablation, which were covered by rich micro/nanostructures and endowed the surface with

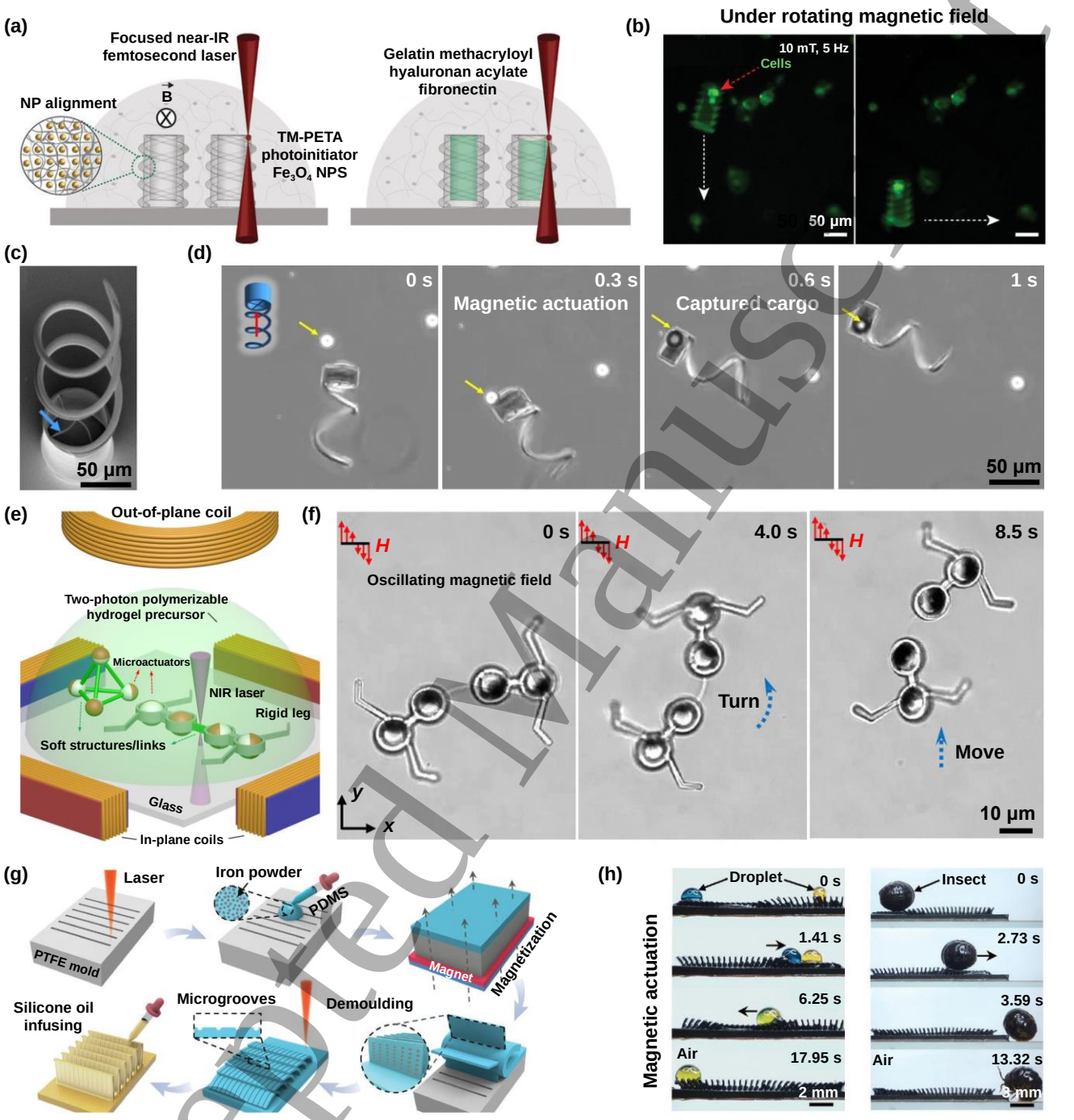

Figure 8. Magneto-responsive structures. (a) Two steps for fabricating a steerable cell microtransporter. (b) Actuation of the microtransporter with encapsulated cells. [179] John Wiley & Sons. © 2019 WILEY-VCH Verlag GmbH & Co. KGaA, Weinheim. (c) SEM image showing the prepared magnetic micromotors. (d) Magnetic actuation of the micromotor for cargo capture. Reproduced from [183]. CC BY-NC 4.0. © 2020 The Authors. (e) Fabrication process schematics of the Janus microparticle-based magnetic micromachines. (f) Locomotion of the lizard-like micromachine. Reproduced from [185]. CC BY 4.0. Copyright © 2021 The Authors. (g) Schematics showing the preparation process for the magnetically responsive microplate array. (h) Active directional transport of droplets and living insects. [163] John Wiley & Sons. © 2022 Wiley-VCH

GmbH.

ultralow-adhesive superhydrophobicity through the modification with fluoroalkylsilane. The superhydrophobicity of the surface would be lost when the micropillar structures underwent deformation through pressing or stretching. Interestingly, after sufficient sunlight irradiation, original morphology and superhydrophobicity of the surface could be completely restored (**Figure 9(f) and (g)**) [200]. In another interesting example, flexible light-responsive intelligent microstructures possessing superior shape-morphing properties were fabricated by using a carbon-nanotube-doped hydrogel composite and two-photon-polymerization-based FsLDW technology (**Figure 9(h)**). The used single-walled carbon nanotubes greatly augmented thermal conductivity, light absorption, and mechanical modulus of the temperature-responsive N-isopropylacrylamide (NIPAM)-based hydrogel composite, thus greatly improving response speed and light sensitivity of these smart micromachines. Impressively, a 3D beating microscale artificial heart (dimension of merely $80 \times 120 \times 60\ \mu m^3$) with excellent spatiotemporal light-induced controllability was manufactured by assembling different cell structures (**Figure 9(i)**), showing great potential in tissue engineering [201].

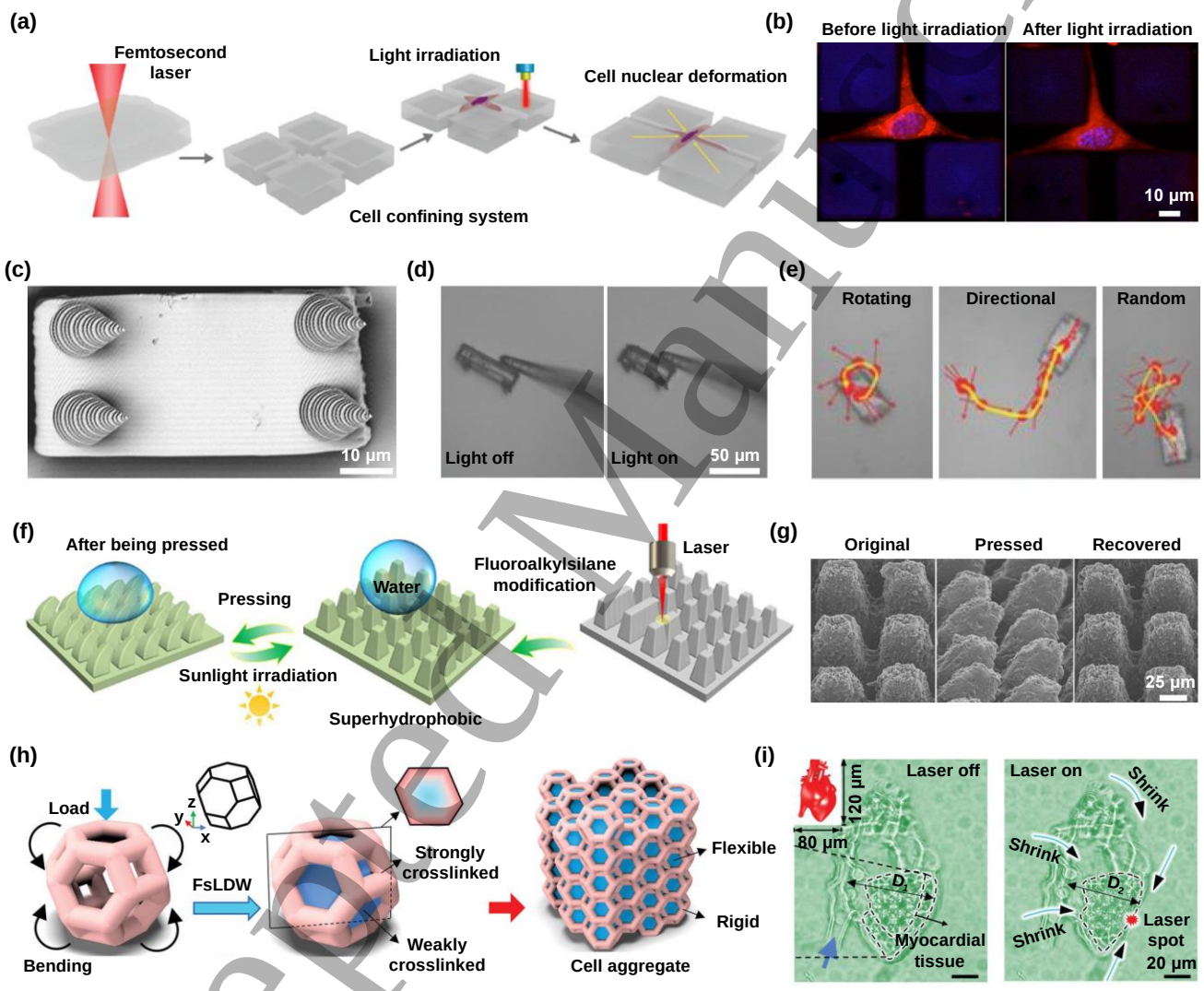

Figure 9. Light-responsive structures. (a) Schematics of the fabrication and working process of the designed cell confining system. (b) Images showing the living cells before and after light irradiation. Reprinted with permission from [57]. Copyright (2017) American Chemical Society. (c) SEM image showing the light-fueled microscopic walker. (d) Actuation of the microwalker. (e) Different dynamic locomotion behaviors of the microwalker. Reproduced from [196]. CC BY-NC 4.0. © 2015 The Authors. (f) Schematics of the preparation for the recoverable sunlight-driven superhydrophobic surface. (g) SEM images of micropillar structures in different states. Reprinted with permission from [200]. Copyright (2022) American Chemical Society. (h) Preparation of the cubic structure assembled by hollow buckyball cells. (i) Micrographs demonstrating the

fabricated microscale heart before and after light stimulation. [201] John Wiley & Sons. © 2023 Wiley-VCH GmbH.

3.3. Temperature-responsive structures

The temperature stimulus response of intelligent structures has been widely used to achieve user-defined functionalities because of the advantages of wide material applicability and simple control [202, 203]. The response processes of most temperature-sensitive materials, including hydrogels, shape-memory materials, and LC polymers, are caused by changes of molecular structure, anisotropic properties, or different swelling behaviors. For thermo-responsive hydrogels, their response principles mainly rely on the change in wettability and solubility with temperature [204, 205]. For example,

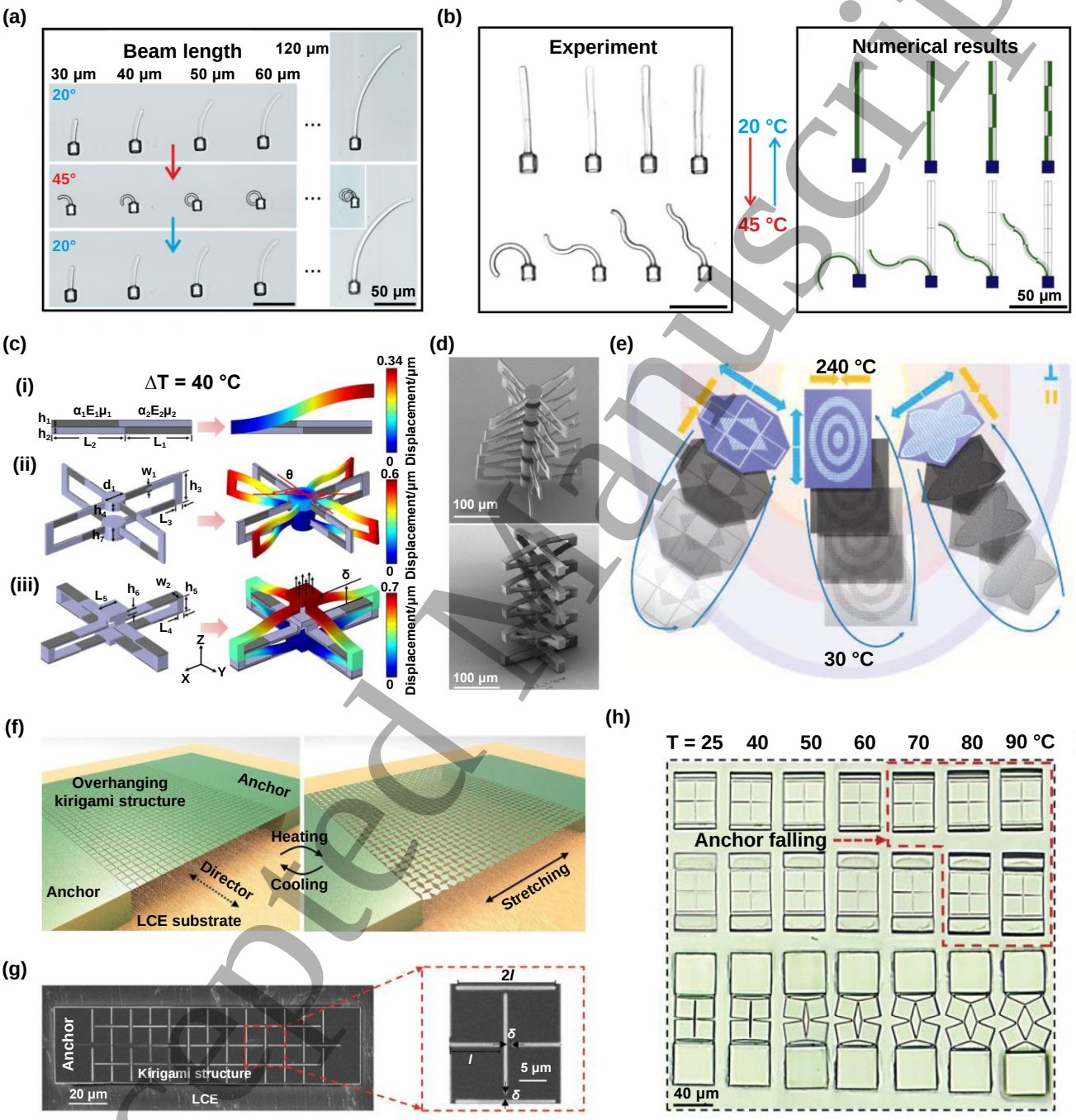

Figure 10. Temperature-responsive structures. (a) Temperature dependence of fabricated microstructures under varying beam lengths. (b) Temperature-responsive hetero-structures with increasing complexity. Reproduced from [18]. CC BY 4.0. Copyright © 2019 The Authors. (c) Illustration of the working principle of thermoelastic-bilayer-plate-based rotational and translational stages. (d) SEM images of the fabricated functional stacks. Reproduced from [206]. CC BY 4.0. Copyright © 2021

The Authors. (e) Thermal actuation of the hybrid temperature-responsive actuators. [207] John Wiley & Sons. © 2019 WILEY-VCH Verlag GmbH & Co. KGaA, Weinheim. (f) Schematics showing the temperature-actuated overhanging kirigami microstructures. (g) Top-view SEM images showing the fabricated kirigami structure. (h) Optical images demonstrating temperature-sensitive transformation of kirigami units. Reproduced from [208]. CC BY 4.0. Copyright © 2021 The Authors.

Hippler and colleagues manufactured functional hetero-microstructures by utilizing poly(N-isopropylacrylamide) (PNIPAM)-based hydrogels and two-photon polymerization strategy. When external temperature exceeded lower hydrogel critical solution temperature (LCST), the hydrogel shrank and stiffened due to the wettability transition from hydrophilicity to hydrophobicity. After being cooled down, the hydrogel reversibly returned to its original state (**Figure 10(a)**). On the other hand, the thermal response of the polymerized hydrogel depended largely on the crosslinking density. Hydrogel with lower crosslinking density exhibited significantly greater shrinkage compared to that with higher crosslinking density, which could be utilized to realize structural deformation. Thus, they flexibly varied the employed exposure dose in fabrication procedure to realize precise and localized control on the crosslinking density and temperature response, enabling complex and controllable actuation of the 3D hetero-microstructures (**Figure 10(b)**) [18]. In a similar fashion, thermomechanical-metamaterial-based 3D soft microrobotics were developed by Ji and coworkers, which consisted of thermoelastic-bilayer-plate-based rotational and translational elements. These two-component elements were prepared through two-photon polymerization with localized control of variable laser exposure using a negative tone photoresist, which enabled expansion and bending upon heating because of the different thermal expansion characteristics (**Figure 10(c) and (d)**) [206].

Temperature-responsive LC elastomers (LCEs) have attracted burgeoning interest because of their large strain and programmable 3D shape morphing capabilities, which are attributed to their anisotropic physical properties caused by their long-range orientational order. Temperature can trigger the order-disorder transition of mesogens to change their molecular alignment [22, 208]. The fascinating anisotropic characteristics of LCEs can be utilized to fabricate temperature-responsive structures. For example, microstructured and hybridized temperature-responsive actuators based on epoxide-based LCEs were manufactured by McCracken and colleagues through femtosecond laser two-photon polymerization (**Figure 10(e)**), which had great locally and spatially controlled actuation performance [207]. Likewise, Guo et al. designed LCE pixels with programmable colors in the visible range from precisely controlled thicknesses of LCE through two-photon polymerization technology [209]. The refractive indexes of LCEs with different molecular alignments were different, which could lead to polarization colors [209-211]. Based on the fact that temperature causes a reduction in order, a decrease in birefringence, and color shifting of the LCE, they fabricated and demonstrated the temperature-responsive 2D (two-dimensional) and 3D LCE-based microstructures with great reversible color-changing capabilities [209]. In another interesting example, Zhang and coworkers designed and demonstrated microscale temperature-responsive reconfigurable kirigami metastructures. They used stimuli-responsive LCEs to fabricate the backing substrate, which could act as an artificial muscle to programmably recon**Figure** the overhanging kirigami microstructures prepared by femtosecond laser two-photon polymerization under proper external thermal stimulation. The stretching and contracting of the kirigami microstructure could be remotely controlled by thermal deformation of the backing LCE substrate (**Figure 10(f)-(h)**). Moreover, they realized temperature-responsive switching and information encryption through the proposed LCE-driven kirigami metastructures [208].

3.4. pH-responsive structures

In addition to the stimulus-responsive structures mentioned above, pH-responsive intelligent structures have also attracted wide attention. Materials capable of responding to pH stimulation include organic polymers [212], hydrogels [213], proteins [116, 214, 215], and SMPs [216], among others. The main reason for the pH-sensitive behaviors of these materials is the ionization/deionization transition of pH-responsive functional groups such as carboxyl and pyridine in certain pH range [17, 24, 217]. By combining FsLDW technology with pH-responsive materials, a lot of interesting smart structures can be manufactured [19, 218-220]. For example, Wang and coworkers developed an intelligent microactuator based on a flytrap-inspired bionic asymmetric structure, which was fabricated by using FsLDW technology and a 2-(dimethylamino)ethyl methacrylate (DMAEMA)-based hydrogel. The protonatable aliphatic tertiary amine groups in the DMAEMA-based hydrogel would be positively charged because of protonation of the hydrogen ions in acidic solution, enabling electrostatic repulsion between molecular chains and thus inducing the swelling of the hydrogel. While the alkaline solution would cause the deprotonation of tertiary ammonium cations and the subsequent shrinkage of the hydrogel (**Figure 11(a)**). These fabricated microstructures could achieve highly controllable capturing and releasing behaviors of target microparticles under proper pH stimulation (**Figure 11(b)**) [221]. Similarly, Hu et al. proposed biomimetic 3D microstructures with versatile shape transformation capabilities, such as expansion/contraction, torsion, and intricate wrinkling and curling distortion, by using FsLDW and a pH-responsive hydrogel. Moreover, they manufactured

functional microcages to realize selective microparticle trapping and release [222].

Bovine serum albumin (BSA) natural proteins have emerged as versatile materials for the fabrication of microstructures with programmable and anisotropic shape-morphing capabilities because of their low cost, stimulation responsiveness, as well as comparable properties to human serum albumin. Wei et al. proposed BSA-protein-based microscale structures possessing adjustable surface morphology and pH-responsive characteristics through FsLDW. The proteins possessed many carboxylic acid groups and amino groups, and the ionization of these charged groups could induce strong electrostatic repulsion and swelling of the microstructures by controlling pH values. The precursor solutions with different concentrations of BSA-based native proteins were used to get varying cross-linking densities within the manufactured structures, enabling various shape morphing and swelling behaviors under external pH stimulation. Intriguingly, they fabricated a panda-face microrelief with unique "facial expression" variations and 3D microsieves with adjustable pore sizes (**Figure 11(c) and (d)**) [116]. Similarly, Ma et al. manufactured micro/nanoscale artificial musculoskeletal systems by programmably integrating the relatively rigid photopolymer SU-8 as framework and pH-sensitive BSA-based protein as responsive muscle component. They developed the successive on-chip femtosecond laser two-photon polymerization strategy for realizing multimaterial integration of complicated micro/nanoscale structures (**Figure 11(e)**). Impressively, they demonstrated a pH-responsive spider microrobot and an intelligent microgripper that could realize on-demand microtarget grasping and release (**Figure 11(f) and (g)**) [215].

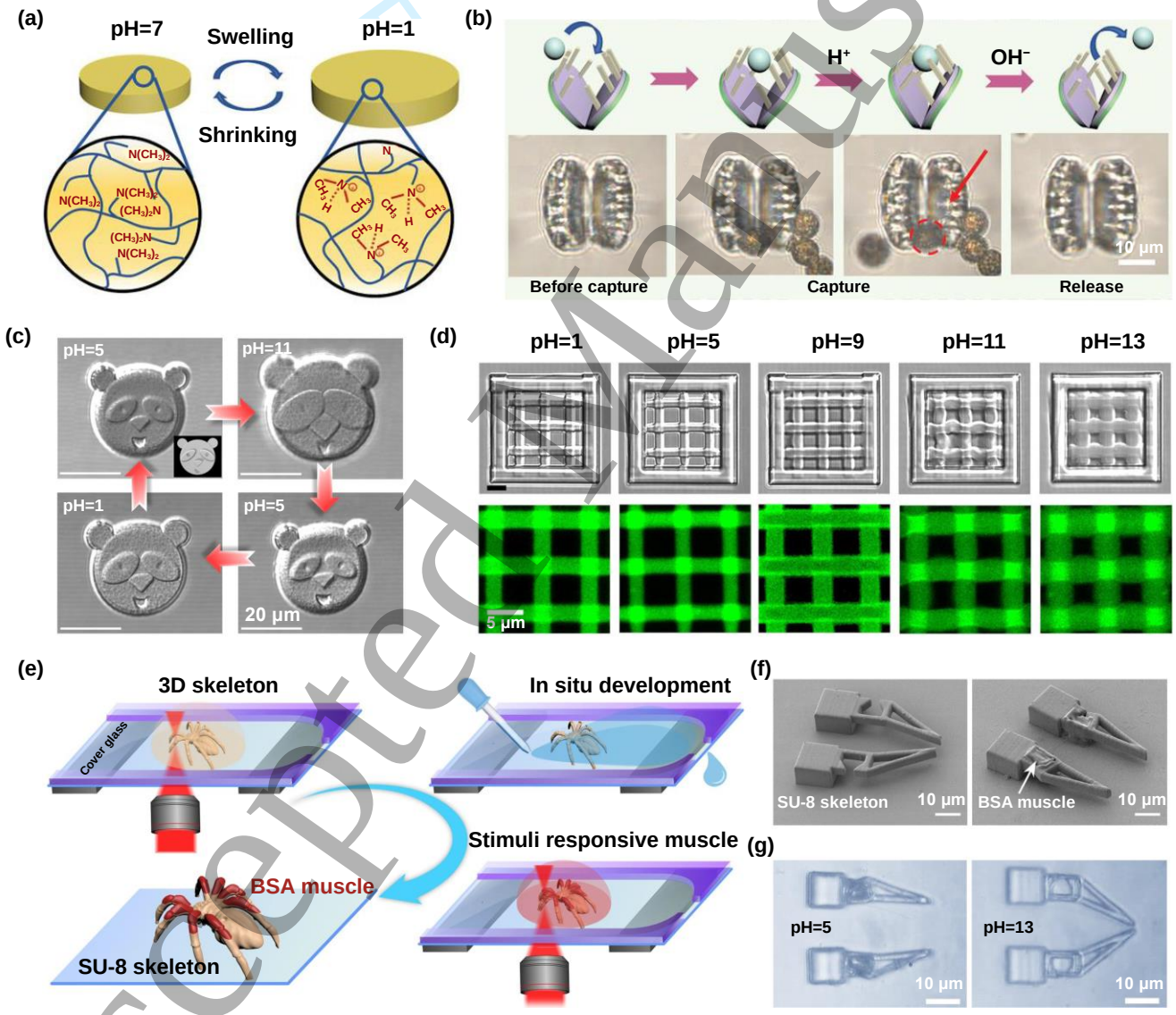

Figure 11. pH-responsive structures. (a) Schematics showing the responsive mechanism of the deformable hydrogel induced by changes in pH. (b) Response behaviors of the pH-driven microactuator for microsphere capture and release. [221] John

Wiley & Sons. © 2022 Wiley-VCH GmbH. (c) 3D panda relief with reversible pH-induced deformation. (d) Microsieves under varying pH. Reprinted with permission from [116]. Copyright (2017) American Chemical Society. (e) Schematics showing programmable fabrication for micro/nanoscale artificial musculoskeletal systems. (f) SEM images showing the fabricated microgripper with or without integration of protein muscles. (g) pH-responsive grasping performance of the fabricated microgripper. Reproduced from [215]. CC BY 4.0. Copyright © 2020 The Authors.

3.5. Humidity-responsive structures

Structures with humidity-responsiveness are prevalent in nature, where they play crucial roles in various biological systems. An illustrative example is the spontaneous opening of pinecone flakes under low humidity, facilitating efficient seed dispersion [3, 223]. Researchers have taken much inspiration from nature and developed diverse humidity-sensitive intelligent structures [17, 224, 225]. Hydrogels are

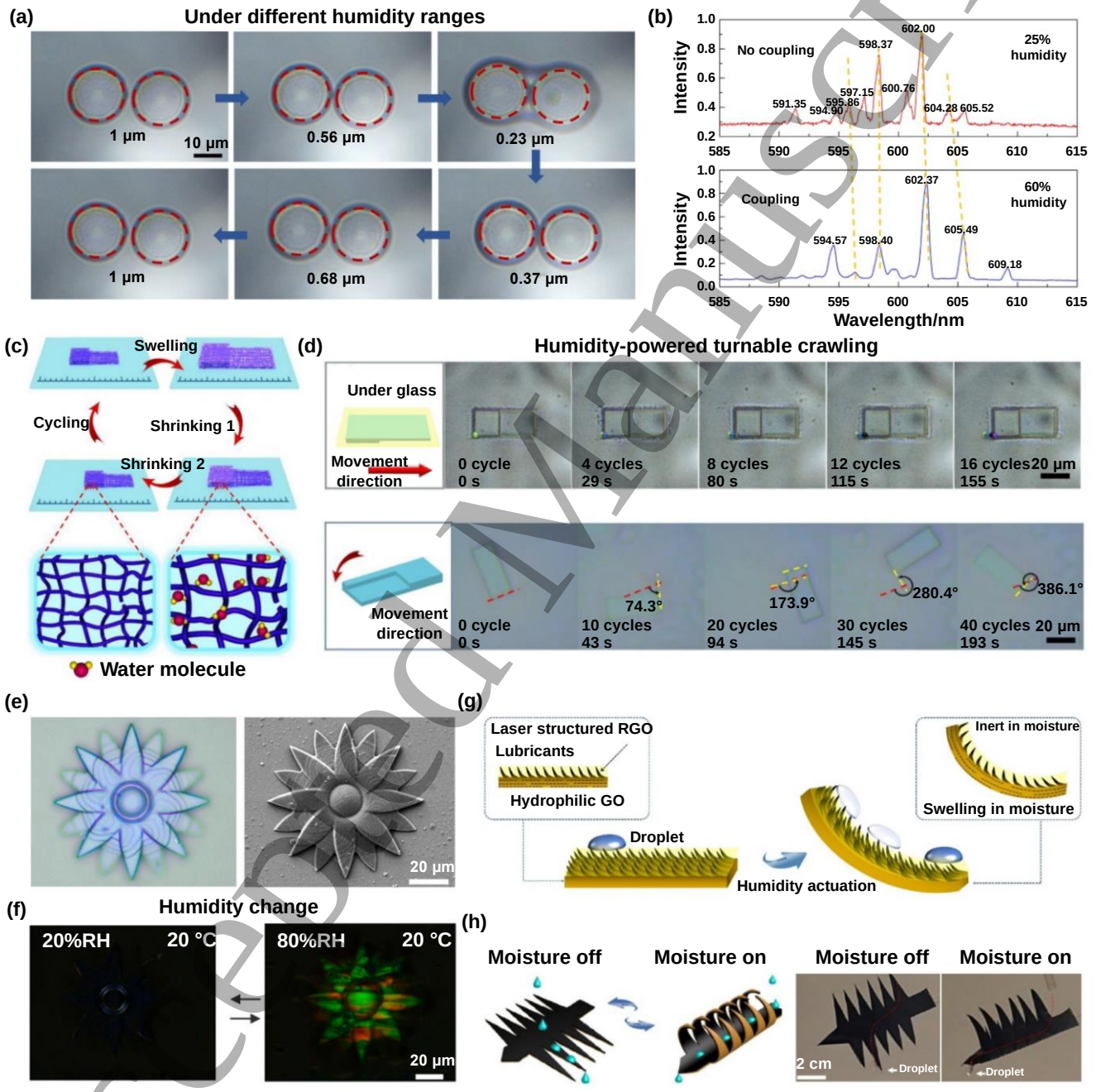

Figure 12. Humidity-responsive structures. (a) Photographs of the photonic molecular microcavity under different humidity ranges. (b) Lasing spectra under different humidities showing optical coupling response of the photonic molecular microcavities.

Reprinted from [226], Copyright (2019), with permission from Elsevier. (c) Schematics showing the crawling motion of a humidity-driven microscopic worm robot in a single cycle. (d) Schematics and images showing humidity-powered turnable crawling movement. Reprinted from [227], Copyright (2020), with permission from Elsevier. (e) Optical microscopy and SEM image of the fabricated micron-sized flower. (f) Micrographs of the flower showing the humidity-induced color change. Reproduced from [228]. CC BY-NC-ND 4.0. Copyright (2020) American Chemical Society. (g) Schematics of the bilayer-actuator-based shape-morphing slippery surfaces. (h) Humidity-responsive deformations of the actuator with a slippery inner surface. Reproduced from [229]. CC BY 4.0. Copyright © 2023 The Authors.

commonly used materials for preparing intelligent structures with humidity response [230, 231]. For example, Li and coworkers fabricated a hydrogel whispering gallery mode (WGM) microcavity resonator that exhibited exceptional sensitivity to environmental humidity through FsLDW technology. The hydrogel-based microcavities demonstrated expansion or contraction behaviors in direct correlation to changes in ambient humidity levels, which enabled modulation of spacing between two microcavities and the subsequent controllable coupling of photonic molecular microcavities (**Figure 12(a) and (b)**) [226]. In another interesting example, Sun et al. developed an ingenious humidity-driven microscopic worm robot with asymmetric structures (thin forefoot and thick hindfoot) by using PEG-DA-based hydrogel and femtosecond laser two-photon polymerization. The microworm robot could swell isotropically with increasing humidity and shrink inhomogeneously with decreasing humidity. Specifically, during the shrinkage process, the thin forefoot exhibited the initial contraction, followed by the subsequent contraction of the thick hindfoot, thus allowing the worm robot to move forward (**Figure 12(c)**). Besides straight crawling movement, the microworm robot could also accomplish more complicated turnable motions when properly designed. The exceptional microcargo-carrying capabilities of the humidity-actuated hydrogel microworm robot were also demonstrated (**Figure 12(d)**) [227]. In addition to hydrogels, LC polymeric materials can also be used for fabricating artificial humidity-responsive structures [232]. For instance, four-dimensional microactuators with humidity-sensitive structural color and shape changes were fabricated based on supramolecular cholesteric liquid crystalline photonic photoresist by Del and colleagues. Networks of the used cholesteric liquid crystals presented a self-organized helical photonic architecture capable of selective light reflection. When the humidity increased or decreased, the microactuators would expand or contract respectively, inducing corresponding alterations in the pitch of ordered cholesteric liquid crystals and leading to a red shift or a blue shift respectively. Interestingly, micron-sized flowers and butterflies were manufactured to demonstrate the structural responsiveness and controllable structural color (**Figure 12(e) and (f)**) [228].

Special structural design can also be utilized to achieve the humidity response of intelligent structures. Han et al. developed bilayer-actuator-based shape-morphing slippery surfaces inspired by carnivorous plants. They used FsLDW technology to process the surface of a graphene oxide (GO) membrane and obtained the Nepenthes-inspired microstructures. Most oxygen-containing groups would be removed in the process because of the photoreduction effect. Due to restricted light penetration and inhibited thermal relaxation of FsLDW, photoreduction only occurred on one surface of the GO membrane, while the other surface was unaffected. Soybean oil was infused into laser-structured reduced GO (LRGO) substrate to fabricate the LRGO/GO-bilayer-based slippery surface with great droplet sliding ability. Upon exposure to moisture, the GO layer preferentially adsorbed water molecules, resulting in strain mismatch at the LRGO/GO bilayer interface and subsequent bending toward the LRGO side (**Figure 12(g)**). Interestingly, several humidity-responsive actuators with active droplet manipulation capabilities, such as a Dionaea muscipula actuator and intelligent frog tongue, were demonstrated (**Figure 12(h)**) [229].

3.6. Other stimulus-responsive structures

Apart from the aforementioned stimuli, other external stimuli, including stress [233, 234], solvent [235, 236], and electric field [237-239], can also be used to trigger the dynamic behaviors of intelligent stimulus-responsive structures manufactured by FsLDW technology. For instance, Gräf et al. demonstrated the mechanically sensitive surface structural color of LIPSS-based diffraction gratings on ductile austenitic stainless steel through FsLDW. The plastic deformation with increasing total strain could cause an increase of the LIPSS period, leading to a subsequent shift of structural coloration from green to yellow and red gradually (**Figure 13(a)**). Furthermore, they fabricated LIPSS on elastomers by using replica casting from metal masters (**Figure 13(b)**), realizing the reversible stress-responsive structure color [240]. Zhang and coworkers designed smart 3D micro/nanostructures using acrylate-based photopolymers and two-photon-polymerization-based FsLDW technology. These intelligent structures could expand in acetone and shrink in n-hexane with rapid response capabilities. Impressively, they fabricated and demonstrated diverse solvent-responsive microactuators, such as a microscale flower and eight-finger microclaw, with highly tunable and reversible dynamic behaviors (**Figure 13(c) and (d)**) [241].

In addition, the electricity-based actuation strategy has attracted wide attention from researchers because it is easy to modulate the electrical amplitude and waveform. Sandford et

al. realized electrically adjustable defects in LC devices and tunable disclination line control using femtosecond laser two-photon polymerization (**Figure 13(e)**). Moreover, they proved that the disclination lines could be utilized for dynamic microparticle manipulation by tuning the external electric field [242]. In another interesting example, Chen and colleagues developed electric-actuated reconfigurable shape-memory shutters by using FsLDW-based laser ablation and soft transfer technology (**Figure 13(f)**). Taking advantage of the electrothermal effect of underlying silver nanowires, the intelligent shutters could be dynamically controlled in situ through an electric field (**Figure 13(g)**), thus enabling thermal management and intelligent display [243].

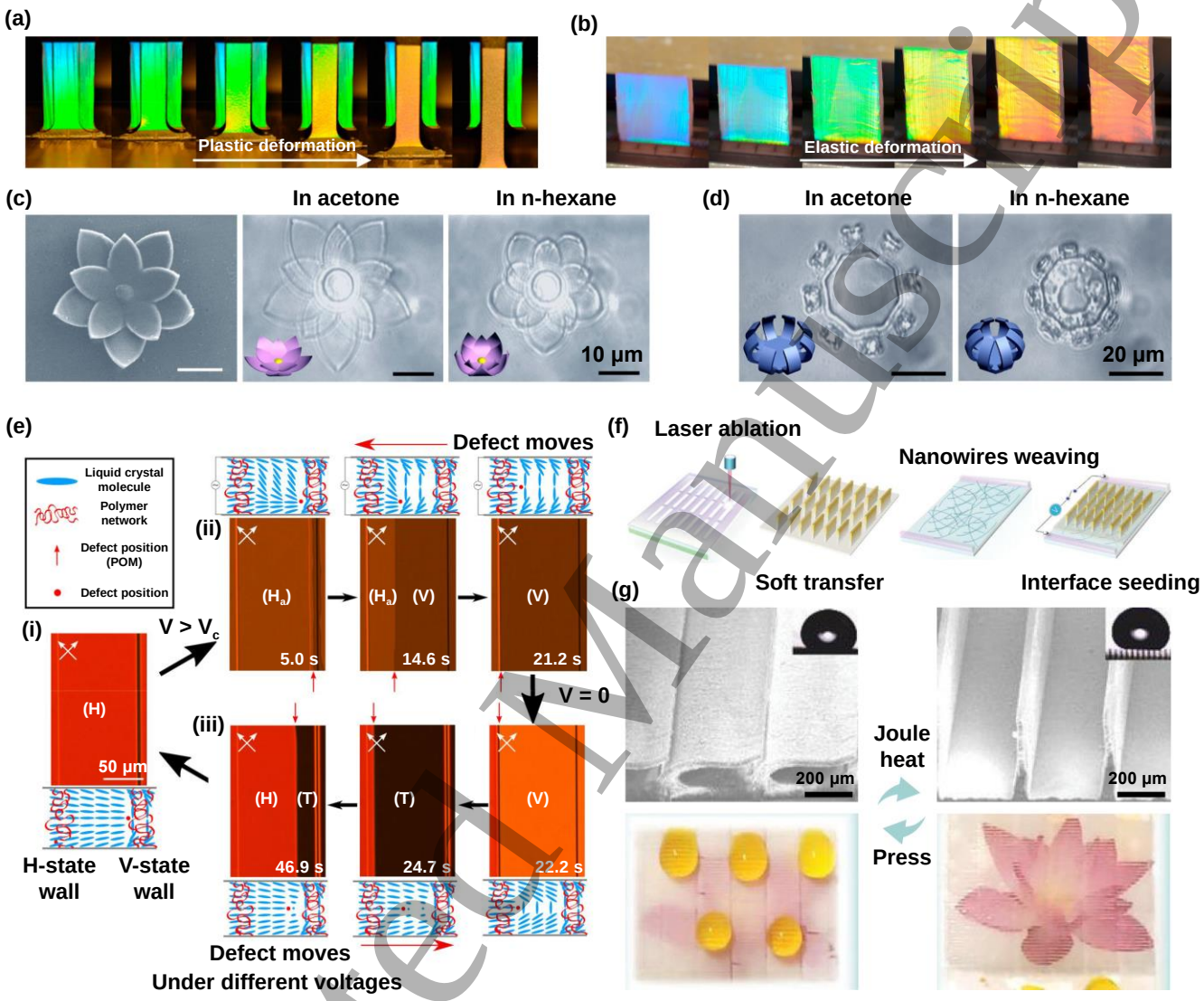

Figure 13. Other stimulus-responsive structures. (a) Structural color shifting on the stainless steel under plastic deformation. (b) Reversible mechano-responsive color change on the elastomer surface. Reprinted from [240], Copyright (2018), with permission from Elsevier. (c) Solvent-responsive microscale flower. (d) Optical images showing the smart microclaw. Reprinted with permission from [241]. Copyright (2019) American Chemical Society. (e) Polarizing microscopy images and director profiles demonstrating dynamics of electrically responsive disclination line. Reproduced from [242]. CC BY 4.0. Copyright © 2020 The Authors. (f) Fabrication schematics of the electrically controllable shape-memory shutters. (g) Reversible switching of the intelligent shutters. [243] John Wiley & Sons. © 2022 Wiley-VCH GmbH.

4. Multifunctional applications

Based on diverse stimulus-responsive structures fabricated by FsLDW technology, various functional applications have been developed in microrobotics, biomedical engineering, optical devices, multifunctional surfaces, droplet/bubble

manipulation, etc.

4.1. Microrobotics

Different from conventional robots, which depend comprehensively on direct-current or alternating-current motor drive systems and complex assembly components, microrobots are usually in the size of micrometers and are generally made based on relatively simple materials but ingenious structural designs [27, 244-246]. FsLDW technology can process and integrate various intelligent materials in an effective and flexible manner, enabling preparation of microrobots with more complex geometric shapes and advanced functionalities, which has aroused widespread interest in the scientific community [99, 174, 178, 247]. Recently, Chen et al. fabricated microcrawlers with

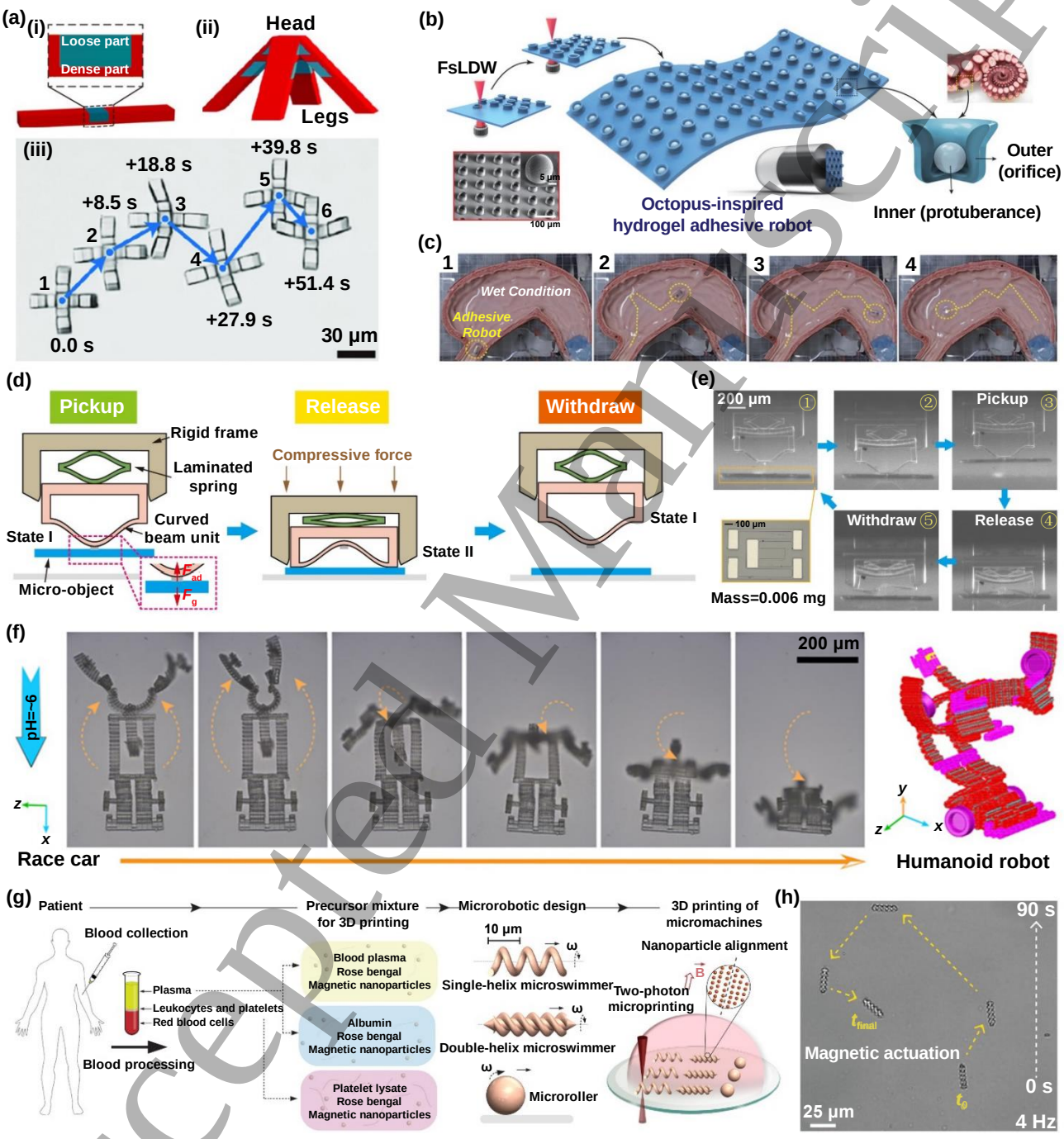

Figure 14. Microrobotics. (a) Schematics of a bilayer-based micro-joint and a starfish-like microcrawler and the locomotion trajectory of the microcrawler. Reproduced from [218]. CC BY 4.0. Copyright © 2020 The Authors. (b) Fabrication process of the octopus-inspired robot. (c) In vitro experiment demonstrating sophisticated locomotion capabilities. Reproduced from

[205]. CC BY-NC 4.0. © 2022 The Authors. (d) Schematics demonstrating the switching principle of the snap-through metastructure. (e) Snapshots showing the underwater pick-and-place process of a silicon chip. From [248]. CC BY-NC 4.0. © 2022 The Authors. Reprinted with permission from AAAS. (f) Complex shape transformation process between the race car configuration and humanoid robot. From [19]. CC BY-NC 4.0. © 2020 The Authors. Reprinted with permission from AAAS. (g) Strategy for fabricating personalized micromachines from patient blood-derivable biomaterials. (h) Magnetic actuation and steering of the fabricated double-helix microswimmer. Reproduced from [249]. CC BY 4.0. Copyright © 2021 The Authors.

stimuli-responsive bilayer-based microjoints by using femtosecond laser two-photon polymerization. The two layers of microjoints were prepared with different crosslinking densities, which would induce interface mismatch during the response process because of the differences in shrinkage capabilities and mechanical properties between the two layers, thus enabling nonmonotonic bending deformations. They demonstrated different kinds of micro crawlers with multifunctional and highly controllable locomotion through diverse programmable structural designs and spatial arrangements of microjoints (**Figure 14(a)**) [218]. Microrobots that can realize robust adhesion to wet and soft biological tissues are very important for effectively completing various biomedical tasks. Lee and coworkers designed a small-scale octopus-inspired robot with robust and biocompatible wet suction-based tissue adhesion capability by using hydrogel heterostructures with varying Young's moduli and two-photon polymerization-based FsLDW technology. The use of a low-modulus PNIPAM-based hydrogel for fabricating an internal dome-like protuberance structure could not only provide strong and controllable tissue adhesion under water, but also simultaneously enable easy detachment through temperature modulation thanks to its temperature-sensitive volume change characteristics. While the use of a high-modulus PEG-DA-based hydrogel to manufacture the outer sucker wall could avoid the collapse of octopus-inspired hydrogel structures during suction. Furthermore, they demonstrated controllable adhesion and detachment of the proposed octopus-inspired robot on wet biological tissues (**Figure 14(b) and (c)**) [205].

At the microscale, there is a substantial increase in the ratio of surface area to volume, resulting in diminished significance of volume-related forces including gravity, inertia, and buoyancy. In this case, surface-related forces including friction, fluid drag and adhesion become more predominant. Therefore, achieving controllable adhesion and release of microobjects at the microscale presents a challenge. Zhang et al. developed a bioinspired snap-through metastructure for gripping and releasing microobjects, which consisted of three parts, including a rigid frame, a laminated spring, and a curved beam unit. The core of this technique was to adjust the boundary conditions for the snap-through instability, enabling the reversible transition from monostable to bistable. During the handling process, the rigid frame could realize the compliant-stiff boundary condition transitions of the curved beam unit assisted by an external compression force. Intriguingly, the snap-through of the curved beam could separate the contact area between the curved beam and pre-adhered micro-object, which enabled the successful release operation. Moreover, the compressed laminated spring could push the curved beam out of the rigid frame after the external force was withdrawn to prepare for the next operation cycle (**Figure 14(d)**). They fabricated and demonstrated a miniaturized snap-through device with two-way switchable adhesive capability through FsLDW, which could realize the picking and placing of micro-objects with smooth and rough surfaces in universal scenes including dry and underwater conditions (**Figure 14(e)**) [248].

In addition to the simple and single structure design, reconfigurable robots based on modular designs have attracted wide attention because they enable the enrichment of morphologies, functionalities, and degrees of motion within a single robot. For an interesting example, diverse 3D reconfigurable microstructures with sophisticated shape-transforming capabilities were proposed based on a programmable modular design and stimulus-responsive micro building blocks assembly strategy by Huang and colleagues. They utilized stimulus-sensitive hydrogel materials and femtosecond laser two-photon polymerization to prepare these multifunctional microscale building blocks. Impressively, they fabricated and demonstrated a micro-transformer based on 3D assembly and movement planning of modular building blocks, which could achieve complex shape transformation between the racing car and humanoid robot (**Figure 14(f)**) [19]. In recent years, the design and manufacturing of biocompatible stimulus-responsive structures have aroused great interest from researchers [121, 250, 251]. Significantly, Ceylan et al. fabricated the multi-responsive microrobots with exceptional biocompatibility based on patient-blood-derived biomaterials (magnetic composites composed of serum albumin protein, plasma, and platelet lysate) through two-photon polymerization-based FsLDW technology. These autologous-biomaterial-based micromachines could avoid cytotoxicity and the immune response to the maximum extent, and they possessed excellent enzymatic degradability, which could minimize the risk of chronic inflammation and long-term toxicity (**Figure 14(g) and (h)**) [249].

4.2. Biomedical engineering

Stimulus-responsive structures prepared by FsLDW technology are being increasingly utilized in biomedical fields including cell delivery and precisely localized therapy because of their controllable dynamic behaviors of manipulating

micro-objects and potential capabilities for loading, delivery, and release of drugs [252-258]. Cells are capable of recognizing and transmitting mechanical strain and stress pattern through mechanically sensitive modules, including cell adhesion sites, ion channels, and cytoskeleton. Exploring the cellular response behaviors to external mechanical stimuli holds significant importance [259-261]. Hippler et al. manufactured stimuli-responsive composite micro scaffolds for cell manipulation by using a β-cyclodextrin acrylamide and adamantane acrylamide-based host-guest hydrogel and two-photon polymerization. The fabricated microstructures through the specially developed host-guest hydrogel could present reversible large volume changes through the application of soluble competitive low-molecular-weight guests (1-adamantanecarboxylic acid, i.e., 1-AdCA) under physiological conditions. They used traditional photoresists and this newly developed host-guest hydrogel to fabricate the

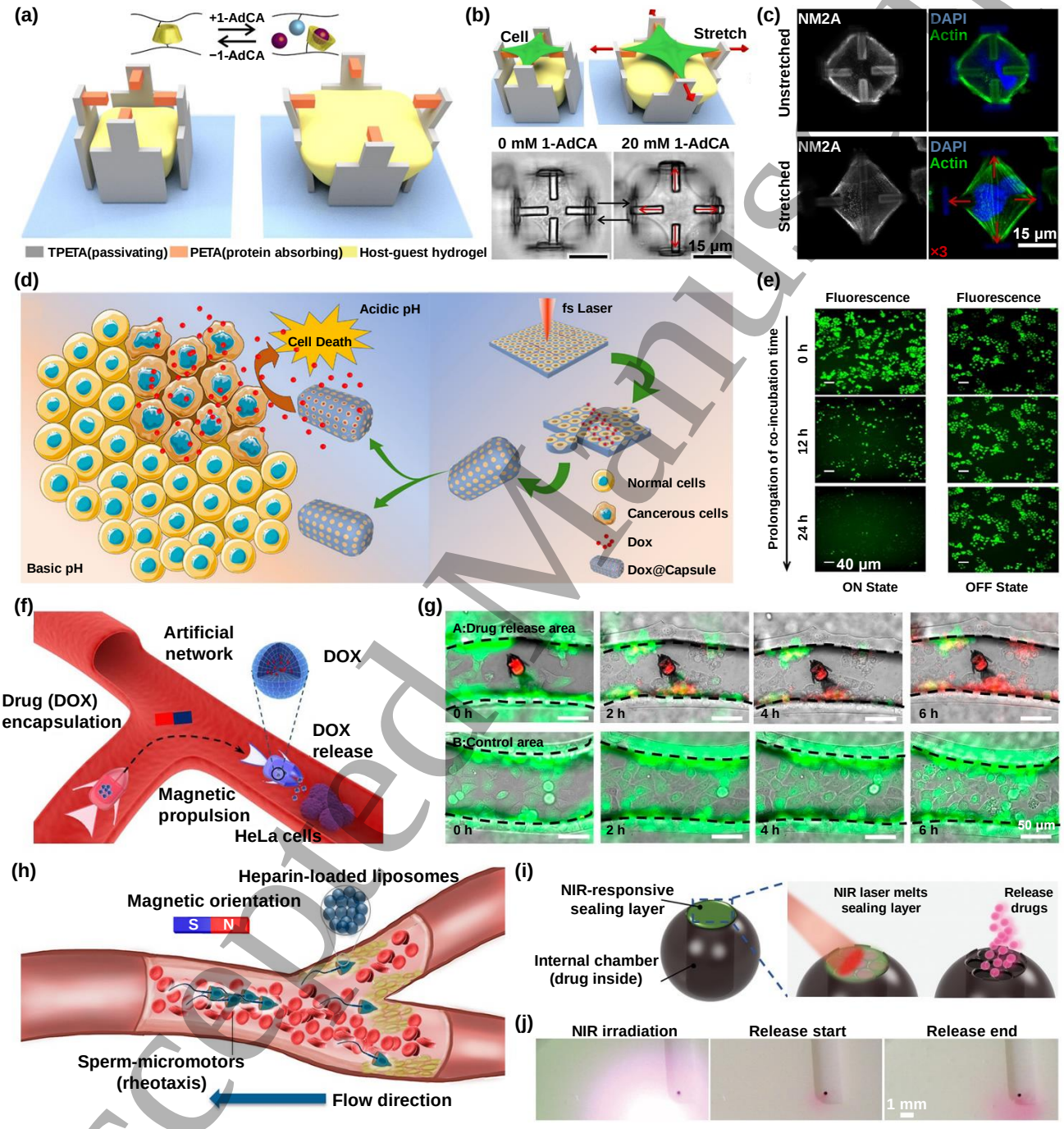

Figure 15. Biomedical engineering. (a) Schematics showing the stimuli-responsive composite microscaffolds. (b) Schematics and optical micrographs showing the cells under unstretched and stretched states. (c) Fixed and stained cells under unstretched

and stretched states. From [262] . CC BY-NC 4.0. © 2020 The Authors. Reprinted with permission from AAAS. (d) Schematics demonstrating design of pH-triggered hydrogel microcapsules for anticancer drug release beside cancer cells. (e) Confocal laser scanning microscopy images showing the fluorescence within tumor cells under pH < 7 (left) and pH > 7 (right). Reprinted with permission from [56]. Copyright (2022) American Chemical Society. (f) Schematics showing targeted drug release utilizing magnetic shape-morphing microfish. (g) Images showing HeLa cells viability at drug release region and control region. Reprinted with permission from [10]. Copyright (2021) American Chemical Society. (h) Illustration for cargo delivery through flowing blood using sperm micromotors. Reprinted with permission from [263]. Copyright (2020) American Chemical Society. (i) Schematics of the puffball-inspired microrobotic system. (j) On-demand drug delivery using the microrobotic system. Reproduced from [176]. CC BY 4.0. Copyright © 2022 The Authors.

microscale composite cell scaffolds composed of protein-repellent base components, protein-adhesive beam components, and central stimuli-sensitive hydrogel host-guest parts, which could be utilized for simultaneously stretching individual cells and studying subsequent dynamic cell behaviors with precise spatial and temporal control under customized microenvironments (**Figure 15(a)-(c)**) [262].

Sustained release of drugs can increase the compliance of patients and reduce the side effects of drugs, which is a very important medical research field. Zhang and coworkers fabricated a biomimetic hydrogel-based porous gating system through FsLDW-based microdrilling and subsequent ultraviolet exposure, which consisted of a pH-sensitive hydrogel-based valve and a frame made of PDMS. The proposed gating systems, including membrane and microcapsule systems inspired by plant stomata, could realize a reversible transition between "OFF" and "ON" states based on pH-triggered valve expansion or contraction, which could be applied to realize sustained drug release and on-demand tumor cells treatment (**Figure 15(d) and (e)**) [56]. Achieving precise drug delivery is a paramount objective in targeted therapy, but it poses significant challenges. Xin et al. successfully engineered shape-morphing microrobots capable of adapting to the surrounding environment by programmatically encoding the heterogeneous architectures in a pH-responsive hydrogel through femtosecond laser two-photon polymerization. These intelligent microscale robots were endowed with magnetic driving capabilities after being immersed in a Fe_3O_4 nanoparticle suspension. They manufactured a magnetic shape-morphing microfish capable of encapsulating and controllably releasing the drug (doxorubicin, DOX) through opening and closing the microfish mouth, which was used to demonstrate localized HeLa cancer cell treatment in the artificial vascular network by stimulation of the magnetic field and pH (**Figure 15(f) and (g)**) [10]. In a similar fashion, Xu and colleagues developed a hybrid streamlined-horned sperm micromotor by using two-photon polymerization. The sperm flagellum of the hybrid micromotor could enable high propulsion, while the synthetic microstructure coated with Fe could be utilized for magnetic guidance and cargo transportation. Medical treatments in blood are accompanied by complex working circumstances, such as diverse cells and substances, complicated hemorheological characteristics, and high fluid velocities, so it is difficult to complete these extremely challenging tasks. However, they demonstrated that the prepared sperm micromotor could efficiently swim against the flow of blood, accomplishing the task of delivering heparin cargo under precise guidance of an external magnetic field for localized anticoagulation therapy (**Figure 15(h)**) [263].

Currently, most stimulus-responsive microstructures used for targeted drug delivery in vivo are largely restricted by inadequate drug loading capacity, inevitable drug leakage or inactivation, as well as stringent drug modification standards. Song et al. proposed a puffball-inspired microrobotic system based on FsLDW technology, which was composed of a spatially segregated inner chamber for high drug payloads, a near-infrared-sensitive sealing layer offering strong drug protection and noninvasive desired drug release, and nickel/titanium composite layers for magnetic propulsion capability. The prepared microrobotic system could flexibly load small-molecule drug payloads and polymeric drug payloads without other complex modification steps (**Figure 15(i)**). Interestingly, they controlled the microrobotic system to move to different designated target positions precisely by a rotating magnetic field and used a near-infrared laser to induce the selective melting of the top sealing layer and following encapsulated drug release (**Figure 15(j)**), thus realizing targeted and on-demand drug delivery [176].

4.3. Optical devices

The unparalleled advantages of FsLDW-based surface and volume processing strategies, including extremely high precision, true 3D manufacturing capability, and wide materials applicability, are particularly helpful for fabricating optical devices with multiple functions [86, 264, 265]. Based on FsLDW technology, a variety of intelligent stimulus-responsive optical devices, such as gratings [189, 233], optical waveguides [53], microlenses [54, 214, 266], and photonic crystals [267, 268], can be manufactured by appropriately integrating smart materials and optimized designs. Optical storage technology has garnered significant attention due to its notable benefits of low energy consumption, cost-effectiveness, and remarkable storage capacity. It is of great significance to explore new optical information storage devices with fast response, 3D storage capacity, and nondestructive rewritability. Xiao et al. developed 3D glass-based optical information storage devices with excellent

rewritability and erasability by utilizing FsLDW technology and transparent photochromic glasses doped with rare earth ions. Reversible modifications of transmittance and upconversion luminescence of photochromic glasses, resulting from the hopping of polarons (W^{6+}/W^{5+} and Sb^{3+}/Sb^{5+}), could be achieved through femtosecond laser irradiation and heat treatment (**Figure 16(a)**). Impressively, they wrote rectangles with different sizes and Chinese characters within inner layers of transparent photochromic glass by internal modifications of solid materials based on FsLDW, thus enabling 3D information storage (**Figure 16(b)**) [269].

Inspired by natural compound eyes found in insects, manufacturing artificial compound eyes that offer expansive field of view, infinite field depth, and dynamic imaging characteristics have aroused widespread interest from researchers because of their potential cutting-edge applications in national defense, industry, and clinical medicine [270-273]. Ma and coworkers designed intelligent stimulus-responsive BSA-protein-based compound eyes through FsLDW, which were inspired by both the compound eyes found in insects and tunable crystalline lens present in human eyes. The adjustable field of view and variable focal

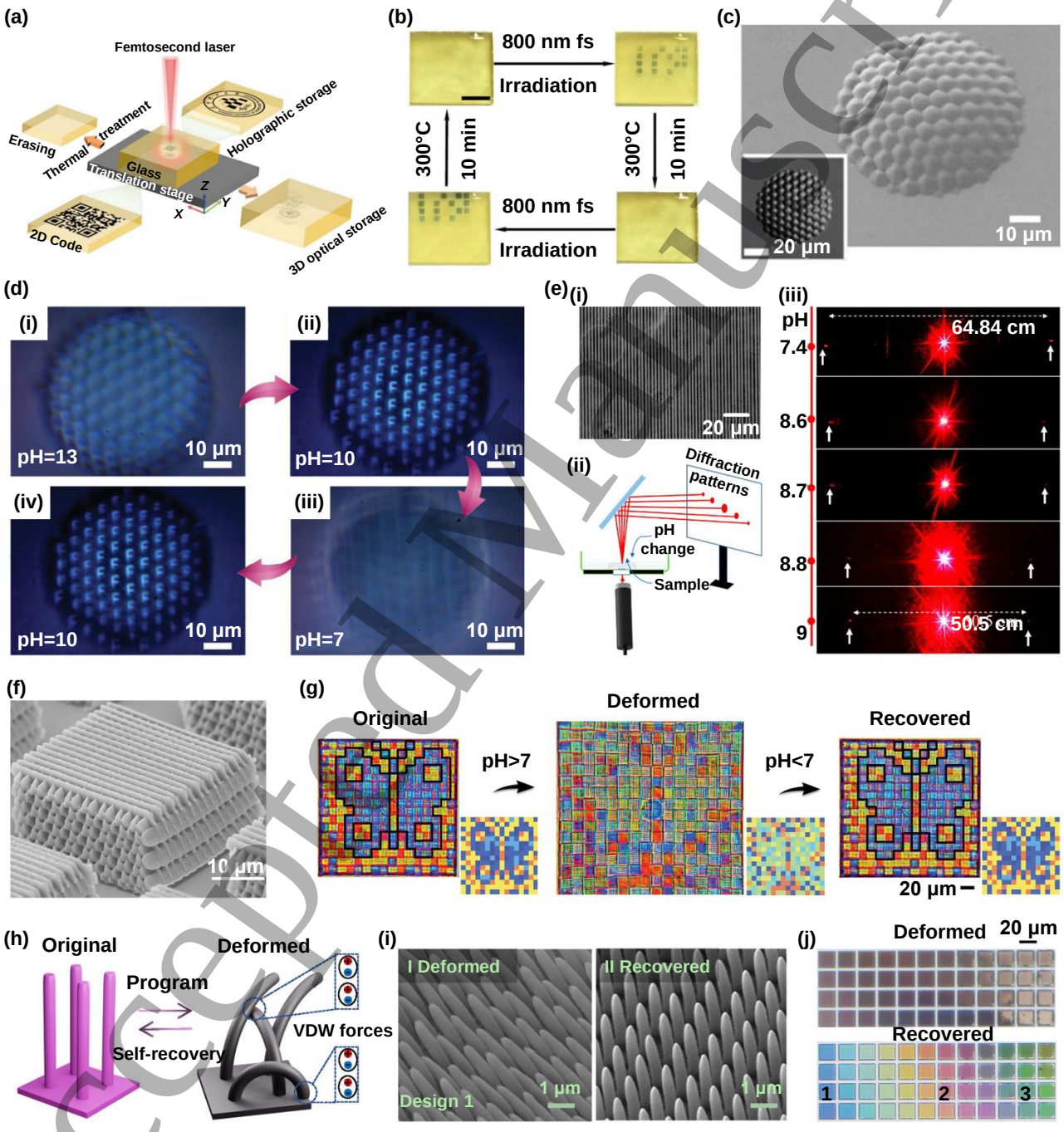

Figure 16. Optical devices. (a) Schematics showing the writing and erasing of 3D glass-based information storage. (b) Images showing the rewritability and erasability of the optical information storage. Reproduced with permission from Springer Nature Customer Service Centre GmbH: Springer Nature, Science China Materials [269], Copyright (2022). (c) SEM image showing the protein compound eye. (d) Varifocal capability of the fabricated compound eye. [52] John Wiley & Sons. © 2019 WILEY-VCH Verlag GmbH & Co. KGaA, Weinheim. (e) Image of the grating and the changes in the distances between first-order maxima under different pH values. Reproduced from [274]. CC BY 4.0. Copyright © 2022 The Authors. (f) SEM image showing the woodpile structure. (g) Images of pH-responsive butterfly painting. [275] John Wiley & Sons. © 2022 Wiley-VCH GmbH. (h) Schematic for the reconfigurable transformation of free-standing nanopillars. (i) Deformed and recovered nanopillars. (j) Optical images showing structural colors. Reprinted with permission from [276]. Copyright (2022) American Chemical Society.

length could be realized by flexibly modulating the pH-induced controllable and reversible expansion and contraction of the compound eyes with sophisticated 3D shapes and ultrafine ommatidia (**Figure 16(c) and (d)**) [52].

Diffraction gratings are periodic-structure-based optical components that can be used to manipulate spatial light distribution and play vital roles across diverse applications, such as spectrometers, monochromators, augmented/virtual reality displays, and structured light [233, 277]. Xiong et al. fabricated tunable volume diffractive gratings by using FsLDW strategy and a partially crosslinked phenylboronic acid hydrogel, which mainly resulted from femtosecond laser densification-induced variations of local refractive index in pH-responsive hydrogel. When exposed to different surrounding pH values, the prepared hydrogel-based subsurface line gratings would swell, inducing grating period changes and subsequently distance changes between the first order maxima of projected diffraction patterns (**Figure 16(e)**) [274].

Structural colors are different from the colors generated from traditional dyes and pigments, and they can be created by light interactions with the specific physical micro/nanostructures within or on the surface of a material, which are eco-friendly and fade-resistant, and are favorable alternatives for future color applications [278-280]. Liu and colleagues achieved stimuli-responsive structure colors under solution conditions by using two-photon polymerization-based FsLDW technology and a modified pH-responsive hydrogel. The fabricated 3D orthogonal grating-stack-based woodpile structures with different designed lateral and axial structural parameters could present a fairly wide range of different colors, resulting from the diffraction of transmitted light beams by different woodpile layers (**Figure 16(f)**). Interestingly, they demonstrated the reversible color-switching behaviors of the prepared woodpile amphichromatic fish and pixelated artwork images with blue butterflies by modulating the pH value of the solution (**Figure 16(g)**) [275]. Similarly, Zhang et al. realized high-resolution reconfigurable structural colors based on the programmable high-aspect-ratio nanopillars (**Figure 16(h)**), which were fabricated by using a newly developed stiff SMP resin and femtosecond laser two-photon polymerization. The slender and narrow nanopillars exhibited the ability to undergo deformations into the collapsed and curled state, and could also be restored to initial upright state upon sufficient heating (**Figure 16(i)**), which could be utilized to reversibly display different structural colors caused by the interaction between the nanopillars and the visible light (**Figure 16(j)**) [276].

4.4. Multifunctional surfaces

With the rapid development of society, surfaces designed with single functionality can no longer fulfill the diverse requirements in practical applications. Imparting intelligent response characteristics to the surface, such as switchable wettability, adjustable adhesion, and light transmittance, has attracted wide interest among researchers [281-285]. Jiang and coworkers fabricated a smart dynamic regulation structured surface composed of a high-aspect-ratio magnetic-responsive microplate array by integrating FsLDW strategy, SMP-based soft transfer, as well as surface modification. Through the overall superhydrophobic treatment and subsequently magnetic-field-assisted selective sunny-side-up laser scanning, a Janus microplate array could be obtained, which had one superhydrophobic side and the other hydrophilic side (**Figure 17(a)**). The application of a magnetic field enables the reversible switching of surface wettability between a superhydrophobic state and a hydrophilic state, thus enabling the function of a magnetic-responsive water droplet switch (**Figure 17(b)**). Similarly, magnetic-sensitive color conversion could be accomplished through painting distinct colors on different sides of the Janus microplates (**Figure 17(c)**) [50]. Bai et al. designed a thermo-actuated SMP-based surface possessing adhesion-switchable capabilities. They used FsLDW to directly prepare a microgroove array on the SMP surface, endowing the micro/nanostructured surface further modified by fluoroalkylsilane with great superhydrophobicity and anisotropic wettability. After being deformed under external force pressing, the microgroove array would undergo a transition from a state of low water adhesion to a state of high water adhesion, and its original morphology and wettability would be completely restored after an adequate heating process (**Figure 17(d)**) [21].

In addition to controllable wettability switching, multifunctional surfaces with synergistically switchable optical transparency are also of great significance for practical applications. Chen and coworkers developed a Joule-heat-

responsive intelligent slippery surface with a sandwich structure, which consisted of impregnated paraffin, elastomer membrane with superhydrophobic micropillars fabricated through FsLDW, and a silver-nanowire-embedded film heater (**Figure 17(e)**). By heating through loading a low voltage, the solid paraffin wax on the microstructured surface would melt, thus forming a slippery surface with augmented transparency and suppressed contact angle hysteresis. Once the electrical heating was removed, the undulating non-slippery surface would be restored due to the coagulated paraffin, which would exhibit low optical transparency and high contact angle hysteresis (**Figure 17(f)**). More intriguingly, they manufactured and demonstrated a homemade smart window with adjustable optical transparency for thermal management in situ and controllable optical visibility (**Figure 17(g)**) [237]. To date, smart surfaces with tunable wettability are mostly limited to switching between two different wetting characteristics. It is of great value to explore the realization of reversible switching of multiple wetting characteristics for intelligent surfaces. Song et al. fabricated a smart biomimetic

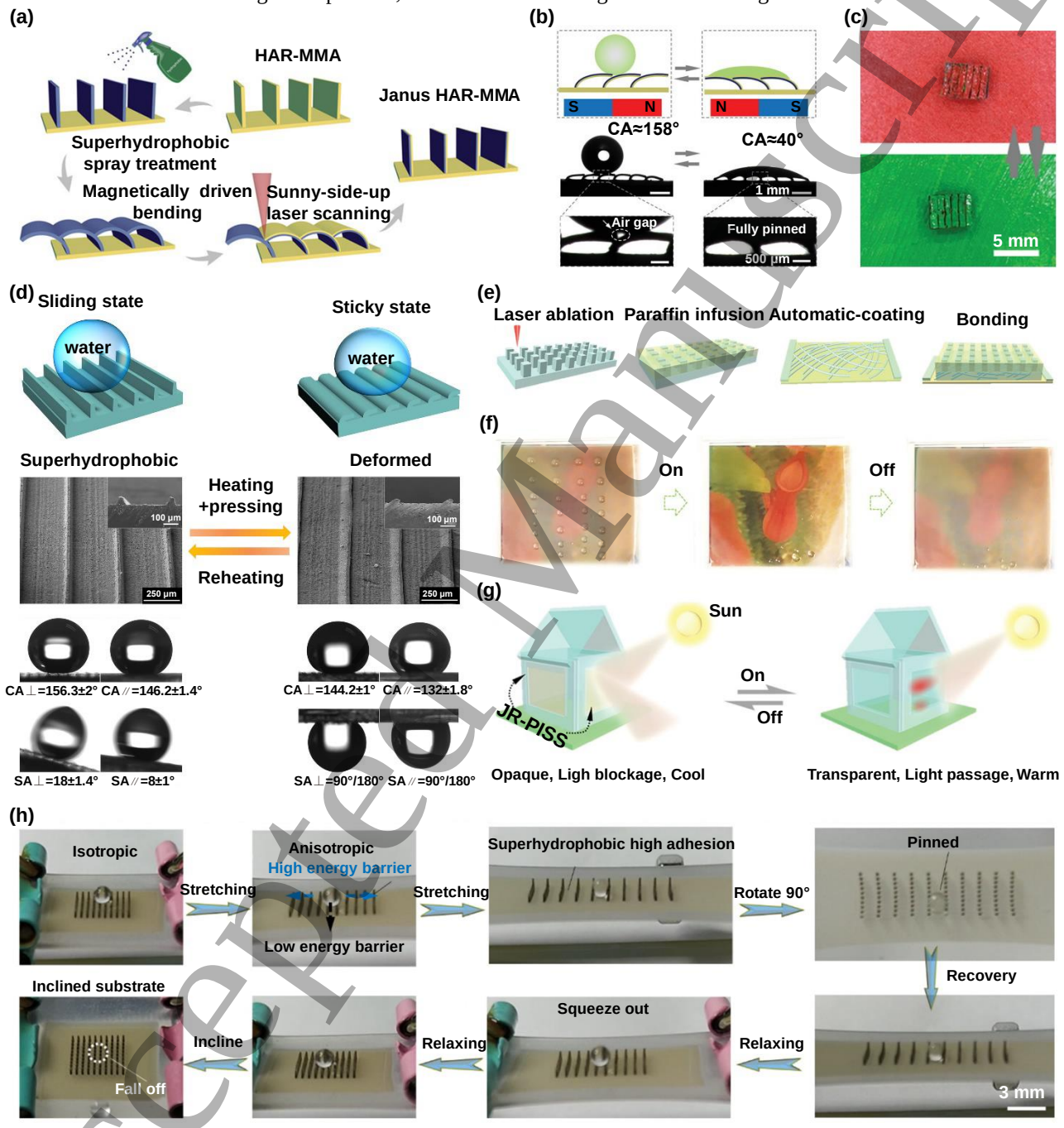

Figure 17. Multifunctional surfaces. (a) Schematics showing the fabrication process for Janus microplate array. (b) Switchable wettability of the Janus microplate array. (c) Images showing the dynamic switching of surface color. [50] John Wiley & Sons.

 (d) Reversible surface wettability switching of the microgroove array. Reprinted from [21], Copyright (2020), with permission from Elsevier. (e) Fabrication strategy of the intelligent slippery surface. (f) Images of regulating optical transparency and wettability. (g) Conceptual schematic of the thermal management. Reproduced from [237]. CC BY 4.0. (h) Optical images showing the reversible tri-switching on the surface in situ. Reprinted with permission from [234].

tensile-dependent surface with flexible tri-switchable wettability, which was composed of a stretchable silicone-based substrate and a PDMS-based microcolumn array obtained through using FsLDW and soft transfer technology. In the absence of external stretching, the cauliflower-like micro/nanostructures uniformly distributed on the femtosecond-laser-ablated top layer of microcolumns could endow the surface with lotus-leaf-like superhydrophobicity, low adhesion, and isotropy. After being stretched uniaxially, the surface exhibited rice-leaf-like anisotropy. Once the increasing tensile force made the microcolumn spacing larger than the droplet diameter, the droplet would completely contact the substrate, thus making the surface present rose-petal-like high adhesion. Therefore, by controlling the uniaxial tensile stress, the reversible switching of triple controllable wettability characteristics could be realized flexibly (**Figure 17(h)**) [234].

4.5. Droplet/bubble manipulation

Controllable manipulation of droplet and bubble, including capture, transport, and merging, is essential for advancing academic research and industrial explorations owing to its vast potential across diverse fields in microfluidics, chemical and biological analysis, sensors, and medicine [286, 287]. Moreover, many researchers have realized multifunctional droplet/bubble manipulation by using stimulus-responsive structures prepared through FsLDW technology [171, 288]. For example, Jiang and colleagues developed a multifunctional magnetic-responsive liquid manipulator by integrating FsLDW technology and the soft transfer technique, which could be utilized for 3D droplet transportation. The controllable droplet manipulation of the proposed manipulator was based on the dynamic behaviors of the magnetic-actuated microplate array subjected to periodic magnetic fields varying spatially. Due to sequential abrupt reversal of the microplates resulting from the particular magnetic field configuration, a droplet could be transported at an unprecedented speed of 58.6 mm s^{-1} (**Figure 18(a)**). Furthermore, they demonstrated the applications of the manipulator in droplet-based chemical reactions and anti-gravity droplet climbing (**Figure 18(b)**) [51].

Recently, microscale drug screening with high throughput has garnered significant attention thanks to its merits in terms of cost-effectiveness and high efficiency. Zhou et al. achieved highly effective and flexible drug toxicity screening through the on-demand manipulation of various prodrug droplets. They proposed a light-sensitive slippery platform, which was fabricated through FsLDW-based ablation of the prepared PDMS film doped with candle-soot nanoparticles and further infused with silicone oil lubricant. The near-infrared-light-induced programmable manipulation of droplets exhibiting varying surface tensions could be realized on the slippery platform, resulting from excellent photothermal conversion capability of candle-soot nanoparticles and temperature-difference-induced wetting gradient force (**Figure 18(c)**). Importantly, they demonstrated the nondestructive droplet merging and sorting of different prodrug droplets under remote control of near-infrared light (**Figure 18(d)**) [289].

In addition, bubble manipulation can also be realized by using FsLDW-based stimulus-dependent intelligent structures. For instance, inspired by pitcher plants and rice leaves, Jiao and coworkers developed a strain-responsive slippery lubricant-infused anisotropic surface for facile bubble manipulation. Initially, a PDMS-based microgrooved surface was fabricated using femtosecond laser ablation. Subsequently, a uniform slippery surface was achieved by spin-coating silicone oil onto the fabricated surface. The microgroove structures played a crucial role in creating a superhydrophobic substrate that effectively trapped the silicone oil, forming a stable lubricant film. When the surface was not subjected to stretching, the lubricant film covered the microgrooves entirely, facilitating easy bubble sliding in a direction perpendicular to the microgrooves. However, when the surface was stretched, the hydrophobic PDMS microgrooves were exposed, resulting in increased contact angle hysteresis and hindering the potential bubble movement. Consequently, the designed surface demonstrated in situ wettability switching, allowing reversible transition between underwater bubble sliding and pinning simply by controlling the mechanical strains (**Figure 18(e) and (f)**) [290].

Besides the conventional adhesion regulation between ultralow and ultrahigh states, tuning the adhesion force between the solid surface and bubble can enable more flexible and accurate bubble manipulation, which is challenging because of the high demand for solid surface topography control. Huo et al. realized controllable bubble manipulation by adjusting the underwater bubble adhesion on a solid surface using FsLDW-based patterned SMP surfaces. They obtained inspiration from fish scales and rose petals. The hierarchically structured SMP surface with microscale protrusions and nanoscale swellings was fabricated through line-by-line femtosecond laser scanning, which endowed the surface with great fish-scale-like underwater superaerophobicity and ultralow bubble adhesion. While the untreated surface exhibited rose-petal-like underwater aerophobicity and high

bubble adhesion. Thus, by controlling the proportion of the FsLDW-induced hierarchically structured square pattern array and untreated planar domain, the underwater bubble/solid adhesion could be flexibly modulated (**Figure 18(g) and (h)**). More importantly, they achieved underwater bubble picking/site-specific release and subsequently programmable tiny-bubble array generation and erasing by using different prepared samples with customized bubble/solid adhesion (**Figure 18(i)**) [291].

5. Conclusions and perspectives

In conclusion, we focus on the state-of-the-art FsLDW-prepared stimulus-responsive structures for multifunctional applications. We first concisely introduce the underlying physical principles of femtosecond-laser-matter interaction and different manufacturing strategies based on FsLDW. Thereafter, according to the response capability to different environmental stimuli, diverse intelligent structures prepared by FsLDW are summarized. Afterwards, multiple potential applications of these stimulus-responsive structures including

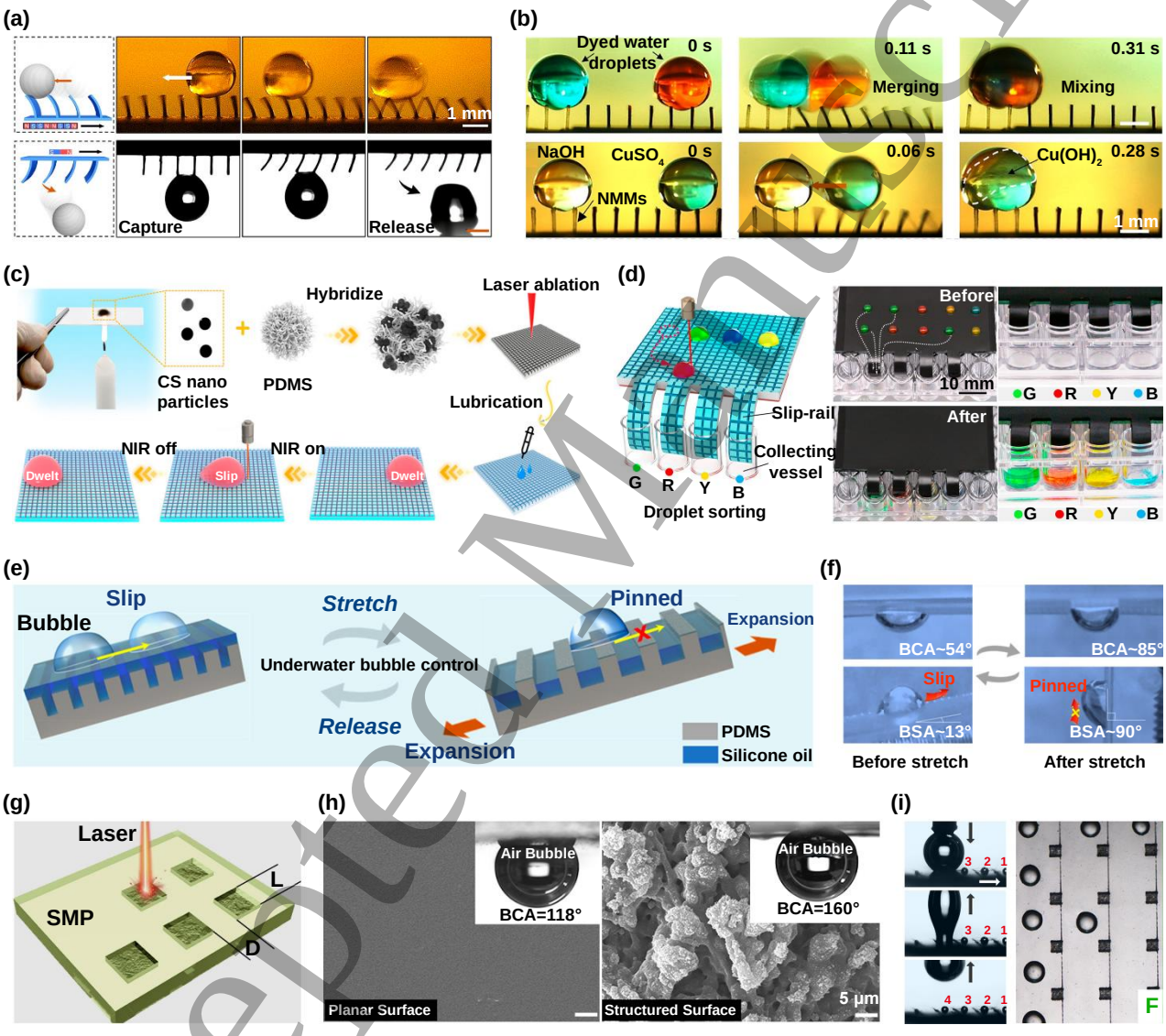

Figure 18. Droplet/bubble manipulation. (a) Horizontal droplet propulsion and vertical droplet capture/release. (b) Images showing the droplet mixing and chemical reaction. Reprinted with permission from [51]. Copyright (2020) American Chemical Society. (c) Schematics for fabrication of the slippery platform and droplet sliding under near infrared light. (d) Schematic and photographs of droplet sorting. Reprinted with permission from [289]. Copyright (2022) American Chemical Society. (e) Schematic showing the reversible bubble manipulation between sliding and pinning under external mechanical excitation. (f) Optical images showing the reversible switching and bubble manipulation. Reprinted with permission from [290]. Copyright

(2021) American Chemical Society. (g) Fabrication schematic of the square-patterned array. (h) SEM images and wettability characterization of the planar surface and laser-structured surface. (i) Images showing the tiny bubble writing and the formed bubble pattern. Reprinted from [291], Copyright (2021), with permission from Elsevier.

microrobotics, biomedical engineering, optical devices, multifunctional surfaces, and droplet/bubble manipulation, are emphasized and described (**Table 1**), which originate from their highly controllable dynamic behaviors.

In spite of remarkable advancements in smart FsLDW-based stimulus-responsive structures, there are still several challenges to be met for better future development. Basically, because of the complicated nonlinear interactions, the interaction mechanisms between femtosecond lasers and various materials have not been fully elucidated, especially some new functional materials. For example, there is still a lack of comprehensive and integrated multiscale theoretical models to scientifically explain the formation mechanism of femtosecond laser-based LIPSS, which requires further extensive experimental and theoretical research, including multiscale observation systems with high spatial-temporal resolution and dynamic continuous observation ability. The mechanisms of femtosecond laser-induced internal physical modification in solid materials have not been completely determined, especially after the energy transfer from the free electron plasma to the lattice.

Apart from the need to explore undisclosed physical mechanisms, novel and more efficient extreme manufacturing techniques should be developed. Achieving high spatial resolution through two-photon polymerization-based FsLDW is of critical significance in the fabrication of high-precision and high-quality stimulus-responsive devices, such as intricate photonic devices and 3D functional micromachines, which is a focal point of numerous researchers. The refinement of the optical system and femtosecond laser writing parameters, including the objective numerical aperture, laser pulse width, wavelength, average power, and exposure dose, holds promise for achieving superior resolution [89, 292, 293]. Another strategy involves fine-tuning the polymerization characteristics of photopolymers through the addition of radical quenchers or highly sensitive and efficient photoinitiators [294-296]. Additionally, employing photoinhibition-lithography techniques, inspired by stimulated emission depletion microscopy, allows for the partial depletion of radicals within the focal region. These techniques can effectively reduce the voxel size, enabling greater resolution at deep sub-diffraction scales and significantly improving the repeatability and consistency [295, 297-299]. Besides high resolution, achieving high throughput and efficiency in the fabrication of stimulus-responsive micro/nano-structures is also of great significance. To enhance fabrication speed, various strategies have been developed, including galvo-mirror-based focus scanning, multifoci parallel processing, and structured light field techniques. These methods usually involve the utilization of auxiliary optical components, such as microlens arrays, beam-splitting devices, spatial light modulators, and digital micromirror devices [300-305]. Currently, the fabrication efficiency and processing quality of FsLDW are restricted by each other, limiting its large-scale and industrial practical applications. Therefore, it is of great necessity to develop novel strategies to overcome the inherent trade-offs between fabrication resolution and efficiency. Although some progress has been made in hybrid processing techniques, more creative and ingenious combinations of different fabrication methods and FsLDW technology are of great significance for endowing the prepared stimulus-responsive structures with more comprehensive advantages, such as sophisticated geometric designability, high resolution, high surface quality, rapid processing capability, high efficiency, and low cost, thus promoting the realization of higher degrees of functionalization, integration, and industrialization.

More significantly, the potential applications should be expanded and truly put into use. We can broaden the application range of FsLDW-based stimulus-responsive structures in sensors and electronic devices by using advanced materials, such as graphene and liquid metal. For example, the synchronous reduction and nanopatterning technology of graphene oxide by a femtosecond laser can be utilized in the field of energy storage electronic devices. Liquid-metal-repellent polymer surfaces based on FsLDW-induced micro/nanostructures can be integrated for intelligent soft electronics. Furthermore, the development of intelligent responsive materials with high performance, multifunctionality, and compatibility for FsLDW is also a key point that cannot be ignored. At present, it is still difficult for stimulus-responsive smart structures manufactured by FsLDW to achieve large-scale industrial applications. The functional capabilities of these intelligent structures can perform well under laboratory conditions, but they may face many difficulties and failures in practical applications. For biomedical applications, the biocompatibility, biodegradability, and self-healing capabilities of stimulus-sensitive materials are crucial but quite challenging. For microrobotic applications, there is a critical need to further optimize the remote control means of stimulus-responsive structures to achieve more efficient and accurate control and meet the special requirements in complicated working environments such as complex biological microenvironments. Moreover, future-oriented functional stimulus-responsive structures need to be further improved in response sensitivity, reversible transformation ability, and response time.

Despite the as-presented challenges, the emerging field of FsLDW-based stimulus-responsive structures still has great prospects. It can be anticipated that various intelligent

structures integrating advanced stimulus-responsive functions and practical applications can be developed through more systematic in-depth research and interdisciplinary integration, which will undoubtedly open up new horizons and make great contributions for both scientific research and practical applications.

Acknowledgements

This work was supported by the National Natural Science Foundation of China (Nos. 52122511, 52105492, and 62005262), the National Key Research and Development Program of China (No. 2021YFF0502700), the Students' Innovation and Entrepreneurship Foundation of USTC (Nos. CY2022G32 and XY2022G02CY), the USTC Research Funds of the Double First-Class Initiative (No.YD2340002009), and CAS Project for Young Scientists in Basic Research (No. YSBR-049).

Table 1. Summary of various FsLDW-prepared stimulus-responsive structures, performances, and applications

Applications	Stimuli	Main materials	Functions	Critical performance	Ref.
Microrobotics	Magnetic	AZ IPS6090 photoresist, CrO_2/NdFeB, silicone elastomer	Microcilia/microrotor, micro-mechanical bits	Heterogeneous multi-material integration, 3D programmable magnetization, complex geometries	[173]
	Magnetic	PEG-DA, PE-TA, Fe_3O_4 nanoparticles	Microswimmer	Superior biodegradability, enhanced structural integrity	[181]
	Magnetic	AZ IPS6050 photoresist, Fe, polymeric materials	Multimaterial micromachines	Mechanical metal/polymer interlocking, unprecedented resolution/topological complexity, multi-locomotion strategies	[184]
	Magnetic	PEG-DA, permalloy Janus microparticle	Versatile micromachines	3D magnetic programmability, programmable deformation and motion, multimaterial integration	[185]
	Magnetic/pH	Blood-derived biomaterials, iron oxide nanoparticles	Micromachines	Multi-responsive, exceptional biocompatibility and biodegradability	[249]
	Light	LCE, acrylic resin IP-Dip, azo dye	Microscopic walkers	Multiple dynamic behaviors	[196]
	Light	LC networks, azobenzene	Microactuators	Deformation dynamics control, non-reciprocal movements, rapid response	[197]
	Light	NIPAM hydrogel, carbon nanotubes	Intelligent micromachines	Programmable shape-morphing, spatiotemporal controllability, microscale artificial heart	[201]
	Temperature/ light	PNIPAM hydrogel	3D heteromicrostructures	Highly localized crosslinking density control, large-amplitude response, complex and controllable actuation response	[18]
	Temperature	PNIPAM and PEG-DA hydrogel	Adhesive microrobot	Robust and biocompatible wet tissue adhesion/detachment	[205]
	Temperature	IP- Dip negative-tone photoresist	Thermoelastic metamaterials	Excellent motion controllability, sensitive thermal-driven behavior, reversible and stable	[206]
	Temperature	IPS780 photoresist, LCE	Microscale kirigami metastructures	Programmable and reconfigurable shape transformation, great scalability	[208]
	Temperature	LCE	Microactuators	Locally/spatially-controlled actuation, multimaterial hybrid integration	[207]
	pH	NIPAM/Acrylic acid (AAc)-based gels	Micromachines/ microtransformer	Programmable modular design, sophisticated shape transformation	[19]
	pH	BSA protein	3D smart microstructures	Controllable morphology and responsive properties, panda-face microrelief, microsieves	[116]
	pH	BSA protein, SU-8	Artificial musculoskeletal systems	Programmable and seamless muiti-material integration, sensitive response, good stability	[215]
	pH	NIPAM/AAc-based gels	Microjoints/ microcrawlers	Multiple controllable/encodable locomotion, excellent speed (0.15 body length s^{-1}) and efficiency (1.1 body length per step)	[218]
	pH	DMAEMA hydrogel	Microactuator	Precise microparticle manipulation, good reversibility/stability, deformation time of 1.2 s and recovery time of 0.3 s	[221]
	pH	AAc-based hydrogel	Microactuator	Multiple degrees of freedom, selective microparticle manipulation, high response speed (<500 ms)	[222]
	Humidity	PEG-DA hydrogel	Micro-worm robot	Motion on smooth glass surface, controllable and excellent carrying capacity	[227]
	Solvent	Methacrylate-based photopolymer	Microactuators	Tunable and reversible deformation, rapid response (1 s for 30% shrinkage, 0.4 s for recovery)	[241]
	Stress	IP-S and urethane(meth)acrylate resin	Microobject manipulator	Wide applicability (dry/wet, smooth/rough), unprecedented switching ratio > 10^4	[248]
Biomedical engineering	Magnetic/ light	IP-S photoresist, nickel, titanium	Targeted drug delivery	Superior locomotion capability, high payloads, strong protection, free from complex drug modification, rapid release	[176]
	Magnetic	TMPETA hydrogel, iron oxide nanoparticles	Therapeutic stem cell delivery	Precise motion control, high mechanical strength and stability	[179]
	Magnetic	IP-Dip photoresist, Fe	Sperm cell delivery/release	Biocompatibility, great swimming ability in complex biofluids	[183]
	Magnetic/ light	IP-S photoresist, iron oxide nanopowder, Au nanostars	Precise drug delivery	High drug-loading efficiency, drug release speed control, biocompatibility	[252]

	Magnetic	IP-S photoresist, nickel/titanium oxide	Neural networks connection	Precise alignment/connections mediation, reproducible/selective/precise connectivity	[257]
	Magnetic	IP-Dip photoresist, Fe	Targeted drug delivery	High propulsion in flowing blood, biocompatibility	[263]
	Light	Acrylamide-modified gelatin hydrogel, azobenzene molecule	Cell confining and stimulation	Great biocompatibility and biodegradability, on-demand mechanical stimulation	[57]
	pH/magnetic	AAc-based hydrogel, Fe_3O_4 nanoparticles	Targeted drug delivery	Complex functions, controllable drug encapsulation/release	[10]
	pH	PDMS, AAc-based hydrogel	Sustained drug release	Dynamic speed control, reversible switch gating, good versatility	[56]
	Solvent	β-cyclodextrin acrylamide and adamantane acrylamide-based host-guest hydrogel, TMPETA/PETA hydrogel	Cell stimulation	Inherent scalability, well-defined microenvironment, flexibility	[262]
Optical devices	Light	Thiol-ene photo-clickable resin, donor-acceptor Stenhouse adducts	3D photochromic microobjects	Reversible photoswitching, dynamic color-tuning, modularity, scalability, highly complex microstructure	[198]
	Temperature	PNIPAM-based hydrogel	Structural colors	Reversible, superior repeatability, convenient in-situ temperature monitoring	[92]
	Temperature	LCE	Polarization colors	Dynamic color-changing capabilities, temperature sensing	[209]
	Temperature	Photochromic glass doped with rare earth ions	Optical information storage	Excellent erasability/rewritability, 3D information storage, nondestructive reading	[269]
	Temperature	Developed AAc-based SMP resin	Reconfigurable nanophotonics	High-resolution reconfigurable structural color prints (DPI ~21 150) and holograms, programmable configuration	[276]
	pH	BSA protein	Artificial compound eyes	Uniform optical focusing capability, adjustable field of view (35 °~80 °), variable focal length (~400%), flexible optical component integration	[52]
	pH	Phenylboronic acid hydrogel	Volume diffractive gratings	Customized subsurface gratings	[274]
	pH	Modified AAc-based hydrogel	Submerged structural colors	Wide color range, reversible colorswitching, biocompatible operation, rapid response	[275]
	Humidity	PEG-DA hydrogel	Photonic-molecular microcavities	Controllable coupling, stable WGM emission, high quality factor ~2.9×10^3	[226]
	Humidity/ temperature	Supramolecular cholesteric LC photonic photoresist	Structural colors	Dual-responsive, high-resolution, feature size < 200 nm	[228]
	Solvent	Acrylamide-based hydrogel	Spiral photonic structures	Great spectral and structural color reproducibility/reversibility, wide gamut of structural colors, improved intensity, predictable uniform color	[236]
	Stress	Ductile stainless steel, polyvinyl siloxane elastomer	Structural colors	Reversible color change, no chemical/biochemical treatment, scalability	[240]
Multifunctional surfaces	Magnetic	Polystyrene SMP, PDMS, carbonyl iron powder	Dynamic regulation structured surfaces	Reversible switching of wettability/color/optical transparency, multiple novel functions	[50]
	Light	Epoxy SMP, RGO	Recoverable superhydrophobic surface	Sunlightdriven fast response, superior durability and chemical stability, complete recoverability	[200]
	Temperature	Epoxy SMP	Smart superhydrophobic surfaces	Anisotropic wettability transition, large-range adhesion switchablity, multifunction platform	[21]
	Electric	PDMS, paraffin, silver nanowires	Smart slippery surfaces	On-demand optical and wetting properties, good flexibility/reconfigurability, fast response (20 s action, 8 s recover), diverse liquids control	[237]
	Electric	PTFE, epoxy resin SMP, silver nanowires	Smart window	Reversible conversion of droplet adhesion and optical transparency, fast response within 60 s, in situ control, robust durability	[243]
	Stress/ magnetic	PTFE, PDMS, carbonyl iron powder, silicone	Tri-switchable wettability surface	In-situ reversible multiple wettability, multimaterial integration, simple but effective	[234]
Droplet/bubble manipulation	Magnetic	Polystyrene SMP, PDMS, carbonyl iron powder	3D multidroplet manipulation	Rapid horizontal propulsion (~58.6 mm s^{-1}), multidroplet parallel-capture/selective-release, continuous fluid and liquid metal manipulation	[51]
	Magnetic/ light	Silica gel, epoxy resin SMP, iron particles	Versatile droplet manipulation, information encryption	Noncontact in-situ reversible reconfiguration, dual response, multifunctionality	[142]

	Magnetic	PTFE, carbonyl iron powder, PDMS, silicone oil	Multi-substance transport	Multi-substance applicability, full-angle active transport, contactless microchemical reaction	[163]
	Magnetic	PTFE, carbonyl iron powder, PDMS	Multiple-droplet selective manipulation	Rapid droplet movement (~80 mm s^{-1}), programmable and multimodal manipulation	[288]
	Light	PDMS, candle-soot nanoparticles, silicone oil	Various prodrug droplets manipulation	Arbitrary-direction actuation (> 1.0 mm s^{-1}), nondestructive merging/sorting, self-cleaning/deicing ability, high-throughput drug toxicity screening	[289]
	Temperature	Diglycidyl ether of bisphenol A-based SMP	Bubble multi-manipulation	Controllable adhesion transition, full-direction loss-less bubble manipulation	[291]
	Humidity	GO membrane, soybean oil	Active and passive droplet manipulation	Enhanced trapping ability, biocompatibility, large deformation curvature (1.4 cm^{-1}), short response/recovery time (7.9/6 s)	[229]
	Stress	PDMS, silicone oil	Facile bubble manipulation	Simple regulation, in situ reversible wettability switching, great durability/repeatability	[290]

References

[1] Chen J, Wu J N and Yan S Z. 2015. Switchable wettability of the honeybee's tongue surface regulated by erectable glossal hairs. *J. Insect Sci*. **15**, 164.

[2] Teyssier J, Saenko S V, van der Marel D and Milinkovitch M C. 2015. Photonic crystals cause active colour change in chameleons. *Nat. Commun*. **6**, 6368.

[3] Reyssat E and Mahadevan L. 2009. Hygromorphs: from pine cones to biomimetic bilayers. *J. Roy. Soc. Interface* **6**, 951-957.

[4] Armon S, Efrati E, Kupferman R and Sharon E. 2011. Geometry and mechanics in the opening of chiral seed pods. *Science* **333**, 1726-1730.

[5] Elbaum R, Zaltzman L, Burgert I and Fratzl P. 2007. The role of wheat awns in the seed dispersal unit. *Science* **316**, 884-886.

[6] Volkov A G, Foster J C, Baker K D and Markin V S. 2010. Mechanical and electrical anisotropy in *Mimosa pudica* pulvini. *Plant Signal. Behav*. **5**, 1211-1221.

[7] Vandenbrink J P, Brown E A, Harmer S L and Blackman B K. 2014. Turning heads: the biology of solar tracking in sunflower. *Plant Sci*. **224**, 20-26.

[8] Li S, Zeng Y, Hou W, Wan W, Zhang J N, Wang Y L, Du X and Gu Z Z. 2020. Photo-responsive photonic hydrogel: *in situ* manipulation and monitoring of cell scaffold stiffness. *Mater. Horiz*. **7**, 2944-2950.

[9] Gelmi A and Schutt C E. 2021. Stimuli-responsive biomaterials: scaffolds for stem cell control. *Adv. Healthcare Mater*. **10**, 2001125.

[10] Xin C *et al*. 2021. Environmentally adaptive shape-morphing microrobots for localized cancer cell treatment. *ACS Nano* **15**, 18048-18059.

[11] Zhang Q Y, He L L, Zhang X F, Tian D L and Jiang L. 2020. Switchable direction of liquid transport *via* an anisotropic microarray surface and thermal stimuli. *ACS Nano* **14**, 1436-1444.

[12] Qu M N, Ma L L, Wang J X, Zhang Y, Zhao Y, Zhou Y C, Liu X R and He J M. 2019. Multifunctional superwettable material with smart pH responsiveness for efficient and controllable oil/water separation and emulsified wastewater purification. *ACS Appl. Mater. Interfaces* **11**, 24668-24682.

[13] Zhao Y H, Wu Y, Wang L, Zhang M M, Chen X, Liu M J, Fan J, Liu J Q, Zhou F and Wang Z K. 2017. Bio-inspired reversible underwater adhesive. *Nat. Commun*. **8**, 2218.

[14] Xiao Y Y, Jiang Z C, Tong X and Zhao Y. 2019. Biomimetic locomotion of electrically powered "janus" soft robots using a liquid crystal polymer. *Adv. Mater*. **31**, 1903452.

[15] Ze Q J, Kuang X, Wu S, Wong J, Montgomery S M, Zhang R D, Kovitz J M, Yang F Y, Qi H J and Zhao R K. 2020. Magnetic shape memory polymers with integrated multifunctional shape manipulation. *Adv. Mater*. **32**, 1906657.

[16] Xin C *et al*. 2019. Conical hollow microhelices with superior swimming capabilities for targeted cargo delivery. *Adv. Mater*. **31**, 1808226.

[17] Hines L, Petersen K, Lum G Z and Sitti M. 2017. Soft actuators for small-scale robotics. *Adv. Mater*. **29**, 1603483.

[18] Hippler M, Blasco E, Qu J Y, Tanaka M, Barner-Kowollik C, Wegener M and Bastmeyer M. 2019. Controlling the shape of 3D microstructures by temperature and light. *Nat. Commun*. **10**, 232.

[19] Huang T Y, Huang H W, Jin D D, Chen Q Y, Huang J Y, Zhang L and Duan H L. 2020. Four-dimensional micro-building blocks. *Sci. Adv*. **6**, eaav8219.

[20] Xia Y L, He Y, Zhang F H, Liu Y J and Leng J S. 2021. A review of shape memory polymers and composites: mechanisms, materials, and applications. *Adv. Mater*. **33**, 2000713.

[21] Bai X, Yang Q, Fang Y, Yong J L, Bai Y K, Zhang J W, Hou X and Chen F. 2020. Anisotropic, adhesion-switchable, and thermal-responsive superhydrophobicity on the femtosecond laser-structured shape-memory polymer for droplet manipulation. *Chem. Eng. J*. **400**, 125930.

[22] del Pozo M, Sol J A H P, Schenning A P H J and Debije M G. 2022. 4D printing of liquid crystals: what's right for me?. *Adv. Mater*. **34**, 2104390.

[23] White T J and Broer D J. 2015. Programmable and adaptive mechanics with liquid crystal polymer networks and elastomers. *Nat. Mater*. **14**, 1087-1098.

[24] Ran C, Wang J C, He Y G, Ren Q, Hu H, Zhu J Q, Gu X X, Li M, Zheng L and Li J. 2022. Recent advances in bioinspired hydrogels with environment-responsive characteristics for biomedical applications. *Macromol. Biosci*. **22**, 2100474.

[25] Downs F G, Lunn D J, Booth M J, Sauer J B, Ramsay W J, Klemperer R G, Hawker C J and Bayley H. 2020. Multi-responsive hydrogel structures from patterned droplet networks. *Nat. Chem*. **12**, 363-371.

[26] Apsite I, Salehi S and Ionov L. 2022. Materials for smart soft actuator systems. *Chem. Rev*. **122**, 1349-1415.

[27] Li J H and Pumera M. 2021. 3D printing of functional microrobots. *Chem. Soc. Rev*. **50**, 2794-2838.

[28] Wallin T J, Pikul J and Shepherd R F. 2018. 3D printing of soft robotic systems. *Nat. Rev. Mater*. **3**, 84-100.

[29] Wu D, Leng Y M, Fan C J, Xu Z Y, Li L, Shi L Y, Yang K K and Wang Y Z. 2022. 4D printing of a fully biobased shape memory copolyester via a UV-assisted FDM strategy. *ACS Sustain. Chem. Eng*. **10**, 6304-6312.

[30] Kuang X, Roach D J, Wu J T, Hamel C M, Ding Z, Wang T J, Dunn M L and Qi H J. 2019. Advances in 4D printing: materials and applications. *Adv. Funct. Mater*. **29**, 1805290.

[31] Jiang P, Zhang Y X, Mu X X, Liu D S, Liu Y H, Guo R, Ji Z Y, Wang X Z and Wang X L. 2022. Grayscale stereolithography of gradient hydrogel with site-selective shape deformation. *Adv. Mater. Technol*. **7**, 2101288.

[32] Zhang Y H, Zhang F, Yan Z, Ma Q, Li X L, Huang Y G and Rogers J A. 2017. Printing, folding and assembly methods for forming 3D mesostructures in advanced materials. *Nat. Rev. Mater*. **2**, 17019.

[33] Namvar N, Zolfagharian A, Vakili-Tahami F and Bodaghi M. 2022. Reversible energy absorption of elasto-plastic auxetic, hexagonal, and AuxHex structures fabricated by FDM 4D printing. *Smart Mater. Struct*. **31**, 055021.

[34] Huang H W, Sakar M S, Petruska A J, Pané S and Nelson B J. 2016. Soft micromachines with programmable motility and morphology. *Nat. Commun*. **7**, 12263.

[35] Kachwal V and Tan J C. 2023. Stimuli-responsive electrospun fluorescent fibers augmented with aggregation-induced emission (AIE) for smart applications. *Adv. Sci*. **10**, 2204848.

[36] Wang W, Li P F, Xie R, Ju X J, Liu Z and Chu L Y. 2022. Designable micro-/nano-structured smart polymeric materials. *Adv. Mater*. **34**, 2107877.

[37] Jaiswal A, Rastogi C K, Rani S, Singh G P, Saxena S and Shukla S. 2023. Two decades of two-photon lithography: materials science perspective for additive manufacturing of 2D/3D nano-microstructures. *iScience* **26**, 106374.

[38] Greant C, Van Durme B, Van Hoorick J and Van Vlierberghe S. 2023. Multiphoton lithography as a promising tool for biomedical applications. *Adv. Funct. Mater*. 2212641.

[39] Xu Y, Yu G, Nie R Q and Wu Z G. 2022. Microfluidic systems toward blood hemostasis monitoring and thrombosis diagnosis: from design principles to micro/nano fabrication technologies. *VIEW* **3**, 20200183.
[40] Zhan Y, Cheng Q F, Song Y L and Li M Z. 2022. Micro-nano structure functionalized perovskite optoelectronics: from structure functionalities to device applications. *Adv. Funct. Mater.* **32**, 2200385.
[41] Huang Z Y, Shao G B and Li L Q. 2023. Micro/nano functional devices fabricated by additive manufacturing. *Prog. Mater. Sci.* **131**, 101020.
[42] Sugioka K and Cheng Y. 2014. Ultrafast lasers—reliable tools for advanced materials processing. *Light Sci. Appl.* **3**, e149.
[43] Sugioka K. 2019. Hybrid femtosecond laser three-dimensional micro-and nanoprocessing: a review. *Int. J. Extrem. Manuf.* **1**, 012003.
[44] Liu H G, Lin W X and Hong M H. 2021. Hybrid laser precision engineering of transparent hard materials: challenges, solutions and applications. *Light Sci. Appl.* **10**, 162.
[45] Chen Z J, Yang J, Liu H B, Zhao Y X and Pan R. 2022. A short review on functionalized metallic surfaces by ultrafast laser micromachining. *Int. J. Adv. Manuf. Technol.* **119**, 6919-6948.
[46] Wang J S, Fang F Z, An H J, Wu S, Qi H M, Cai Y X and Guo G Y. 2023. Laser machining fundamentals: micro, nano, atomic and close-to-atomic scales. *Int. J. Extrem. Manuf.* **5**, 012005.
[47] Lin Z Y and Hong M H. 2021. Femtosecond laser precision engineering: from micron, submicron, to nanoscale. *Ultrafast Sci.* **2021**, 9783514.
[48] Wang A D, Sopeña P and Grojo D. 2022. Burst mode enabled ultrafast laser inscription inside gallium arsenide. *Int. J. Extrem. Manuf.* **4**, 045001.
[49] Liu H, Zhang L, Huang J Y, Mao J J, Chen Z, Mao Q H, Ge M Z and Lai Y K. 2022. Smart surfaces with reversibly switchable wettability: concepts, synthesis and applications. *Adv. Colloid Interface Sci.* **300**, 102584.
[50] Jiang S J *et al*. 2019. Multifunctional janus microplates arrays actuated by magnetic fields for water/light switches and bio-inspired assimilatory coloration. *Adv. Mater.* **31**, 1807507.
[51] Jiang S J *et al*. 2020. Three-dimensional multifunctional magnetically responsive liquid manipulator fabricated by femtosecond laser writing and soft transfer. *Nano Lett.* **20**, 7519-7529.
[52] Ma Z C, Hu X Y, Zhang Y L, Liu X Q, Hou Z S, Niu L G, Zhu L, Han B, Chen Q D and Sun H B. 2019. Smart compound eyes enable tunable imaging. *Adv. Funct. Mater.* **29**, 1903340.
[53] Hou Z S, Sun S M, Zheng B Y, Yang R Z and Li A W. 2015. Stimuli-responsive protein-based micro/nano-waveguides. *RSC Adv.* **5**, 77847-77850.
[54] He Z Q, Lee Y H, Chanda D and Wu S T. 2018. Adaptive liquid crystal microlens array enabled by two-photon polymerization. *Opt. Express* **26**, 21184-21193.
[55] Jin D D, Chen Q Y, Huang T Y, Huang J Y, Zhang L and Duan H L. 2020. Four-dimensional direct laser writing of reconfigurable compound micromachines. *Mater. Today* **32**, 19-25.
[56] Zhang J *et al*. 2022. Ultrafast laser-ablated bioinspired hydrogel-based porous gating system for sustained drug release. *ACS Appl. Mater. Interfaces* **14**, 35366-35375.
[57] Pennacchio F A, Fedele C, De Martino S, Cavalli S, Vecchione R and Netti P A. 2018. Three-dimensional microstructured azobenzene-containing gelatin as a photoactuable cell confining system. *ACS Appl. Mater. Interfaces* **10**, 91-97.
[58] Eaton S M, Cerullo G and Osellame R. 2012. Fundamentals of femtosecond laser modification of bulk dielectrics. *In Femtosecond Laser Micromachining* (eds Osellame R, Cerullo G & Ramponi R). 3-18. (Springer, Berlin).
[59] Schaffer C B, Brodeur A and Mazur E. 2001. Laser-induced breakdown and damage in bulk transparent materials induced by tightly focused femtosecond laser pulses. *Meas. Sci. Technol.* **12**, 1784-1794.
[60] Stoian R, Rosenfeld A, Ashkenasi D, Hertel I V, Bulgakova N M and Campbell E E B. 2002. Surface charging and impulsive ion ejection during ultrashort pulsed laser ablation. *Phys. Rev. Lett.* **88**, 097603.
[61] Nedialkov N N, Imamova S E and Atanasov P A. 2004. Ablation of metals by ultrashort laser pulses. *J. Phys. D: Appl. Phys.* **37**, 638-643.
[62] Ashitkov S I, Komarov P S, Ovchinnikov A V, Struleva E V, Zhakhovskii V V, Inogamov N A and Agranat M B. 2014. Ablation and nanostructuring of metals by femtosecond laser pulses. *Quantum Electron.* **44**, 535-539.
[63] Anisimov S I and Luk'yanchuk B S. 2002. Selected problems of laser ablation theory. *Phys.-Usp.* **45**, 293-324.
[64] Yang J, Zhao Y and Zhu X. 2007. Theoretical studies of ultrafast ablation of metal targets dominated by phase explosion. *Appl. Phys. A* **89**, 571-578.
[65] Bulgakova N M and Bourakov I M. 2002. Phase explosion under ultrashort pulsed laser ablation: modeling with analysis of metastable state of melt. *Appl. Surf. Sci.* **197-198**, 41-44.
[66] Bouilly D, Perez D and Lewis L J. 2007. Damage in materials following ablation by ultrashort laser pulses: a molecular-dynamics study. *Phys. Rev. B* **76**, 184119.
[67] Perez D and Lewis L J. 2002. Ablation of solids under femtosecond laser pulses. *Phys. Rev. Lett.* **89**, 255504.
[68] von der Linde D, Sokolowski-Tinten K and Bialkowski J. 1997. Laser–solid interaction in the femtosecond time regime. *Appl. Surf. Sci.* **109-110**, 1-10.
[69] Rethfeld B, Sokolowski-Tinten K, von der Linde D and Anisimov S I. 2004. Timescales in the response of materials to femtosecond laser excitation. *Appl. Phys. A* **79**, 767-769.
[70] Hohlfeld J, Wellershoff S S, Güdde J, Conrad U, Jähnke V and Matthias E. 2000. Electron and lattice dynamics following optical excitation of metals. *Chem. Phys.* **251**, 237-258.
[71] Liu X, Du D and Mourou G. 1997. Laser ablation and micromachining with ultrashort laser pulses. *IEEE J. Quantum Electron.* **33**, 1706-1716.
[72] Mannion P T, Magee J, Coyne E, O'Connor G M and Glynn T J. 2004. The effect of damage accumulation behaviour on ablation thresholds and damage morphology in ultrafast laser micro-machining of common metals in air. *Appl. Surf. Sci.* **233**, 275-287.
[73] Anisimov S I, Kapeliovich B L and Perel'man T L. 1974. Electron emission from metal surfaces exposed to ultrashort laser pulses. *Sov. Phys.-JETP* **39**, 375-377.
[74] Jiang L and Tsai H L. 2005. Improved two-temperature model and its application in ultrashort laser heating of metal films. *J. Heat Transfer* **127**, 1167-1173.
[75] Darkins R and Duffy D M. 2018. Modelling radiation effects in solids with two-temperature molecular dynamics. *Comp. Mater. Sci.* **147**, 145-153.
[76] Povarnitsyn M E, Fokin V B and Levashov P R. 2015. Microscopic and macroscopic modeling of femtosecond laser ablation of metals. *Appl. Surf. Sci.* **357**, 1150-1156.
[77] Li X and Jiang L. 2012. Size distribution control of metal nanoparticles using femtosecond laser pulse train: a molecular dynamics simulation. *Appl. Phys. A* **109**, 367-376.

[78] Ahmmed K M T, Grambow C and Kietzig A M. 2014. Fabrication of micro/nano structures on metals by femtosecond laser micromachining. *Micromachines* **5**, 1219-1253.
[79] Sundaram S K and Mazur E. 2002. Inducing and probing non-thermal transitions in semiconductors using femtosecond laser pulses. *Nat. Mater.* **1**, 217-224.
[80] Balling P and Schou J. 2013. Femtosecond-laser ablation dynamics of dielectrics: basics and applications for thin films. *Rep. Prog. Phys.* **76**, 036502.
[81] Mihailov S J, Grobnic D, Hnatovsky C, Walker R B, Lu P, Coulas D and Ding H M. 2017. Extreme environment sensing using femtosecond laser-inscribed fiber bragg gratings. *Sensors* **17**, 2909.
[82] Wu M T, Guo B, Zhao Q L, He P, Zeng Z Q and Zang J. 2018. The influence of the ionization regime on femtosecond laser beam machining mono-crystalline diamond. *Opt. Laser Technol.* **106**, 34-39.
[83] Henyk M, Mitzner R, Wolfframm D and Reif J. 2000. Laser-induced ion emission from dielectrics. *Appl. Surf. Sci.* **154-155**, 249-255.
[84] Maruo S, Nakamura O and Kawata S. 1997. Three-dimensional microfabrication with two-photon-absorbed photopolymerization. *Opt. Lett.* **22**, 132-134.
[85] Skliutas E, Lebedevaite M, Kabouraki E, Baldacchini T, Ostrauskaite J, Vamvakaki M, Farsari M, Juodkazis S and Malinauskas M. 2021. Polymerization mechanisms initiated by spatio-temporally confined light. *Nanophotonics* **10**, 1211-1242.
[86] Gonzalez-Hernandez D, Varapnickas S, Bertoncini A, Liberale C and Malinauskas M. 2023. Micro-optics 3D printed via multi-photon laser lithography. *Adv. Opt. Mater.* **11**, 2201701.
[87] Cumpston B H *et al*. 1999. Two-photon polymerization initiators for three-dimensional optical data storage and microfabrication. *Nature* **398**, 51-54.
[88] Bin F C, Guo M, Li T, Zheng Y C, Dong X Z, Liu J, Jin F and Zheng M L. 2023. Carbazole-based anion ionic water-soluble two-photon initiator for achieving 3D hydrogel structures. *Adv. Funct. Mater.* 2300293.
[89] Harinarayana V and Shin Y C. 2021. Two-photon lithography for three-dimensional fabrication in micro/nanoscale regime: a comprehensive review. *Opt. Laser Technol.* **142**, 107180.
[90] Liaros N and Fourkas J T. 2017. The characterization of absorptive nonlinearities. *Laser Photonics Rev.* **11**, 1700106.
[91] Fischer J, Mueller J B, Kaschke J, Wolf T J A, Unterreiner A N and Wegener M. 2013. Three-dimensional multi-photon direct laser writing with variable repetition rate. *Opt. Express* **21**, 26244-26260.
[92] Liu K L, Ding H B, Li S, Niu Y F, Zeng Y, Zhang J N, Du X and Gu Z Z. 2022. 3D printing colloidal crystal microstructures via sacrificial-scaffold-mediated two-photon lithography. *Nat. Commun.* **13**, 4563.
[93] Wang X D, Yu H B, Li P W, Zhang Y Z, Wen Y D, Qiu Y, Liu Z, Li Y P and Liu L Q. 2021. Femtosecond laser-based processing methods and their applications in optical device manufacturing: a review. *Opt. Laser Technol.* **135**, 106687.
[94] Xing J F, Dong X Z, Chen W Q, Duan X M, Takeyasu N, Tanaka T and Kawata S. 2007. Improving spatial resolution of two-photon microfabrication by using photoinitiator with high initiating efficiency. *Appl. Phys. Lett.* **90**, 131106.
[95] Ligon S C, Husár B, Wutzel H, Holman R and Liska R. 2014. Strategies to reduce oxygen inhibition in photoinduced polymerization. *Chem. Rev.* **114**, 557-589.
[96] Yang L, Münchinger A, Kadic M, Hahn V, Mayer F, Blasco E, Barner-Kowollik C and Wegener M. 2019. On the schwarzschild effect in 3D two-photon laser lithography. *Adv. Opt. Mater.* **7**, 1901040.
[97] Bauer J, Guell Izard A, Zhang Y F, Baldacchini T and Valdevit L. 2019. Programmable mechanical properties of two-photon polymerized materials: from nanowires to bulk. *Adv. Mater. Technol.* **4**, 1900146.
[98] Henning I, Woodward A W, Rance G A, Paul B T, Wildman R D, Irvine D J and Moore J C. 2020. A click chemistry strategy for the synthesis of efficient photoinitiators for two-photon polymerization. *Adv. Funct. Mater.* **30**, 2006108.
[99] Xia H, Wang J, Tian Y, Chen Q D, Du X B, Zhang Y L, He Y and Sun H B. 2010. Ferrofluids for fabrication of remotely controllable micro-nanomachines by two-photon polymerization. *Adv. Mater.* **22**, 3204-3207.
[100] Xin C *et al*. 2022. Rapid and multimaterial 4D printing of shape-morphing micromachines for narrow micronetworks traversing. *Small* **18**, 2202272.
[101] Ennis A, Nicdao D, Kolagatla S, Dowling L, Tskhe Y, Thompson A J, Trimble D, Delaney C and Florea L. 2023. Two-photon polymerization of sugar responsive 4D microstructures. *Adv. Funct. Mater.* 2213947.
[102] Sugioka K and Cheng Y. 2014. Femtosecond laser three-dimensional micro- and nanofabrication. *Appl. Phys. Rev.* **1**, 041303.
[103] Kawata S, Sun H B, Tanaka T and Takada K. 2001. Finer features for functional microdevices. *Nature* **412**, 697-698.
[104] Calin B S and Paun I A. 2022. A review on stimuli-actuated 3D micro/nanostructures for tissue engineering and the potential of laser-direct writing via two-photon polymerization for structure fabrication. *Int. J. Mol. Sci.* **23**, 14270.
[105] Seet K K, Mizeikis V, Matsuo S, Juodkazis S and Misawa H. 2005. Three-dimensional spiral-architecture photonic crystals obtained by direct laser writing. *Adv. Mater.* **17**, 541-545.
[106] Dadras-Toussi O, Khorrami M, Louis Sam Titus A S C, Majd S, Mohan C and Abidian M R. 2022. Multiphoton lithography of organic semiconductor devices for 3D printing of flexible electronic circuits, biosensors, and bioelectronics. *Adv. Mater.* **34**, 2200512.
[107] Jia Y X *et al*. 2022. Covalent adaptable microstructures via combining two-photon laser printing and alkoxyamine chemistry: toward living 3D microstructures. *Adv. Funct. Mater.* 2207826.
[108] Gauci S C, Gernhardt M, Frisch H, Houck H A, Blinco J P, Blasco E, Tuten B T and Barner-Kowollik C. 2022. 3D printed microstructures erasable by darkness. *Adv. Funct. Mater.* 2206303.
[109] Ocier C R *et al*. 2020. Direct laser writing of volumetric gradient index lenses and waveguides. *Light Sci. Appl.* **9**, 196.
[110] Aderneuer T, Fernández O and Ferrini R. 2021. Two-photon grayscale lithography for free-form micro-optical arrays. *Opt. Express* **29**, 39511-39520.
[111] Porte X, Dinc N U, Moughames J, Panusa G, Juliano C, Kadic M, Moser C, Brunner D and Psaltis D. 2021. Direct (3+1)D laser writing of graded-index optical elements. *Optica* **8**, 1281-1287.
[112] Sun Y L, Dong W F, Niu L G, Jiang T, Liu D X, Zhang L, Wang Y S, Chen Q D, Kim D P and Sun H B. 2014. Protein-based soft micro-optics fabricated by femtosecond laser direct writing. *Light Sci. Appl.* **3**, e129.
[113] Serbin J, Egbert A, Ostendorf A, Chichkov B, Houbertz R, Domann G, Schulz J, Cronauer C, Fröhlich L and Popall M. 2003. Femtosecond laser-induced two-photon polymerization of inorganic–organic hybrid materials for applications in photonics. *Opt. Lett.* **28**, 301-303.

[114] Tian Z N, Yao W G, Xu J J, Yu Y H, Chen Q D and Sun H B. 2015. Focal varying microlens array. *Opt. Lett.* **40**, 4222-4225.
[115] Zhang Y L, Chen Q D, Xia H and Sun H B. 2010. Designable 3D nanofabrication by femtosecond laser direct writing. *Nano Today* **5**, 435-448.
[116] Wei S X, Liu J, Zhao Y Y, Zhang T B, Zheng M L, Jin F, Dong X Z, Xing J F and Duan X M. 2017. Protein-based 3D microstructures with controllable morphology and pH-responsive properties. *ACS Appl. Mater. Interfaces* **9**, 42247-42257.
[117] Li Q, Kulikowski J, Doan D, Tertuliano O A, Zeman C J, Wang M M, Schatz G C and Gu X W. 2022. Mechanical nanolattices printed using nanocluster-based photoresists. *Science* **378**, 768-773.
[118] Huang Z J, Tsui G C P, Deng Y and Tang C Y. 2020. Two-photon polymerization nanolithography technology for fabrication of stimulus-responsive micro/nano-structures for biomedical applications. *Nanotechnol. Rev.* **9**, 1118-1136.
[119] Lao Z X, Xia N, Wang S J, Xu T T, Wu X Y and Zhang L. 2021. Tethered and untethered 3D microactuators fabricated by two-photon polymerization: a review. *Micromachines* **12**, 465.
[120] Ren L Q, Nama N, Mcneill J M, Soto F, Yan Z F, Liu W, Wang W, Wang J and Mallouk T E. 2019. 3D steerable, acoustically powered microswimmers for single-particle manipulation. *Sci. Adv.* **5**, eaax3084.
[121] Jeon S *et al*. 2019. Magnetically actuated microrobots as a platform for stem cell transplantation. *Sci. Robot.* **4** eaav4317.
[122] Li G Q *et al*. 2016. Multifunctional ultrathin aluminum foil: oil/water separation and particle filtration. *J. Mater. Chem. A* **4**, 18832-18840.
[123] Albu C, Dinescu A, Filipescu M, Ulmeanu M and Zamfirescu M. 2013. Periodical structures induced by femtosecond laser on metals in air and liquid environments. *Appl. Surf. Sci.* **278**, 347-351.
[124] Zhang Z *et al*. 2017. A Janus oil barrel with tapered microhole arrays for spontaneous high-flux spilled oil absorption and storage. *Nanoscale* **9**, 15796-15803.
[125] Wu D *et al*. 2020. High-performance unidirectional manipulation of microdroplets by horizontal vibration on femtosecond laser-induced slant microwall arrays. *Adv. Mater.* **32**, 2005039.
[126] Jia T Q, Chen H X, Huang M, Zhao F L, Qiu J R, Li R X, Xu Z Z, He X K, Zhang J and Kuroda H. 2005. Formation of nanogratings on the surface of a ZnSe crystal irradiated by femtosecond laser pulses. *Phys. Rev. B* **72**, 125429.
[127] van Driel H M, Sipe J E and Young J F. 1982. Laser-induced periodic surface structure on solids: a universal phenomenon. *Phys. Rev. Lett.* **49**, 1955-1958.
[128] Birnbaum M. 1965. Semiconductor surface damage produced by ruby lasers. *J. Appl. Phys.* **36**, 3688-3689.
[129] Wang Y, Wang Y Y and Zhdanov A. 2019. Review of femtosecond laser induced surface periodic structure. *In Proceedings of SPIE 11193, Nanophotonics and Micro/Nano Optics V*. (SPIE, Hangzhou, China).
[130] Zhang D S, Liu R J and Li Z G. 2022. Irregular LIPSS produced on metals by single linearly polarized femtosecond laser. *Int. J. Extrem. Manuf.* **4**, 015102.
[131] Volkov S N, Kaplan A E and Miyazaki K. 2009. Evanescent field at nanocorrugated dielectric surface. *Appl. Phys. Lett.* **94**, 041104.
[132] Rudenko A, Mauclair C, Garrelie F, Stoian R and Colombier J P. 2019. Self-organization of surfaces on the nanoscale by topography-mediated selection of quasi-cylindrical and plasmonic waves. *Nanophotonics* **8**, 459-465.
[133] Sipe J E, Young J F, Preston J S and van Driel H M. 1983. Laser-induced periodic surface structure. I. Theory. *Phys. Rev. B* **27**, 1141-1154.
[134] Bonse J, Rosenfeld A and Krüger J. 2009. On the role of surface plasmon polaritons in the formation of laser-induced periodic surface structures upon irradiation of silicon by femtosecond-laser pulses. *J. Appl. Phys.* **106**, 104910.
[135] Nathala C S R, Ajami A, Ionin A A, Kudryashov S I, Makarov S V, Ganz T, Assion A and Husinsky W. 2015. Experimental study of fs-laser induced sub-100-nm periodic surface structures on titanium. *Opt. Express* **23**, 5915-5929.
[136] Wu M T, Guo B, Zhao Q L, Fan R W, Dong Z W and Yu X. 2018. The influence of the focus position on laser machining and laser micro-structuring monocrystalline diamond surface. *Opt. Laser. Eng.* **105**, 60-67.
[137] Qi L T, Nishii K and Namba Y. 2009. Regular subwavelength surface structures induced by femtosecond laser pulses on stainless steel. *Opt. Lett.* **34**, 1846-1848.
[138] Liu Y, Li S Y, Niu S C, Cao X W, Han Z W and Ren L Q. 2016. Bio-inspired micro-nano structured surface with structural color and anisotropic wettability on Cu substrate. *Appl. Surf. Sci.* **379**, 230-237.
[139] Bonse J, Koter R, Hartelt M, Spaltmann D, Pentzien S, Höhm S, Rosenfeld A and Krüger J. 2015. Tribological performance of femtosecond laser-induced periodic surface structures on titanium and a high toughness bearing steel. *Appl. Surf. Sci.* **336**, 21-27.
[140] Long J Y, Fan P X, Zhong M L, Zhang H J, Xie Y D and Lin C. 2014. Superhydrophobic and colorful copper surfaces fabricated by picosecond laser induced periodic nanostructures. *Appl. Surf. Sci.* **311**, 461-467.
[141] Jiang H B, Zhang Y L, Liu Y, Fu X Y, Li Y F, Liu Y Q, Li C H and Sun H B. 2016. Bioinspired few-layer graphene prepared by chemical vapor deposition on femtosecond laser-structured Cu foil. *Laser Photonics Rev.* **10**, 441-450.
[142] Li C Z *et al*. 2021. Noncontact all-in-situ reversible reconfiguration of femtosecond laser-induced shape memory magnetic microcones for multifunctional liquid droplet manipulation and information encryption. *Adv. Funct. Mater.* **31**, 2100543.
[143] Wu J R, He J, Yin K, Zhu Z, Xiao S, Wu Z P and Duan J A. 2021. Robust hierarchical porous PTFE film fabricated via femtosecond laser for self-cleaning passive cooling. *Nano Lett.* **21**, 4209-4216.
[144] Guo Y, Qiu P, Xu S L and Cheng G J. 2022. Laser-induced microjet-assisted ablation for high-quality microfabrication. *Int. J. Extrem. Manuf.* **4**, 035101.
[145] Sohn I B, Choi H K, Noh Y C, Kim J and Ahsan S. 2019. Laser assisted fabrication of micro-lens array and characterization of their beam shaping property. *Appl. Surf. Sci.* **479**, 375-385.
[146] Shimotsuma Y, Hirao K, Kazansky P G and Qiu J R. 2005. Three-dimensional micro-and nano-fabrication in transparent materials by femtosecond laser. *Jpn. J. Appl. Phys.* **44**, 4735-4748.
[147] Chen F and de Aldana J R V. 2014. Optical waveguides in crystalline dielectric materials produced by femtosecond-laser micromachining. *Laser Photonics Rev.* **8**, 251-275.
[148] Zhang X L, Yu F, Chen Z G, Tian Z N, Chen Q D, Sun H B and Ma G C. 2022. Non-Abelian braiding on photonic chips. *Nat. Photonics* **16**, 390-395.
[149] Wei D Z *et al*. 2018. Experimental demonstration of a three-dimensional lithium niobate nonlinear photonic crystal. *Nat. Photonics* **12**, 596-600.

[150] Liao C R, Li Y H, Wang D N, Sun T and Grattan K T V. 2010. Morphology and thermal stability of fiber bragg gratings for sensor applications written in H_2-free and H_2-loaded fibers by femtosecond laser. *IEEE Sens. J.* **10**, 1675-1681.

[151] Zhang C, Dong N N, Yang J, Chen F, de Aldana J R V and Lu Q M. 2011. Channel waveguide lasers in Nd:GGG crystals fabricated by femtosecond laser inscription. *Opt. Express* **19**, 12503-12508.

[152] Jia Y C, Dong N N, Chen F, de Aldana J R V, Akhmadaliev S and Zhou S Q. 2012. Continuous wave ridge waveguide lasers in femtosecond laser micromachined ion irradiated Nd: YAG single crystals. *Opt. Mater. Express* **2**, 657-662.

[153] Ams M, Dekker P, Marshall G D and Withford M J. 2012. Ultrafast laser-written dual-wavelength waveguide laser. *Opt. Lett.* **37**, 993-995.

[154] Della Valle G, Taccheo S, Osellame R, Festa A, Cerullo G and Laporta P. 2007. 1.5 μm single longitudinal mode waveguide laser fabricated by femtosecond laser writing. *Opt. Express* **15**, 3190-3194.

[155] Wang M H, Zhao K H, Wu J Y, Li Y Q, Yang Y, Huang S, Zhao J R, Tweedle T, Carpenter D and Zheng G Q. 2021. Femtosecond laser fabrication of nanograting-based distributed fiber sensors for extreme environmental applications. *Int. J. Extrem. Manuf.* **3**, 025401.

[156] Watanabe W, Asano T, Yamada K, Itoh K and Nishii J. 2003. Wavelength division with three-dimensional couplers fabricated by filamentation of femtosecond laser pulses. *Opt. Lett.* **28**, 2491-2493.

[157] Butkutė A and Jonušauskas L. 2021. 3D manufacturing of glass microstructures using femtosecond laser. *Micromachines* **12**, 499.

[158] Itoh K, Watanabe W, Nolte S and Schaffer C B. 2006. Ultrafast processes for bulk modification of transparent materials. *MRS Bull.* **31**, 620-625.

[159] Sakakura M, Lei Y H, Wang L, Yu Y H and Kazansky P G. 2020. Ultralow-loss geometric phase and polarization shaping by ultrafast laser writing in silica glass. *Light Sci. Appl.* **9**, 15.

[160] Sun Y K, Zhang X L, Yu F, Tian Z N, Chen Q D and Sun H B. 2022. Non-Abelian Thouless pumping in photonic waveguides. *Nat. Phys.* **18**, 1080-1085.

[161] Wolf A, Dostovalov A, Bronnikov K and Babin S. 2019. Arrays of fiber Bragg gratings selectively inscribed in different cores of 7-core spun optical fiber by IR femtosecond laser pulses. *Opt. Express* **27**, 13978-13990.

[162] Li Y, Liu H G and Hong M H. 2020. High-quality sapphire microprocessing by dual-beam laser induced plasma assisted ablation. *Opt. Express* **28**, 6242-6250.

[163] Shao K X, Jiang S J, Hu Y L, Zhang Y Y, Li C Z, Zhang Y X, Li J W, Wu D and Chu J R. 2022. Bioinspired lubricated slippery magnetic responsive microplate array for high performance multi-substance transport. *Adv. Funct. Mater.* **32**, 2205831.

[164] Deng C, Kim H and Ki H. 2019. Fabrication of a compound infrared microlens array with ultrashort focal length using femtosecond laser-assisted wet etching and dual-beam pulsed laser deposition. *Opt. Express* **27**, 28679-28691.

[165] Liu X Q, Bai B F, Chen Q D and Sun H B. 2019. Etching-assisted femtosecond laser modification of hard materials. *Opto Electron. Adv.* **2**, 190021.

[166] Juodkazis S, Nishimura K, Misawa H, Ebisui T, Waki R, Matsuo S and Okada T. 2006. Control over the crystalline state of sapphire. *Adv. Mater.* **18**, 1361-1364.

[167] Liu X Q, Yang S N, Yu L, Chen Q D, Zhang Y L and Sun H B. 2019. Rapid engraving of artificial compound eyes from curved sapphire substrate. *Adv. Funct. Mater.* **29**, 1900037.

[168] Ródenas A, Gu M, Corrielli G, Paiè P, John S, Kar A K and Osellame R. 2019. Three-dimensional femtosecond laser nanolithography of crystals. *Nat. Photonics* **13**, 105-109.

[169] Liu H G, Li Y, Lin W X and Hong M H. 2020. High-aspect-ratio crack-free microstructures fabrication on sapphire by femtosecond laser ablation. *Opt. Laser Technol.* **132**, 106472.

[170] Li M J, Yang T Z, Yang Q, Fang Z, Bian H, Zhang C J, Hou X and Chen F. 2022. Bioinspired anti-fogging and anti-fouling artificial compound eyes. *Adv. Opt. Mater.* **10**, 2200861.

[171] Li C Z *et al*. 2022. Laser-induced morphology-switchable slanted shape memory microcones for maneuvering liquid droplets and dry adhesion. *Appl. Phys. Lett.* **120**, 061603.

[172] Zhang Y X *et al*. 2022. Reconfigurable magnetic liquid metal robot for high-performance droplet manipulation. *Nano Lett.* **22**, 2923-2933.

[173] Liu Z M, Li M, Dong X G, Ren Z Y, Hu W Q and Sitti M. 2022. Creating three-dimensional magnetic functional microdevices via molding-integrated direct laser writing. *Nat. Commun.* **13**, 2016.

[174] Tiryaki M E and Sitti M. 2022. Magnetic resonance imaging-based tracking and navigation of submillimeter-scale wireless magnetic robots. *Adv. Intell. Syst.* **4**, 2100178.

[175] Li R *et al*. 2022. Magnetically encoded 3D mesostructure with high-order shape morphing and high-frequency actuation. *Natl. Sci. Rev.* **9**, nwac163.

[176] Song X, Sun R J, Wang R, Zhou K, Xie R X, Lin J L, Georgiev D, Paraschiv A A, Zhao R B and Stevens M M. 2022. Puffball-inspired microrobotic systems with robust payload, strong protection, and targeted locomotion for on-demand drug delivery. *Adv. Mater.* **34**, 2204791.

[177] Tang Y C, Li M T, Wang T L, Dong X G, Hu W Q and Sitti M. 2022. Wireless miniature magnetic phase-change soft actuators. *Adv. Mater.* **34**, 2204185.

[178] Kim S, Lee S, Lee J, Nelson B J, Zhang L and Choi H. 2016. Fabrication and manipulation of ciliary microrobots with non-reciprocal magnetic actuation. *Sci. Rep.* **6**, 30713.

[179] Yasa I C, Tabak A F, Yasa O, Ceylan H and Sitti M. 2019. 3D-printed microrobotic transporters with recapitulated stem cell niche for programmable and active cell delivery. *Adv. Funct. Mater.* **29**, 1808992.

[180] Bozuyuk U, Yasa O, Yasa I C, Ceylan H, Kizilel S and Sitti M. 2018. Light-triggered drug release from 3D-printed magnetic chitosan microswimmers. *ACS Nano* **12**, 9617-9625.

[181] Sun H C M, Liao P, Wei T Y, Zhang L and Sun D. 2020. Magnetically powered biodegradable microswimmers. *Micromachines* **11**, 404.

[182] Mhanna R, Qiu F M, Zhang L, Ding Y, Sugihara K, Zenobi-Wong M and Nelson B J. 2014. Artificial bacterial flagella for remote-controlled targeted single-cell drug delivery. *Small* **10**, 1953-1957.

[183] Xu H F, Medina-Sánchez M and Schmidt O G. 2020. Magnetic micromotors for multiple motile sperm cells capture, transport, and enzymatic release. *Angew. Chem. Int. Ed.* **59**, 15029-15037.

[184] Alcântara C C J, Landers F C, Kim S, De Marco C, Ahmed D, Nelson B J and Pané S. 2020. Mechanically interlocked 3D multi-material micromachines. *Nat. Commun.* **11**, 5957.

[185] Hu X H, Yasa I C, Ren Z Y, Goudu S R, Ceylan H, Hu W Q and Sitti M. 2021. Magnetic soft micromachines made of linked microactuator networks. *Sci. Adv.* **7**, eabe8436.

[186] Hsu L Y, Mainik P, Münchinger A, Lindenthal S, Spratte T, Welle A, Zaumseil J, Selhuber-Unkel C, Wegener M and Blasco E. 2023. A facile approach for 4D microprinting of multi-photoresponsive actuators. *Adv. Mater. Technol.* **8**, 2200801.

[187] Flatae A M, Burresi M, Zeng H, Nocentini S, Wiegele S, Parmeggiani C, Kalt H and Wiersma D. 2015. Optically controlled elastic microcavities. *Light Sci. Appl.* **4**, e282.

[188] Yong J L, Chen F, Yang Q, Farooq U and Hou X. 2015. Photoinduced switchable underwater superoleophobicity–superoleophilicity on laser modified titanium surfaces. *J. Mater. Chem. A* **3**, 10703-10709.

[189] Nocentini S, Martella D, Parmeggiani C, Zanotto S and Wiersma D S. 2018. Structured optical materials controlled by light. *Adv. Opt. Mater.* **6**, 1800167.

[190] Nocentini S, Riboli F, Burresi M, Martella D, Parmeggiani C and Wiersma D S. 2018. Three-dimensional photonic circuits in rigid and soft polymers tunable by light. *ACS Photonics* **5**, 3222-3230.

[191] Chen L, Dong Y Q, Tang C Y, Zhong L, Law W C, Tsui G C P, Yang Y K and Xie X L. 2019. Development of direct-laser-printable light-powered nanocomposites. *ACS Appl. Mater. Interfaces* **11**, 19541-19553.

[192] Zanotto S, Sgrignuoli F, Nocentini S, Martella D, Parmeggiani C and Wiersma D S. 2019. Multichannel remote polarization control enabled by nanostructured liquid crystalline networks. *Appl. Phys. Lett.* **114**, 201103.

[193] Nishiguchi A, Zhang H, Schweizerhof S R, Schulte M F, Mourran A and Möller M. 2020. 4D printing of a light-driven soft actuator with programmed printing density. *ACS Appl. Mater. Interfaces* **12**, 12176-12185.

[194] Jamil F, Pokharel M and Park K. 2022. Light-controlled microbots in biomedical application: a review. *Appl. Sci.* **12**, 11013.

[195] Münchinger A, Hsu L Y, Fürniß F, Blasco E and Wegener M. 2022. 3D optomechanical metamaterials. *Mater. Today* **59**, 9-17.

[196] Zeng H, Wasylczyk P, Parmeggiani C, Martella D, Burresi M and Wiersma D S. 2015. Light-fueled microscopic walkers. *Adv. Mater.* **27**, 3883-3887.

[197] Martella D, Antonioli D, Nocentini S, Wiersma D S, Galli G, Laus M and Parmeggiani C. 2017. Light activated non-reciprocal motion in liquid crystalline networks by designed microactuator architecture. *RSC Adv.* **7**, 19940-19947.

[198] Ulrich S, Wang X P, Rottmar M, Rossi R M, Nelson B J, Bruns N, Müller R, Maniura-Weber K, Qin X H and Boesel L F. 2021. Nano-3D-printed photochromic micro-objects. *Small* **17**, 2101337.

[199] Zheng C L, Jin F, Zhao Y Y, Zheng M L, Liu J, Dong X Z, Xiong Z, Xia Y Z and Duan X M. 2020. Light-driven micron-scale 3D hydrogel actuator produced by two-photon polymerization microfabrication. *Sens. Actuators B: Chem.* **304**, 127345.

[200] Bai X, Yang Q, Li H Y, Huo J L, Liang J, Hou X and Chen F. 2022. Sunlight recovering the superhydrophobicity of a femtosecond laser-structured shape-memory polymer. *Langmuir* **38**, 4645-4656.

[201] Deng C S, Liu Y C, Fan X H, Jiao B Z, Zhang Z X, Zhang M D, Chen F Y, Gao H, Deng L M and Xiong W. 2023. Femtosecond laser 4D printing of light-driven intelligent micromachines. *Adv. Funct. Mater.* **33**, 2211473.

[202] Woska S *et al*. 2020. Tunable photonic devices by 3D laser printing of liquid crystal elastomers. *Opt. Mater. Express* **10**, 2928-2943.

[203] Tudor A, Delaney C, Zhang H R, Thompson A J, Curto V F, Yang G Z, Higgins M J, Diamond D and Florea L. 2018. Fabrication of soft, stimulus-responsive structures with sub-micron resolution via two-photon polymerization of poly(ionic liquid)s. *Mater. Today* **21**, 807-816.

[204] Spratte T, Geiger S, Colombo F, Mishra A, Taale M, Hsu L Y, Blasco E and Selhuber-Unkel C. 2023. Increasing the efficiency of thermoresponsive actuation at the microscale by direct laser writing of pNIPAM. *Adv. Mater. Technol.* **8**, 2200714.

[205] Lee Y W, Chun S, Son D, Hu X H, Schneider M and Sitti M. 2022. A tissue adhesion-controllable and biocompatible small-scale hydrogel adhesive robot. *Adv. Mater.* **34**, 2109325.

[206] Ji Q X *et al*. 2021. 4D Thermomechanical metamaterials for soft microrobotics. *Commun. Mater.* **2**, 93.

[207] McCracken J M *et al*. 2019. Microstructured photopolymerization of liquid crystalline elastomers in oxygen-rich environments. *Adv. Funct. Mater.* **29**, 1903761.

[208] Zhang M C, Shahsavan H, Guo Y B, Pena-Francesch A, Zhang Y Y and Sitti M. 2021. Liquid-crystal-elastomer-actuated reconfigurable microscale kirigami metastructures. *Adv. Mater.* **33**, 2008605.

[209] Guo Y B, Shahsavan H and Sitti M. 2020. Microscale polarization color pixels from liquid crystal elastomers. *Adv. Opt. Mater.* **8**, 1902098.

[210] Kubota H. 1952. On hypersensitive polarization colors. *J. Opt. Soc. Am.* **42**, 144-145.

[211] Zhang P, de Haan L T, Debije M G and Schenning A P H J. 2022. Liquid crystal-based structural color actuators. *Light Sci. Appl.* **11**, 248.

[212] Ye C H, Nikolov S V, Calabrese R, Dindar A, Alexeev A, Kippelen B, Kaplan D L and Tsukruk V V. 2015. Self-(Un)rolling biopolymer microstructures: rings, tubules, and helical tubules from the same material. *Angew. Chem. Int. Ed.* **54**, 8490-8493.

[213] Hu L, Wan Y, Zhang Q and Serpe M J. 2020. Harnessing the power of stimuli-responsive polymers for actuation. *Adv. Funct. Mater.* **30**, 1903471.

[214] Sun Y L, Dong W F, Yang R Z, Meng X, Zhang L, Chen Q D and Sun H B. 2012. Dynamically tunable protein microlenses. *Angew. Chem. Int. Ed.* **51**, 1558-1562.

[215] Ma Z C, Zhang Y L, Han B, Hu X Y, Li C H, Chen Q D and Sun H B. 2020. Femtosecond laser programmed artificial musculoskeletal systems. *Nat. Commun.* **11**, 4536.

[216] Chen H M, Li Y, Liu Y, Gong T, Wang L and Zhou S B. 2014. Highly pH-sensitive polyurethane exhibiting shape memory and drug release. *Polym. Chem.* **5**, 5168-5174.

[217] Chen J K and Chang C J. 2014. Fabrications and applications of stimulus-responsive polymer films and patterns on surfaces: a review. *Materials* **7**, 805-875.

[218] Chen Q Y, Lv P Y, Huang T Y, Huang J Y and Duan H L. 2020. Encoding smart microjoints for microcrawlers with enhanced locomotion. *Adv. Intell. Syst.* **2**, 1900128.

[219] Lao Z X, Sun R, Jin D D, Ren Z G, Xin C, Zhang Y C, Jiang S J, Zhang Y Y and Zhang L. 2021. Encryption/decryption and microtarget capturing by pH-driven Janus microstructures fabricated by the same femtosecond laser printing parameters. *Int. J. Extrem. Manuf.* **3**, 025001.

[220] Wen H J, Zeng X Z, Xu X X, Li W Y, Xie F, Xiong Z, Song S C, Wang B, Li X P and Cao Y Y. 2021. Reversible data encryption-decryption using a pH stimuli-responsive hydrogel. *J. Mater. Chem. C* **9**, 2455-2463.

[221] Wang J Y, Jin F, Dong X Z, Liu J and Zheng M L. 2022. Flytrap inspired pH-driven 3D hydrogel actuator by

femtosecond laser microfabrication. *Adv. Mater. Technol.* **7**, 2200276.
[222] Hu Y L *et al*. 2020. Botanical-inspired 4D printing of hydrogel at the microscale. *Adv. Funct. Mater.* **30**, 1907377.
[223] Fratzl P and Barth F G. 2009. Biomaterial systems for mechanosensing and actuation. *Nature* **462**, 442-448.
[224] Cesnik S, Perrotta A, Cian A, Tormen M, Bergmann A and Coclite A M. 2022. Humidity responsive reflection grating made by ultrafast nanoimprinting of a hydrogel thin film. *Macromol. Rapid Commun.* **43**, 2200150.
[225] Wang G, Xia H, Sun X C, Lv C, Li S X, Han B, Guo Q, Shi Q, Wang Y S and Sun H B. 2018. Actuator and generator based on moisture-responsive PEDOT: PSS/PVDF composite film. *Sens. Actuators B: Chem.* **255**, 1415-1421.
[226] Li M T, Hou Z S, Huang Q L, Xu S and Li A W. 2020. Laser printing controllable photonic-molecule microcavities. *Opt. Commun.* **459**, 125036.
[227] Sun X C, Xia H, Xu X L, Lv C and Zhao Y. 2020. Ingenious humidity-powered micro-worm with asymmetric biped from single hydrogel. *Sens. Actuators B: Chem.* **322**, 128620.
[228] del Pozo M, Delaney C, Bastiaansen C W M, Diamond D, Schenning A P H J and Florea L. 2020. Direct laser writing of four-dimensional structural color microactuators using a photonic photoresist. *ACS Nano* **14**, 9832-9839.
[229] Han D D, Zhang Y L, Chen Z D, Li J C, Ma J N, Mao J W, Zhou H and Sun H B. 2023. Carnivorous plants inspired shape-morphing slippery surfaces. *Opto Electron. Adv.* **6**, 210163.
[230] Huang Q L, Xu H L, Li M T, Hou Z S, Lv C, Zhan X P, Li H L, Xia H, Wang H Y and Sun H B. 2018. Stretchable PEG-DA hydrogel-based whispering-gallery-mode microlaser with humidity responsiveness. *J. Lightwave Technol.* **36**, 819-824.
[231] Lv C *et al*. 2018. Humidity-responsive actuation of programmable hydrogel microstructures based on 3D printing. *Sens. Actuators B: Chem.* **259**, 736-744.
[232] de Haan L T, Verjans J M N, Broer D J, Bastiaansen C W M and Schenning A P H J. 2014. Humidity-responsive liquid crystalline polymer actuators with an asymmetry in the molecular trigger that bend, fold, and curl. *J. Am. Chem. Soc.* **136**, 10585-10588.
[233] Chen B H, Zhao Z M, Nourshargh C, He C, Salter P S, Booth M J, Elston S J and Morris S M. 2022. Laser written stretchable diffractive optic elements in liquid crystal gels. *Crystals* **12**, 1340.
[234] Song Y G *et al*. 2022. Flexible tri-switchable wettability surface for versatile droplet manipulations. *ACS Appl. Mater. Interfaces* **14**, 37248-37256.
[235] Sun Y L, Hou Z S, Sun S M, Zheng B Y, Ku J F, Dong W F, Chen Q D and Sun H B. 2015. Protein-based three-dimensional whispering-gallery-mode micro-lasers with stimulus-responsiveness. *Sci. Rep.* **5**, 12852.
[236] Qian J, Kolagatla S, Pacalovas A, Zhang X, Florea L, Bradley A L and Delaney C. 2023. Responsive spiral photonic structures for visible vapor sensing, pattern transformation and encryption. *Adv. Funct. Mater.* 2211735.
[237] Chen C, Huang Z C, Zhu S W, Liu B R, Li J W, Hu Y L, Wu D and Chu J R. 2021. In situ electric-induced switchable transparency and wettability on laser-ablated bioinspired paraffin-impregnated slippery surfaces. *Adv. Sci.* **8**, 2100701.
[238] Münchinger A, Hahn V, Beutel D, Woska S, Monti J, Rockstuhl C, Blasco E and Wegener M. 2022. Multi-photon 4D printing of complex liquid crystalline microstructures by in situ alignment using electric fields. *Adv. Mater. Technol.* **7**, 2100944.
[239] Fleisch M, Gao S, Bošnjaković D, Zhang X, Rupp R A and Drevenšek-Olenik I. 2019. Laser-written polymeric scaffolds for micro-patterned liquid crystal alignment. *Liq. Cryst.* **46**, 2075-2084.
[240] Gräf S, Kunz C, Undisz A, Wonneberger R, Rettenmayr M and Müller F A. 2019. Mechano-responsive colour change of laser-induced periodic surface structures. *Appl. Surf. Sci.* **471**, 645-651.
[241] Zhang Y L, Tian Y, Wang H, Ma Z C, Han D D, Niu L G, Chen Q D and Sun H B. 2019. Dual-3D femtosecond laser nanofabrication enables dynamic actuation. *ACS Nano* **13**, 4041-4048.
[242] Sandford O'neill J J, Salter P S, Booth M J, Elston S J and Morris S M. 2020. Electrically-tunable positioning of topological defects in liquid crystals. *Nat. Commun.* **11**, 2203.
[243] Chen C, Yao H, Guo S J, Lao Z X, Xu Y D, Li S Y and Wu S Z. 2023. Ultra-robust joule-heated superhydrophobic smart window: dually-switching droplets adhesion and transparency via in situ electric-actuated reconfigurable shape-memory shutters. *Adv. Funct. Mater.* **33**, 2210495.
[244] Wu Y D, Dong X G, Kim J K, Wang C X and Sitti M. 2022. Wireless soft millirobots for climbing three-dimensional surfaces in confined spaces. *Sci. Adv.* **8**, eabn3431.
[245] Li W B *et al*. 2023. Self-vectoring electromagnetic soft robots with high operational dimensionality. *Nat. Commun.* **14**, 182.
[246] Kim H, Ahn S K, Mackie D M, Kwon J, Kim S H, Choi C, Moon Y H, Lee H B and Ko S H. 2020. Shape morphing smart 3D actuator materials for micro soft robot. *Mater. Today* **41**, 243-269.
[247] Guo Y B, Shahsavan H and Sitti M. 2020. 3D microstructures of liquid crystal networks with programmed voxelated director fields. *Adv. Mater.* **32**, 2002753.
[248] Zhang X, Wang Y, Tian Z H, Samri M, Moh K, Mcmeeking R M, Hensel R and Arzt E. 2022. A bioinspired snap-through metastructure for manipulating micro-objects. *Sci. Adv.* **8**, eadd4768.
[249] Ceylan H, Dogan N O, Yasa I C, Musaoglu M N, Kulali Z U and Sitti M. 2021. 3D printed personalized magnetic micromachines from patient blood-derived biomaterials. *Sci. Adv.* **7**, eabh0273.
[250] Gantenbein S, Colucci E, Käch J, Trachsel E, Coulter F B, Rühs P A, Masania K and Studart A R. 2023. Three-dimensional printing of mycelium hydrogels into living complex materials. *Nat. Mater.* **22**, 128-134.
[251] Afzali Naniz M, Askari M, Zolfagharian A, Afzali Naniz M and Bodaghi M. 2022. 4D printing: a cutting-edge platform for biomedical applications. *Biomed. Mater.* **17**, 062001.
[252] Zheng S R *et al*. 2022. Microrobot with gyroid surface and gold nanostar for high drug loading and near-infrared-triggered chemo-photothermal therapy. *Pharmaceutics* **14**, 2393.
[253] van Kesteren S, Shen X T, Aldeghi M and Isa L. 2023. Printing on particles: combining two-photon nanolithography and capillary assembly to fabricate multimaterial microstructures. *Adv. Mater.* **35**, 2207101.
[254] Mohanty S, Paul A, Matos P M, Zhang J N, Sikorski J and Misra S. 2022. CeFlowBot: a biomimetic flow-driven microrobot that navigates under magneto-acoustic fields. *Small* **18**, 2105829.
[255] Lüken A, Stüwe L, Rauer S B, Oelker J, Linkhorst J and Wessling M. 2022. Fabrication, flow assembly, and permeation of microscopic any-shape particles. *Small* **18**, 2107508.
[256] Lee Y W, Kim J K, Bozuyuk U, Dogan N O, Khan M T A, Shiva A, Wild A M and Sitti M. 2023. Multifunctional 3D-printed pollen grain-inspired hydrogel microrobots for on-

demand anchoring and cargo delivery. *Adv. Mater.* **35**, 2209812.
[257] Kim E, Jeon S, An H K, Kianpour M, Yu S W, Kim J Y, Rah J C and Choi H. 2020. A magnetically actuated microrobot for targeted neural cell delivery and selective connection of neural networks. *Sci. Adv.* **6**, eabb5696.
[258] Abele T, Messer T, Jahnke K, Hippler M, Bastmeyer M, Wegener M and Göpfrich K. 2022. Two-photon 3D laser printing inside synthetic cells. *Adv. Mater.* **34**, 2106709.
[259] Zhang J G, Yang H, Abali B E, Li M J, Xia Y and Haag R. 2019. Dynamic mechanics-modulated hydrogels to regulate the differentiation of stem-cell spheroids in soft microniches and modeling of the nonlinear behavior. *Small* **15**, 1901920.
[260] Xi W, Saw T B, Delacour D, Lim C T and Ladoux B. 2019. Material approaches to active tissue mechanics. *Nat. Rev. Mater.* **4**, 23-44.
[261] De Belly H, Paluch E K and Chalut K J. 2022. Interplay between mechanics and signalling in regulating cell fate. *Nat. Rev. Mol. Cell Biol.* **23**, 465-480.
[262] Hippler M *et al*. 2020. Mechanical stimulation of single cells by reversible host-guest interactions in 3D microscaffolds. *Sci. Adv.* **6**, eabc2648.
[263] Xu H F, Medina-Sánchez M, Maitz M F, Werner C and Schmidt O G. 2020. Sperm micromotors for cargo delivery through flowing blood. *ACS Nano* **14**, 2982-2993.
[264] Cai C K and Wang J. 2022. Femtosecond laser-fabricated photonic chips for optical communications: a review. *Micromachines* **13**, 630.
[265] Chen M Q, He T Y and Zhao Y. 2022. Review of femtosecond laser machining technologies for optical fiber microstructures fabrication. *Opt. Laser Technol.* **147**, 107628.
[266] Lu D X, Zhang Y L, Han D D, Wang H, Xia H, Chen Q D, Ding H and Sun H B. 2015. Solvent-tunable PDMS microlens fabricated by femtosecond laser direct writing. *J. Mater. Chem. C* **3**, 1751-1756.
[267] Hu Y Y, Miles B T, Ho Y L D, Taverne M P C, Chen L F, Gersen H, Rarity J G and Faul C F J. 2017. Toward direct laser writing of actively tuneable 3D photonic crystals. *Adv. Opt. Mater.* **5**, 1600458.
[268] Ho C H, Cheng Y C, Maigyte L, Zeng H, Trull J, Cojocaru C, Wiersma D S and Staliunas K. 2015. Controllable light diffraction in woodpile photonic crystals filled with liquid crystal. *Appl. Phys. Lett.* **106**, 021113.
[269] Xiao D W *et al*. 2022. Large reversible upconversion luminescence modification and 3D optical information storage in femtosecond laser irradiation-subjected photochromic glass. *Sci. China Mater.* **65**, 1586-1593.
[270] Zhu L, Zhang Y L and Sun H B. 2021. Miniaturising artificial compound eyes based on advanced micronanofabrication techniques. *Light Adv. Manuf.* **2**, 7.
[271] Jin G X, Hu X Y, Ma Z C, Li C H, Zhang Y L and Sun H B. 2019. Femtosecond laser fabrication of 3D templates for mass production of artificial compound eyes. *Nanotechnol. Precis. Eng.* **2**, 110-117.
[272] Hu Z Y, Zhang Y L, Pan C, Dou J Y, Li Z Z, Tian Z N, Mao J W, Chen Q D and Sun H B. 2022. Miniature optoelectronic compound eye camera. *Nat. Commun.* **13**, 5634.
[273] Xu Q, Dai B, Jiao Z, Hong R J, Yang Z Q, Zhang D W and Zhuang S L. 2018. Fabrication of large micro-structured high-numerical-aperture optofluidic compound eyes with tunable angle of view. *Opt. Express* **26**, 33356-33365.
[274] Xiong Z, Poudel A, Narkar A R, Zhang Z, Kunwar P, Henderson J H and Soman P. 2022. Femtosecond laser densification of hydrogels to generate customized volume diffractive gratings. *ACS Appl. Mater. Interfaces* **14**, 29377-29385.
[275] Liu B R *et al*. 2023. 4D direct laser writing of submerged structural colors at the microscale. *Small* **19**, 2204630.
[276] Zhang W *et al*. 2022. Stiff shape memory polymers for high-resolution reconfigurable nanophotonics. *Nano Lett.* **22**, 8917-8924.
[277] Wang Y, Fu X H, Chen Y Y, Qin L, Ning Y Q and Wang L J. 2022. The development progress of surface structure diffraction gratings: from manufacturing technology to spectroscopic applications. *Appl. Sci.* **12**, 6503.
[278] Li K X, Li C, Li H Z, Li M Z and Song Y L. 2021. Designable structural coloration by colloidal particle assembly: from nature to artificial manufacturing. *iScience* **24**, 102121.
[279] del Pozo M, Delaney C, da Cunha M P, Debije M G, Florea L and Schenning A P H J. 2022. Temperature-responsive 4D liquid crystal microactuators fabricated by direct laser writing by two-photon polymerization. *Small Structures* **3**, 2100158.
[280] Li W Y, Zeng X Z, Dong Y J, Feng Z W, Wen H J, Chen Q, Wen L, Song S C, Li X P and Cao Y Y. 2021. Laser nanoprinting of floating three-dimensional plasmonic color in pH-responsive hydrogel. *Nanotechnology* **33**, 065302.
[281] Bai X, Gou X D, Zhang J L, Liang J, Yang L J, Wang S P, Hou X and Chen F. 2023. A review of smart superwetting surfaces based on shape-memory micro/nanostructures. *Small* **19**, 2206463.
[282] Lou X D, Huang Y, Yang X, Zhu H, Heng L P and Xia F. 2020. External stimuli responsive liquid-infused surfaces switching between slippery and nonslippery states: fabrications and applications. *Adv. Funct. Mater.* **30**, 1901130.
[283] Yong J L, Chen F, Yang Q, Fang Y, Huo J L and Hou X. 2015. Femtosecond laser induced hierarchical ZnO superhydrophobic surfaces with switchable wettability. *Chem. Commun.* **51**, 9813-9816.
[284] Bai X, Yang Q, Fang Y, Zhang J Z, Yong J L, Hou X and Chen F. 2020. Superhydrophobicity-memory surfaces prepared by a femtosecond laser. *Chem. Eng. J.* **383**, 123143.
[285] Ke Y J, Chen J W, Lin G J, Wang S C, Zhou Y, Yin J, Lee P S and Long Y. 2019. Smart windows: electro-, thermo-, mechano-, photochromics, and beyond. *Adv. Energy Mater.* **9**, 1902066.
[286] Yang C, Zeng Q H, Huang J X and Guo Z G. 2022. Droplet manipulation on superhydrophobic surfaces based on external stimulation: a review. *Adv. Colloid Interface Sci.* **306**, 102724.
[287] Guo P, Wang Z B, Heng L P, Zhang Y Q, Wang X and Jiang L. 2019. Magnetocontrollable droplet and bubble manipulation on a stable amphibious slippery gel surface. *Adv. Funct. Mater.* **29**, 1808717.
[288] Wu S Z, Li D Y, Zhang J, Zhang Y Y, Zhang Y X, Li S Y, Chen C, Guo S J, Li C Z and Lao Z X. 2023. Multiple-droplet selective manipulation enabled by laser-textured hydrophobic magnetism-responsive slanted micropillar arrays with an ultrafast reconfiguration rate. *Langmuir* **39**, 2589-2597.
[289] Zhou S N, Chen C, Yang J F, Liao L R, Wang Z K, Wu D, Chu J R, Wen L and Ding W P. 2022. On-demand maneuvering of diverse prodrug liquids on a light-responsive candle-soot-hybridized lubricant-infused slippery surface for highly effective toxicity screening. *ACS Appl. Mater. Interfaces* **14**, 31667-31676.
[290] Jiao Y L, Zhang Y Y, Lv X D, Ji J W, Wang Z C, Su Y H, Liu X J and Liu K. 2021. In situ tuning underwater bubble movement on slippery lubricant-infused anisotropic microgrooved surface by unidirectional mechanical strain. *Langmuir* **37**, 2140-2145.

[291] Huo J L, Bai X, Yong J L, Fang Y, Yang Q, Hou X and Chen F. 2021. How to adjust bubble's adhesion on solid in aqueous media: Femtosecond laser-ablated patterned shape-memory polymer surfaces to achieve bubble multi-manipulation. *Chem. Eng. J.* **414**, 128694.

[292] Liu Y H, Zhao Y Y, Jin F, Dong X Z, Zheng M L, Zhao Z S and Duan X M. 2021. λ/12 super resolution achieved in maskless optical projection nanolithography for efficient cross-scale patterning. *Nano Lett.* **21**, 3915-3921.

[293] Tan D F, Li Y, Qi F J, Yang H, Gong Q H, Dong X Z and Duan X M. 2007. Reduction in feature size of two-photon polymerization using SCR500. *Appl. Phys. Lett.* **90**, 071106.

[294] Stocker M P, Li L J, Gattass R R and Fourkas J T. 2011. Multiphoton photoresists giving nanoscale resolution that is inversely dependent on exposure time. *Nat. Chem.* **3**, 223-227.

[295] Liaros N and Fourkas J T. 2019. Ten years of two-color photolithography [Invited]. *Opt. Mater. Express* **9**, 3006-3020.

[296] Takada K, Sun H B and Kawata S. 2005. Improved spatial resolution and surface roughness in photopolymerization-based laser nanowriting. *Appl. Phys. Lett.* **86**, 071122.

[297] Fischer J and Wegener M. 2013. Three-dimensional optical laser lithography beyond the diffraction limit. *Laser Photonics Rev.* **7**, 22-44.

[298] He M F, Zhang Z M, Cao C, Zhou G Z, Kuang C F and Liu X. 2022. 3D sub-diffraction printing by multicolor photoinhibition lithography: from optics to chemistry. *Laser Photonics Rev.* **16**, 2100229.

[299] Gan Z S, Cao Y Y, Evans R A and Gu M. 2013. Three-dimensional deep sub-diffraction optical beam lithography with 9 nm feature size. *Nat. Commun.* **4**, 2061.

[300] Balena A, Bianco M, Pisanello F and De Vittorio M. 2023. Recent advances on high-speed and holographic two-photon direct laser writing. *Adv. Funct. Mater.* 2211773.

[301] Hahn V, Kiefer P, Frenzel T, Qu J Y, Blasco E, Barner-Kowollik C and Wegener M. 2020. Rapid assembly of small materials building blocks (voxels) into large functional 3D metamaterials. *Adv. Funct. Mater.* **30**, 1907795.

[302] Zhu D Z *et al*. 2022. Direct laser writing breaking diffraction barrier based on two-focus parallel peripheral-photoinhibition lithography. *Adv.Photonics* **4**, 066002.

[303] Zhang L R *et al*. 2022. Functional shape-morphing microarchitectures fabricated by dynamic holographically shifted femtosecond multifoci. *Nano Lett.* **22**, 5277-5286.

[304] Ouyang W Q, Xu X Y, Lu W P, Zhao N, Han F and Chen S C. 2023. Ultrafast 3D nanofabrication via digital holography. *Nat. Commun.* **14**, 1716.

[305] Saha S K, Wang D E, Nguyen V H, Chang Y N, Oakdale J S and Chen S C. 2019. Scalable submicrometer additive manufacturing. *Science* **366**, 105-109.